A numerical study of heat and mass transfer in non-Newtonian nanofluid models

UNIVERSITY OF
KWAZULU-NATAL ™

INYUVESI
YAKWAZULU-NATALI

A THESIS SUBMITTED TO THE UNIVERSITY OF KWAZULU-NATAL

FOR THE DEGREE OF DOCTOR OF PHILOSOPHY IN THE COLLEGE

OF AGRICULTURE, ENGINEERING AND SCIENCE

by

Hloniphile Mildred Sithole Mthethwa

SCHOOL OF MATHEMATICS, STATISTICS AND COMPUTER SCIENCE.

August 2019

This thesis is dedicated to my mother Thembisile Sebenzile Sithole, with gratitude.
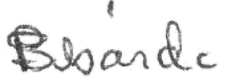
DECLARATION 1 - STUDENT AND SUPERVISORS

The work described in this thesis was carried out under the supervision of Prof. P. Sibanda and Prof. S.S. Motsa in the School of Mathematics, Statistics and Computer Science, College of Agriculture, Engineering and Science, University of KwaZulu-Natal, Pietermaritzburg, from September 2014 to August 2019.

I hereby declare that no portion of the work referred to in this thesis has been submitted in support of an application for another degree or qualification of this or any other university or institution of learning. The thesis is my original work except where due reference and credit is given.

Signature: 03/08/2020

Hloniphile Mildred Sithole Mthethwa Date

Signature: 3-Aug-2020

Prof. P. Sibanda Date

Signature: 6-Aug-2020

Prof. S.S. Motsa Date

DECLARATION 2 - PLAGIARISM

I, **Hloniphile Mildred Sithole Mthethwa** declare that

1. The research reported in this thesis, except where otherwise indicated, is my original research.

2. This thesis has not been submitted for any degree or examination at any other university.

3. This thesis does not contain other persons' data, pictures, graphs or other information, unless specifically acknowledged as being sourced from other persons.

4. This thesis does not contain other persons' writing, unless specifically acknowledged as being sourced from other researchers. Where other written sources have been quoted, then:

    (a) Their words have been re-written but the general information attributed to them has been referenced.

    (b) Where their exact words have been used, then their writing has been placed in italics and inside quotation marks, and referenced.

5. This thesis does not contain text, graphics or tables copied and pasted from the Internet, unless specifically acknowledged, and the source being detailed in the thesis and in the References sections.

Signature: ....   03/08/2020 ....

Hloniphile Mildred Sithole Mthethwa   Date

DECLARATION 3 - PUBLICATIONS

This thesis includes 4 published papers and 1 submitted paper. All papers were written under the supervision of Prof. P. Sibanda and Prof. S.S. Motsa.

1. Sithole, H.M., Mondal, S., Sibanda, P. and Motsa, S.S., 2017. An unsteady MHD Maxwell nanofluid flow with convective boundary conditions using spectral local linearization method. Open Physics, 15(1), pp.637-646.

2. Sithole, H., Mondal, H., Goqo, S., Sibanda, P. and Motsa, S., 2018. Numerical simulation of couple stress nanofluid flow in magneto-porous medium with thermal radiation and a chemical reaction. Applied Mathematics and Computation, 339, pp.820-836.

3. Sithole, H., Mondal, H. and Sibanda, P., 2018. Entropy generation in a second grade magnetohydrodynamic nanofluid flow over a convectively heated stretching sheet with nonlinear thermal radiation and viscous dissipation. Results in Physics, 9, pp.1077-1085.

4. Sithole, H., Mondal, H., Magagula, V.M., Sibanda, P. and Motsa, S., 2019. Bivariate Spectral Local Linearisation Method (BSLLM) for unsteady MHD Micropolar-nanofluids with Homogeneous–Heterogeneous chemical reactions over a stretching surface. International Journal of Applied and Computational Mathematics, 5(1), pp.12.

Signature: ....

Hloniphile Mildred Sithole Mthethwa

03/08/2020

....

Date

Acknowledgements

Abstract

A theoretical study of boundary layer flow, heat and mass transport in non-Newtonian nanofluids is presented. Because of the diversity in the physical structure and properties of non-Newtonian fluids, it is not possible to describe their behaviour using a single constitutive model. In the literature, several constitutive models have been proposed to predict the behaviour and rheological properties of non-Newtonian fluids. The question of interest is how the fluid physical parameters affect the boundary layer flow, and heat and mass transfer in various nanofluids.

In this thesis, nanofluid models in various geometries and subject to different boundary conditions are constructed and analyzed. A range of fluid models from simple to complex are studied, leading to highly nonlinear and coupled differential equations, which require advanced numerical methods for their solution.

This thesis is a conjoin between mathematical modeling of non-Newtonian nanofluid flows and numerical methods for solving differential equations. Some recent spectral techniques for finding numerical solutions of nonlinear systems of differential equations that model fluid flow problems are used. The numerical methods of primary interest are spectral quasilinearization, local linearization and bivariate local linearization methods. Consequently, one of the objectives of this thesis is to test the accuracy, robustness and general validity of these methods.

The dependency of heat and mass transfer, and skin friction coefficients on the physical parameters is quantified and discussed. Results show that nanofluids and physical parameters have an important and significant impact on boundary layer flows, and on heat and mass transfer processes.

Table of contents

Chapter 1

Introduction

Non-Newtonian fluid flow has generated a considerable amount of research in the last few decades because of its extensive applications in the biomedical, petroleum and chemical industries (Mushtaq et al. [1]). The flow properties of non-Newtonian fluids differ in many ways from those of Newtonian fluids. In particular, in contrast to Newtonian fluids, a constant coefficient of viscosity cannot always be defined. This is because the relationship between the strain rate and the shear stress is nonlinear, and may be time-dependent (Sochi [2]). The fluid viscosity depends on the applied shear force and, for some fluids, also on the rate at which the resultant shear occurs. It is important to understand the non-Newtonian viscous properties, how to characterize such physical fluid properties and how to use these properties to predict flow behaviour.

Due to the complexity and the broad diversity in the physical structure of fluids, it is not possible to suggest a single constitutive equation to describe the flow and properties of fluids. For example, Cioranescu et al. [3] indicate that the Navier–Stokes equations cannot adequately describe the flow of some non-Newtonian fluids. For this reason, non-Newtonian fluid models involve a number of different constitutive relations to predict their behaviour and rheological characteristics. The equations representing such constituent relations tend to be highly nonlinear and intricate in comparison with those of a Newtonian fluid. Furthermore, the viscosity of non-Newtonian fluids is usually greater than that of Newtonian fluids. Consequently, in the process of flow and heat transfer, the pressure drop is high and the heat transfer coefficient is particularly low (Chhabra and Richardson [4]).

To enrich heat transfer in fluids, a recent innovation has been to suspend nanosized solid particles in the fluids, in such a way that no sedimentation takes place. Such a fluid is called a nanofluid (Choi and Eastman [5]). Suspending very small solid particles in the energy transmission fluids can improve their thermal conductivity and so provide an effective way to significantly enhance their heat transfer characteristics (Das et al. [6]). The high thermal

conductivity of the suspended nanoparticles results in improved thermophysical properties or thermal performance of the nanofluid over conventional fluids (Bhanvase et al. [7]). When the nanoparticles are added to fluids they form non-Newtonian nanofluids.

Non-Newtonian nanofluids are considered to be the future of heat transfer in fluids, with a key role in many industrial, biomedical and transportation applications. Consequently, there has been a growing interest and need to study their flow characteristics and behaviour (Goyal and Bhargava [8]). However, being non-Newtonian means the motion of nanofluids is complicated and difficult to model because of the nonlinear relationship between the stress and the rate of strain, which as with most phenomena in the real world, is described by nonlinear equations. Solving such transport equations, means using the newly developed accurate and fast converging spectral methods.

In this study, we investigate theoretically the flow, heat and mass transfer in five non-Newtonian nanofluids. To illustrate the complete properties of all these fluids, any single fluid model is inadequate because it may address only some properties and fail to predict others. The non-Newtonian fluids of interest in this thesis are Maxwell fluids, second grade fluids, couple stress fluids, non-Darcy power-law fluids and micropolar fluids. We chose these five models for the following various reasons. A Maxwell fluid can be seen to possess both viscous and elastic characteristics. It is a subclass of rate type fluids and can predict the stress relaxation (Sadeghy et al. [9]). However, according to Choi et al. [10], the Maxwell model does not properly describe the typical relation between shear rate and shear stress in a simple shear flow. The second grade fluid model is the simplest class of differential type fluid, which can show normal stress (Wu et al. [11]). The couple stress fluid model have a nonlinear constitutive correlation between strain and stress. It is not suitable for fluids having viscosities that depend on the shear rate. On the other hand, the viscosity of a power-law model is shear dependent. The model predicts thinning and thickening behaviour due to the shear. However, the couple stress model is limited because at low and high shear rates it fails to produce sensible results in the shear regions. It does not predict the zero and infinite shear viscosities (Barnes et al. [12]). We also investigate a subclass of microfluids called micropolar fluids, which exhibit micro-rotational effects and micro-inertia.

In the remainder of this chapter we give a brief discussion and literature review of the various types of fluids that will be investigated in this study. We start with an outline of the relevant fluid models. This is followed by the discussion on nanofluids, heat and mass transfer, convective boundary condition, thermal radiation, entropy generation, and numerical methods. The chapter ends with the research aims and objectives together with an outline of the remainder of the thesis.

1.1 Non-Newtonian fluid models

The study of Newtonian and non-Newtonian fluid flows has been an active area of research interest for several decades, specifically in relation to heat and mass transfer processes found in commercial and industrial processes. Non-Newtonian fluids have a diverse range of applications in nature and engineering; for example, blood rheology, food processing, petroleum engineering, polymer blending and pharmaceutical products.

1.1.1 Maxwell fluids

A Maxwell fluid is an example of a viscoelastic fluid, (Özkaya et al. [13]). Viscoelasticity is a property of materials that exhibit both viscous and elastic characteristics when undergoing deformation (Papanicolaou and Zaoutsos [14]). Polymeric fluids show strong viscoelastic effects. For these materials, stress at the present time depends upon the rate of strain at past times, but with diminishing memory (Gargallo and Radic, [15]). Viscoelastic behaviours may be linear or nonlinear. Linear viscoelastic materials are such that under very small deformation or strain, the flow regime can be approximated by a linear relationship between stress and the rate of strain (Tanner and Walters [16]). The limitation of the linear viscoelastic model is that it cannot describe the strain rate dependence of viscocity on normal stress phenomena as these are nonlinear effects.

The upper convected Maxwell (UCM) model is an example of a nonlinear viscoelastic model. Unlike the Newtonian model, the UCM model incorporates relaxation time. The UCM model is a generalization of the Maxwell material for the case of large deformations using the upper convected time derivative (Souvaliotis and Beris [17]). Limitations of the UCM model noted by Joseph [18] include the lack of multiple relaxation time scales as well as unbounded stress growth for extensional flow. A model of an upper convected Maxwell fluid flow is discussed in Chapter 2.

The UCM model has been studied by many researchers. For example Choi et al. [10] gave an analysis of incompressible steady two-dimensional UCM fluid flow in a porous channel, where they included inertia and fluid elasticity. Hayat and Sajid [19] used the homotopy analysis method to find the analytical solutions of a magnetohydrodynamic (MHD) boundary layer flow in a UCM fluid model. Yang and Zhu [20] studied the unidirectional startup flow of a viscoelastic fluid in a pipe using the fractional Maxwell model. This flow, in an infinite straight pipe, starting from rest was driven by a constant pressure gradient. Mukhopadhyay and Gorla [21] analysed the unsteady two-dimensional flow of a Maxwell fluid over a stretching surface with a first order constructive or destructive chemical reaction. They found that flow fields and mass transfer were significantly influenced by the governing parameters.

Specifically, fluid velocity initially decreased with increasing unsteadiness parameter and concentration decreased significantly due to unsteadiness. The homotopy analysis method was used by Rashidi et al. [22] to find solutions to the conservation equations for heat and mass transfer in a two dimensional steady magnetohydrodynamic (MHD) fluid flow in a porous medium. The Falkner–Skan flow of a magnetohydrodynamic Maxwell fluid was also studied by Abbasbandy et al. [23]. Awais et al. [24] used the UCM fluid model to investigate heat absorption and generation in steady flow over a surface stretched linearly in its own plane.

Ramzan et al. [25] discussed the effects of Soret and Dufour parameters on mixed convection flow of a Maxwell nanofluid with variable conditions for temperature and concentration. They further investigated the impact of changes in parameter values on the local Nusselt and Sherwood numbers. Their study showed that the concentration field decreases with increased Brownian motion and increases with increased thermophoretic parameters.

Bilal et al. [26] presented an investigation of three-dimensional UCM nanofluid flow over a stretching surface to determine the effects of nanoparticles on MHD heat and mass transfer. A nonlinear radiative heat flux was incorporated in the formulation of the energy equation. Liu et al. [27] presented an analysis of the unsteady Maxwell nanofluid flow and mass transfer in a finite thin film induced by an unsteady stretching sheet. They further investigated the effects of heat generation, thermophoresis and Brownian motion on the flow behaviour.

Many fluid flow studies with the UCM model are limited in the number of parameters they included. For instance, Nandy [28] focused on the unsteady boundary layer flow of a Maxwell nanofluid over a permeable shrinking sheet with a Navier slip condition at the surface. The conventional no-slip condition at the surface and the Navier's slip condition were applied at the surface. However there was no evaluation of the impact and significance of thermophoresis and Brownian motion when the nanofluid particle volume fraction at the boundary is not actively controlled. This limitation will be addressed in this thesis. They explored the simultaneous impact of a magnetic field, thermal radiation, and unsteadiness on the heat transfer and flow properties of the fluid. Nandy et al. [29] studied forced convection in an unsteady nanofluid flow past a permeable shrinking sheet subject to heat loss due to thermal radiation. They explored the simultaneous impact of a magnetic field, thermal radiation, and unsteadiness on the heat transfer and flow properties of the fluid. The study did not, however, consider nonlinear thermal radiation. The study in this thesis will consider the nonlinear thermal radiation for some of the models. Such extensions should make the UCM model more realistic.

1.1.2 Second grade fluids

A second grade fluid is a subclass of viscoelastic fluids that was first proposed by Rivlin and Ericksen [30]. Second grade fluid flows with constant viscosity are the subject of considerable attention in many boundary layer studies. This model is able to the normal stress effects, as well as shear thinning and thickening effects, in steady flows (Man and Sun [31]).

Second grade nanofluids are non-Newtonian fluids with both viscoelastic and magnetic properties, which have biomedical applications, such as in treatment of wounds or tumors, as well as in heat removal processes. (Ramzan and Bilal [32]). As a result second grade fluids have generated research interest. Hayat et al. [33] investigated the stagnation point flow of a second grade fluid with variable free stream properties. Das et al. [34] studied a second grade fluid flow passing along semi-infinite stretching sheet with convective surface heat flux. They provided the exact solutions of the equations for this flow using the Fourier sine transform method. Helical flows of a second grade fluid between two coaxial cylinders, where the flow was due to the inner cylinder motion, were investigated by Jamil et al. [35]. Nadeem et al. [36] examined the boundary layer flow and heat transfer in a second grade fluid flow through a horizontal cylinder. Akinbobola and Okoya [37] studied a steady two-dimensional non-Newtonian second grade fluid flow under the influence of temperature dependent viscosity and thermal conductivity. They found that viscosity varies inversely as a linear function of temperature while the thermal conductivity varies directly as a linear function of temperature.

Turkyilmazoglu [38] presented dual and triple solutions of an MHD second grade non-Newtonian fluid with a slip condition. Erdogan and Imrak [39] gave an exact solution for equations describing incompressible second grade fluid flow between two coaxial cylinders with porous walls. The study assumed that the inner cylinder was rotating with a constant angular velocity and the outer cylinder was at rest. Hayat et al. [40] studied the magnetohydrodynamic (MHD) flow of a second grade nanofluid over a nonlinear stretching sheet. The nanofluid was assumed to be electrically conducting and subjected to a non-uniform applied magnetic field. Ramzan et al. [41] studied a three dimensional second grade nanofluid flow over an exponentially stretched surface, with thermal radiation and convective boundary conditions. The study of steady two-dimensional flow of a magnetohydrodynamic second grade nanofluid was presented by Zuhra et al. [42]. Their primary focus was the mixed convection in gravity driven MHD second grade nanofluid flow containing both nanoparticles and gyrotactic microorganisms along a convectively heated vertical solid surface. Entropy generation is one of the key factors responsible for energy losses in thermal and engineering systems. None of the studies reviewed in this thesis incorporated the entropy generation in the second grade nanofluid models. In Chapter 5, entropy generation in a second grade nanofluid flow is investigated.

1.1.3   Couple stress fluids

The main feature of couple stresses in fluids is that they introduce a size-dependent effect. The theory of couple stress fluids, first introduced by Stokes [43], has been widely studied by researchers such as Islam and coworkers [44, 45].

According to Stokes [43], couple stresses appear in fluids with very large molecules, such as polymeric suspensions, animal and human blood and lubrication fluids. These fluids are therefore of scientific interest and have numerous industrial applications, such as in the extrusion of polymers and solidification of liquid crystals. Walicki and Walicka [46] modeled synovial fluids (which contain long chain hylauronic acid molecules) in human joints as couple stress fluids.

Other examples of studies of the flow of couple stress fluids include that of Hiremath and Patil [47], who investigated the oscillatory flow of a couple stress fluid through a porous medium, and the investigation by Hayat et al. [48] of melting heat transfer in the boundary layer flow of a couple stress fluid over a stretching surface. Bakhti and Azrar [49] studied steady flow of a couple stress fluid in a constricted tapered artery under the effects of a transverse magnetic field, moving catheter, and slip velocity. Takhar et al. [50] examined the unsteady MHD flow of an ambient fluid with heat transfer over a rotating disk. Khan et al. [51] extended this study to incorporate the couple stress effects when a magnetic field and heat transfer analysis are taken into account. The analytical solution for a fully developed laminar flow between vertical parallel plates filled with two immiscible viscous and couple stress fluids in a composite porous medium was presented by Umavathi et al. [52]. The study by Sarojini et al. [53] considered the steady hydro magnetic flow of a couple stress fluid in a channel through a porous medium under the influence of a uniform inclined magnetic field. The equations for the couple stress fluid flow incorporated the Brinkman model for a porous medium.

The boundary layer nanofluid flow subject to couple stress effects has been studied by various researchers. Some studies have assumed that the nanoparticle volume fraction at the boundary surface may be actively controlled. However, a more realistic boundary condition is that there is no active control of the nanoparticle volume fraction at the boundary, as was suggested by Awad et al. [54], who investigated the couple stress effects on unsteady nanofluid flow over stretching surfaces with a vanishing nanoparticle flux at the wall. Their results showed that the effect of Brownian motion on the mass volume fraction within the boundary is much more significant rather than on the temperature.

Applications of nanoparticles in medical science has opened a new dimension for researchers. Nanoparticles may be used in treating different diseases by means of the peristaltic movement of blood or magnetic drug targeting of tumours. Ellahi et al. [55] used a single

model to investigate the simultaneous effects of a chemical reaction and activation energy on the peristaltic flow of couple stress nanofluids. The non-Newtonian power-law fluid relations were extended to the couple stress theory by Hajesfaniari and Dargush [56]. In Chapter 4 a study of a couple stress nanofluid flow is presented.

1.1.4 Power-law fluids

A power-law fluid model is a generalized non-Newtonian fluid model that gives a basic relationship between the fluid viscosity and the strain rate. It is sometimes known as the Ostwald-de Waele model. A power-law fluid is represented by the rheological equation of state given by

$$\tau_{xy} = -\kappa \left(\frac{\partial u}{\partial y} \right)^n \tag{1.1}$$

where τ_{xy} is the stress tensor, κ is the fluid consistency, and n is the power-law exponent.

The power-law fluid model can be subdivided into three different type of fluids based on values of the flow behaviour index. That is for $n < 1$, we have pseudoplastic or shear-thinning fluids, when $n = 1$ we have a Newtonian fluid and for $n > 1$ the fluid is dilatant. The power-law is the simplest model that approximates the behaviour of a non-Newtonian fluid. However, its limitations are that it cannot predict the effects of elasticity and it is valid over only a limited range of shear rates. The model fails to provide sensible results at low and high shear regimes. Nevertheless, the power-law model is the most widely used model in process engineering applications. The power-law model can be used to describe accurately the rheology of lubricants. Schowalter [57] and Acrivos et al. [58] were among the first to consider the boundary layer flow of non-Newtonian power-law fluids. Schowalter [57] derived the equations for self-similar flow of a pseudoplastic fluid, while Acrivos et al. [58] provided numerical solutions to the equations for self-similar flow in both shear-thinning and shear-thickening fluids. More recently, Ishak and Bachok [59] investigated the steady boundary-layer flow of a non- Newtonian power-law fluid over a flat plate in a moving fluid. Then Reddy et al. [60] studied the magnetic effects on a steady, two-dimensional laminar flow of a power-law fluid along a moving flat plate. The numerical solutions to the resulting equations were solved using the implicit finite difference scheme.

The problem of turbulence modeling of non-Newtonian power-law fluids inside ducts was investigated by Cruz et al. [61]. This important problem appears in many applications in chemical and mechanical engineering, including food processing. Non-Newtonian power-law fluids have particular applications in cavity flows. The magnetohydrodynamic mixed convection flow of a non-Newtonian power-law fluid through a round cavity was analyzed numerically by Bose et al. [62]. For their study the cavity was kept at a uniformly high

temperature, with the bottom wall being insulated and the top wall of the channel being maintained at a temperature lower than the cavity temperature. Sojoudi et al. [63] carried out a numerical investigation of free convection and heat transfer in a differentially heated trapezoidal cavity filled with a non-Newtonian power-law fluid. More recently, a numerical simulation of a non-Newtonian laminar fluid flow in a lid-driven skewed cavity was studied by Thohura et al. [64] using the power-law viscosity model.

A porous medium is a solid material comprising a solid matrix with interconnected voids [65, 66]. Flows through porous media have been extensively studied because of their important applications. For instance catalysts are frequently supported by, or made as, a porous medium through which the chemicals flow. Flows through porous media have two characteristics; namely their porosity and their permeability, both of which control the movement and storage of fluids. According to Lehr and Lehr [67], porosity is defined as the ratio of the void space to the total volume of the porous medium. According to [68], permeability is defined as a measure of the ability of porous materials to conduct flow and is dictated by the geometry of the pore network.

Darcy's law, proposed by Darcy [69] in 1856 assumes that viscous forces dominate the inertial forces in porous media, The law is valid where the flow rate is low in porous media or through fractures. In such cases the flow rate and the pressure gradient have a linear relationship. Deviations from this linear relation are termed non-Darcy flow. The non-Darcy law is important for describing fluid flow in porous media in situations where high velocity occurs.

Zeng and Grigg [70] reviewed the two non-Darcy criteria for fluid flow in porous media namely, the Reynolds number and the Forchheimer number. They recommended a revised Forchheimer number, which has the advantage of having wide applicability. Prasad et al. [71] analyzed the effect of melting and thermal dispersion-radiation on steady mixed convective heat transfer from a vertical plate embedded in a non-Newtonian power-law fluid that saturated a non-Darcy porous medium, with aiding and opposing external flows. The effect of the power-law index parameter of the non-Newtonian fluid on free convection heat and mass transfer from a vertical wall was studied by Kairi et al. [72]. Their study considered double dispersion in a non-Darcy porous medium with constant wall temperature and concentration. They used the Ostwald–de Waele power-law model to characterize the non-Newtonian fluid behaviour. Kumari and Jayanthi [73] used the implicit finite-difference method developed by Keller to find the steady state solutions for non-Darcy free convection flow through the walls of a horizontal cylinder, that are a saturated porous medium. Hadim [74] presented a numerical study of non-Darcy natural convection in a porous enclosure saturated with a power-law fluid. The flow in the porous medium was modeled using

the modified Brinkman–Forchheimer extended Darcy model for power-law fluids, which accounts for both inertia and boundary effects. The results indicated that when the power-law index is reduced, the circulation within the enclosure increases, thereby leading to a higher Nusselt number. These effects were enhanced as the Darcy number was increased.

Chamka et al. [75] studied the impact of a uniform lateral mass flux on non-Darcy natural convection of a non-Newtonian nanofluid along a vertical cone embedded in a porous. Kameswaran et al. [76] studied the effects of thermal dispersion on non-Newtonian power-law nanofluid flow over an impermeable vertical plate. Their mathematical model for the nanofluid incorporated the effects of Brownian motion of the nanoparticles and thermophoresis. The non- Newtonian nature of the fluid was modeled by the power-law index n, and cases of both shear thinning and thickening were investigated.

1.1.5   Micropolar fluids

The idea of a micropolar fluid was first introduced by Eringen [77] in an attempt to explain the behaviour of some naturally occurring fluids and certain fluids containing polymeric additives.

Micropolar fluids are non-Newtonian fluids that consist of solid particles suspended in a viscous medium. Ferro-fluids, bubbly liquids, cerebrospinal fluid and blood are some examples of micropolar fluids. Uddin et al. [78] mention their application in industrial or engineering of colloidal or polymeric suspensions, such as are found in engine lubricants, radial diffusion, paint rheology, and thrust bearing technologies. In the theory of micropolar fluids, the local effects arising from the microstructure and the intrinsic motion of fluid elements are taken into account. Peddieson and McNitt [79] extended the pioneering work of Eringen [77] in boundary layer theory by studying the stagnation flow of a micropolar fluid. They considered both planar and axisymmetric flows, and imposed the condition that the spin should vanish on the solid boundary. Eringen [80] later developed the theory of thermomicropolar fluids by taking into account the effect of microelements of fluids on both the kinematics and conduction of heat. Kümmerer [81] used a shooting method for a numerical investigation of a steady boundary layer flow of a micropolar fluid. The results showed that the macroscopic properties of steady boundary layer flows are little affected by coupling, microdiffusivity and microinertia parameters, while the microrotation is very sensitive to all three parameters. Sankara and Watson [82] investigated the boundary layer flow of a micropolar fluid over a stretching surface. Heruska et al. [83] investigated the boundary layer flow of a micropolar fluid with suction or injection through a porous sheet. In both the studies [82, 83] the flow equations were solved numerically using a globally convergent method in conjunction with a quasi-Newtonian algorithm.

The heat transfer from a micropolar fluid flow over a non-isothermal stretching sheet with suction and blowing was examined by Hassanien and Gorla [84] while, the heat transfer in a two-dimensional steady hydromagnetic natural convective flow of a micropolar fluid over an inclined permeable plate subjected to a constant heat flux condition was studied by Rahman et al. [85]. Results in both studies showed that the thermal conductivity parameter promotes higher velocities and higher temperatures in the respective boundary layers. Das [86] investigated the effect of thermophoresis and chemical reaction on heat and mass transfer in a hydromagnetic micropolar fluid flow over an inclined permeable plate with constant heat flux and non-uniform heat source/sink in the presence of variable fluid properties such as thermal radiation. Das [86] did not consider the homogeneous-heterogeneous chemical reaction. Bhattacharyya et al. [87] investigated the effects of thermal radiation on both the flow of a micropolar fluid and the heat transfer past a porous shrinking sheet. Mishra et al. [88] studied free convection in a micropolar fluid along a stretching sheet embedded in a porous medium with a volumetric non-uniform heat source. Their study considered the effects of thermal diffusion and a first order chemical reaction on the flow characteristics.

Atif et al. [89] studied the heat and mass transfer in a magnetohydrodynamic micropolar Carreau nanofluid flowing over a stretching sheet. Their study included important parameters such as induced magnetic field, internal heating, thermal radiation, and Ohmic and viscous dissipation effects. Alizader et al. [90] studied the steady laminar flow and heat transfer in an MHD micropolar nanofluid in a two-dimensional channel with penetrable walls and thermal radiation. The outcomes showed that by increasing the micropolar parameter, the temperature profile slightly increased. Abbas et al. [91] investigated the stagnation point flow of an MHD micropolar nanomaterial fluid over a circular cylinder having sinusoidal radius variation, while taking into account a velocity slip phenomenon. They mathematically modeled the flow of the micropolar fluid for both weak and strong concentrations. Shah et al. [92] studied the flow of a micropolar Casson fluid between two parallel plates in a rotating frame, with thermal radiation and taking into account the influence of Hall current. It was found that the combined Hall impact decreases the operative conductivity, which tends to increase the velocity field.

Mixed convection due to homogeneous–heterogeneous chemical reactions arises in many science and engineering applications, such as in the production of plastics including polythene, polymer extrusion, and cooling of elastic sheets. Many chemical systems involve both homogeneous and heterogeneous reactions, with examples arising in combustion, catalysis and biochemical systems. The interaction between the homogeneous reactants in the bulk fluid and heterogeneous reactions on catalytic surfaces is generally very complex. A simple mathematical model for homogeneous-heterogeneous reactions in stagnation-

point boundary-layer flow was given by Chaudhary and Merkin [93]. They modeled the homogeneous reaction using isothermal cubic kinetics and the heterogeneous reaction using first-order kinetics. Chaudhary and Merkin [94] extended their earlier work to include the effect of loss of the autocatalyst. Two studies, by Kameswaran et al. [95] and Ravikiran and Radhakrishnamacharya [96], considered the effects of combined homogeneous and heterogeneous chemical reactions on the peristaltic motion of a micropolar fluid through a porous medium with wall effects and a slip boundary condition. Shaw et al. [97] investigated the effects of a homogeneous-heterogeneous reaction on steady micropolar fluid flow along a permeable stretching or shrinking sheet in a porous medium. This study extended the model developed by Chaudhary and Merkin [93] for a homogeneous-heterogeneous reaction in boundary layer flow with equal diffusivities of a reactant and autocatalysis. In Chapter 6 of the current thesis, an unsteady MHD micropolar model with homogeneous–heterogeneous chemical reactions over a stretching surface is studied.

1.2   Nanofluids

All fluid flows studied in this thesis incorporate nanofluids. The low thermal conductivity of common fluids often limits their effectiveness in applications such as heat exchangers. A wide variety of techniques are often used to enhance thermal conductivity of fluids and subsequently improve heat transfer. One such innovative method is suspending nanometre-sized solid particles in the fluids. Different types of powders such as metallic, non-metallic and polymeric particles are added to common fluids to form slurries. Even at low particle volume concentration, the thermal conductivity, thermal diffusivity, viscosity and heat transfer performance of such fluids with suspended particles have been shown to be higher than those of common base fluids such as water and oil [98, 99]. A nanofluid is defined by Choi [5] as a fluid with suspended solid nanometer-sized particles (termed nanoparticles) such as, nanofibers, nanotubes, nanowires, nanorods, or droplets that are less than 100 nm in size, and solid volume fraction less than 4%. The study by Xuan and Li [99] presented a procedure for preparing a nanofluid through a suspension of nanophase powders in a base liquid. They presented a theoretical study of the thermal conductivity of nanofluids and the heat transfer performance of a nanofluid flowing in a tube. The study revealed that nanofluids has great potential for enhancing the heat transfer process. The reason is that the suspended ultrafine particles generally increase the thermal conductivity of the nanofluid. The volume fraction, shape, dimensions and properties of the nanoparticles have been shown to affect the thermal conductivity of nanofluids.

Many researchers have presented experimental or theoretical studies of the thermo-physical properties of, and the convective heat transfer in, nanofluids. Nanofluids have great potential for applications in many fields, including the intensification of heat transfer and the cooling of electronic equipments. For instance, a novel cooler designed by Jang and Choi [100] combined the use of a microchannel heat sink with nanofluids. These nanofluids had better cooling performance than pure water when used as the cooling medium. Nanofluids reduced both the thermal resistance and the temperature difference between the heated microchannel wall and the coolant. Nanofluids have further been used in applications in such fields as energy extraction, mechanical engineering, biomedical systems and transportation. Tzeng et al. [101] studied the use of nanofluids in cooling of automatic transmissions. Nanofluids have been used in building heating and cooling systems. Kulkarni et al. [102] evaluated how nanofluids perform when heating buildings in cold regions. Otanicar et al. [103] reported experimental results of solar collectors that used nanofluids made from a variety of nanoparticles (graphite, and silver). The efficiency improvement was shown to improve by a factor of up to 5% in solar thermal collectors when utilizing nanofluids as the absorption media.

Various experimental and theoretical studies have been carried out on the characteristics of nanofluids in convective heat transfer and thermal conductivity. Arifin et al. [104] studied both free and mixed convection in a nanofluid flow past a horizontal surface in order to investigate the effect of the solid volume fraction or nanoparticle volume fraction of the nanofluid on the flow and heat transfer characteristics. It was found that the solid volume fraction affects the fluid flow and heat transfer characteristics. Chamkha et al. [105] investigated non-Darcy natural convection flow in non-Newtonian nanofluids over a cone in a porous medium with uniform heat and volume fraction fluxes. Their nanofluid model incorporated the effects of Brownian motion and thermophoresis. It was assumed that the cone surface was permeable for possible nanofluid wall suction/injection. They concluded that increasing the Brownian motion parameter led to enhancing the local Sherwood number and to reducing the local Nusselt number. Mondal et al. [106] presented a model for the unsteady boundary-layer flow and heat transfer of a Maxwell nanofluid fluid over a permeable shrinking sheet with convective boundary conditions and a variable magnetic field applied normal to the sheet. More recent work by Bilal et al. [107] has identified the novel characteristics of nanofluid flow induced by a vertically rotating cone with a consideration of both the heat and mass transport. All fluid flows studied in this thesis incorporate nanofluids.

1.3   Heat and mass transfer

In modern engineering designs it is essential to account for heat transfer. Sobhan and Peterson [108] highlight the need to account for efficiencies in heat exchanges when designing and operating devices such as air-conditioners and refrigeration systems. A successful design makes provision for maintaining reasonable temperatures by means of adequate transfer of heat. The study of heat transfer entails understanding the physical processes whereby thermal energy is transferred as a result of a temperature gradient. There are three different processes by which energy is transported; namely, conduction, convection and radiation. Conduction is the mechanism of heat transfer that takes place between particles immediately adjacent to one another or through molecular action, supplemented by free flow of electrons from a high temperature region to a low temperature region, as explained by Bergman et al. [109]. Çengel and Ghajar [110] explain that in convection, the thermal energy transport is influenced by the relative motions within the fluid, so the resultant heat transfer occurs between the layers of a fluid. These two authors also note that heat transfer can occur by thermal radiation when solid bodies, as well as liquids and gases, emit thermal energy in the form of electromagnetic waves and absorb similar energy from neighboring bodies. Thermal radiation is considered further in Section 1.5.

Many fluid flows involve mass transfer. Yunus and Afshin [111] note that the transport of one constituent chemical species from a region of higher concentration to that of a lower concentration constitutes mass transfer. Mass transfer occurs in two ways, as outlined by Bergman et al. [109]; firstly through the bulk fluid motion or mass convection and secondly through diffusion. Cengel and Ghajar [110] state that the rate of mass diffusion of species is proportionally related to the concentration gradient in the specific direction. Heat and mass transfer in various fluid flows is investigated in this thesis.

1.4   Convective boundary conditions

The convective boundary condition is also commonly known as a Newton boundary condition. This boundary condition describes the existence of heating or cooling at the surface and comes from the surface energy balance. Kays et al. [112] explain that surface energy balance infers that the heat conduction at the surface of the material is equal to the heat convection at the surface in the same direction. The net heat entering the surface from the convective side must equal the net heat leaving the surface from the conduction side. The convective boundary condition is derived from the Fourier law of heat conduction applied to a solid boundary. Sisko et al. [113] highlight the importance of heat transfer analysis associated

with convective boundary conditions in designing thermal energy storage, studying cooling problems, reducing the drag, and in controling boundary layer separation. Makinde and Aziz [114] investigated the importance of a convective boundary condition on boundary layer flow and heat transfer. This study was later extended by Uddin et al. [115] who investigated MHD free convection of a nanofluid over a vertical flat plate, taking into account a Newtonian heating boundary condition. Models in this thesis consider the convective boundary condition.

1.5 Thermal radiation

Thermal radiation plays a significant role in controlling heat transfer processes in polymer processing industries. Additionally, the effect of thermal radiation on flow and heat transfer processes is of major importance in the design of many advanced systems that operate at high temperatures. Thermal radiation in these systems is usually the result of emission from hot walls and from the working fluid. Thermal radiation becomes important when the difference between the ambient temperature and that at the surface and is large. Thus an understanding of radiation heat transfer in a system may assist in achieving products with desired characteristics. The influence of thermal radiation on hydromagnetic Darcy-Forchheimer mixed convection in a flow past a stretching sheet embedded in a porous medium was studied by, among others, Pal and Mondal [116].

Thermal radiation is often approximated using the Rosseland approximation, with the heat flux q_r given by Pal [117] as

$$q_r = -\frac{\partial T^4}{\partial y}\left(\frac{4\sigma^*}{3k^*}\right), \tag{1.2}$$

where k^* and σ^* are the Rosseland mean spectral absorption coefficient and the Stefan–Boltzmann constant, respectively. If the temperature differences are small, T^4 may be expanded using the Taylor series about T_∞, to obtain

$$T^4 \approx -3T_\infty^4 + 4T_\infty^3. \tag{1.3}$$

The relative heat flux can then be written as

$$q_r = -\frac{\partial T}{\partial y}\left(\frac{16\sigma^* T_\infty^3}{3k^*}\right). \tag{1.4}$$

Both linear and the nonlinear thermal radiation is incorporated in the models in this thesis.

1.6   Entropy generation

Entropy generation plays a major role in controlling the rate of heat transfer in the proximity of a surface. Entropy production depletes the available energy in the engineering and industrial processes. For this reason, it is important to determine the rate of entropy generation in a system. Irreversibility which is expressed as entropy generation, is due to heat transfer, mass transfer, vis- cous dissipation, chemical reactions, or magnetic field, etc. Aiboud and Saouli [118] studied entropy generation in viscoelastic MHD flow over a stretching surface. Butt et al. [119] studied the effects of velocity slip on entropy generation in the boundary layer flow over a vertical sheet with a convective boundary condition. Magherbi et al. [120] studied entropy generation in convective heat and mass transfer within a square cavity in the case of assisting buoyancy forces. For the case of a binary perfect gas mixture, Hidouri et al. [121] studied the influence of the Soret effect on entropy generation during double diffusive convection for both aiding and opposing buoyancy forces in a square cavity. López et al. [122] investigated entropy generation in MHD nanofluid flow in a porous vertical microchannel with nonlinear thermal radiation. Entropy generation in second grade nanofluid flow is investigated in this thesis. In Chapter 5, the focus is on entropy generation analysis in order to improve the system's performance.

1.7   Numerical methods

In recent years, various numerical methods have been used to solve systems of coupled, nonlinear equations. These include methods such as that of Runge-Kutta, which is applicable only for first order initial value ODE's. Khan et al. [123] solved a system of equations with the aid of shooting algorithm supported by a fifth order Runge-Kutta integration scheme. The developed element free Galerkin method, is another new computational method, which has been used effectively to solve problems with discontinuities, moving boundaries and large deformations. Using this method Sharma et al. [124] presented a numerical solution for unsteady MHD convection heat and mass transfer past a semi-infinite vertical porous moving plate. The famous discretized method, the finite element method (FEM), has been widely used in many simulations of engineering problem; however, it has limitations such as interpolation failing when elements become too distorted. Another major difficulty in FEM analysis is the preparation of an effective mesh leading to a good response solution. In order

to remove many of the meshing difficulties, Bathe and Zhang [125] suggested a new finite element solution scheme including meshing in which the elements can overlap.

The numerical methods for solving differential equations by approximating them with difference equations, in which finite differences approximate the derivatives, are called the finite difference methods (FDMs). The FDMs are unique; as Vajravelu and Prasad [126] indicate they differ from other numerical techniques in a sense that they allow for an effective control on the rate of convergence via an initial approximation. Saithambi [127] studied and demonstrated the effectiveness of a second order FDM by applying it successfully to variations of the Falkner–Skan equation, and by demonstrating its second order accuracy. The Keller box method is an implicit finite difference scheme. It has been successfully applied to parabolic partial differential equations. A shooting method accompanied by the Runge-Kutta-Fehlberg scheme has been recently used by Bin-Moshin [128] to explore the magnetohydrodynamic nanofluid flow over a vertical expanding surface. The disadvantage of this method, as highlighted by Anderson et al. [129], lies in the computational effort per time step being expensive due to its step having to replace the higher derivative by first derivatives.

The methods mentioned above have been used to find approximate solutions of highly nonlinear coupled systems. These methods have some disadvantages, such as requiring many grid points for accurate approximations of the solutions, being computationally expensive and possibly not being very effective, as pointed out by Motsa et al. [130], where there are discontinuities, singularities or problems with multiple solutions. Instead, spectral methods are often the preferred tools for solving ordinary and partial differential equations, because of their elegance and high accuracy in resolving problems with smooth functions. In comparing spectral methods to finite difference methods, Solecki [131] indicate that, particularly for problems with smooth solutions, spectral methods are computationally less expensive, they converge faster and are more accurate.

In this study, the spectral quasilinearization methods and the local linearization method are used to find solutions for unsteady boundary layer flow problems. These methods give better accuracy than do the finite element and finite differences methods. Motsa and Shateyi [132] used the successive linearization method to solve the equations describing an unsteady boundary layer flow.

In this study, the spectral quasilinearization methods and the local linearization method are used to find solutions for unsteady boundary layer flow problems. These methods give better accuracy compared to those from finite element and finite differences methods. Motsa and Shateyi [132] used the successive linearization method to solve the equations describing an unsteady boundary layer flow.

1.7.1   The spectral quasilinearization methods

The spectral quasilinearization method (SQLM) assumes a small difference between the approximation at the current iteration level and the approximation at the previous iteration. The SQLM was used by Motsa [130] to solve nonlinear partial differential equations (PDEs) describing unsteady boundary layer flow due to an impulsively stretching surface. The resulting sequence of equations was integrated using a Chebyshev spectral collocation method. In the SQLM the nonlinear terms are linearized using the quasilinearization method (QLM), developed by Bellman and Kalaba [133]. The SQLM has been described as being efficient with faster convergence than for numerical methods such as the Runge–Kutta methods. It gives accurate results with rapid convergence, according to Motsa et al. [134]. However, if a poor initial guess is chosen, the quasilinearization method performs poorly. In this thesis, the SQLM is used in Chapters 3 and 4.

The spectral quasilinearization method (SQLM) assumes a small difference between the approximation at the current iteration level and the approximation at the previous iteration. The SQLM was used by Motsa et al. [130] to solve nonlinear partial differential equations (PDEs) describing unsteady boundary layer flow due to an impulsively stretching surface. The resulting sequence of equations was integrated using a Chebyshev spectral collocation method. In the SQLM the nonlinear terms are linearised using the quasilinearisation method (QLM), developed by Bellman and Kalaba [133]. The SQLM has been described as being efficient with faster convergence compared to numerical methods such as the Runge–Kutta methods. It gives accurate results with rapid convergence, according to Motsa et al. [134]. However, if a poor initial guess is chosen, the quasilinearisation method performs poorly. In this thesis, the SQLM is used in Chapters 3 and 4.

1.7.2   The spectral local linearization method

The spectral local linearization method (SLLM) was developed by Motsa [130]. In principle the aim of the SLLM algorithm is to linearize and decouple the system of equations using the combination of a univariate linearization technique and spectral collocation discretization. It breaks down a large coupled system of equations into a sequence of smaller systems which can be solved iteratively in a computationally efficient manner using a Chebyshev pseudospectral method. Shateyi and Marewo [135] used the SLLM to solve equations that model an unsteady MHD flow and heat transfer in a boundary layer. Motsa et al. [136] used the spectral local linearization method to solve the equations that model natural convection in glass-fibre production processes. In this thesis, the SLLM is used to solve the nonlinear transport equations in Chapters 2 and 5.

1.7.3   The bivariate spectral local linearization methods

While the spectral local linearization method (SLLM) described in Section 1.7.2 is an efficient method for solving coupled systems of nonlinear ordinary differential equations that model boundary layer equations, the method has limitations. The SLLM is used to solve the system of ODEs, that is in space only. It may not be used to solve a system of PDEs in both space and time. This method was extended to a PDE system by Motsa [137], where he used the Chebyshev spectral collocation method to discretize the equations in one independent variable and still used finite differences for discretization in the second independent variable. However, as already noted, finite differences require very fine grids to give accurate solution. To eliminate the need for finite differences and so improve the convergence rate of the SLLM, Motsa [138] presented a new approach wherein spectral collocation is used independently in all independent variables of the PDE. The applied collocation method uses bivariate Lagrange interpolation polynomials as basis functions and so the method is termed the bivariate spectral local linearization method (BSLLM). The BSLLM converges fast and gives very accurate results, which are obtained in a computationally efficient manner. In this thesis, the BSLLM is used to solve PDEs in Chapter 6.

1.8   Aims and Objectives

The aim of this thesis is to study different mathematical models of non-Newtonian nanofluid flows under various boundary conditions and in different geometries. The question of interest concerns how the fluid physical parameters affect the boundary layer flow, heat and mass transfer in various non-Newtonian nanofluids.

In this study we are further interested in the solution methods for solving the underlying differential equations. The flow equations are solved numerically using the spectral local linearization, spectral quasilinearization and the bivariate spectral local linearization methods. Consequently, one of the objectives of this thesis is to test the accuracy, robustness and general validity of these methods. To show the accuracy of the numerical schemes, analysis of the residual errors is given for different physical parameter values. Detailed characterization and interpretation of the physical results is given. Further validation of the results comes from comparing them with existing results from literature.

The effect of several physical parameters on the fluid properties are given. We seek to study the impact of key physical parameters including Brownian motion, thermal radiation, and thermophoresis parameters on the flow velocity, temperature and concentration profiles and entropy generation.

1.9   Thesis structure

This thesis is organized as follows, in Chapter 2 the SLLM is used to solve the equations that model an unsteady MHD Maxwell nanofluid flow with convective and boundary conditions over a shrinking sheet. In Chapter 3, the SQLM is used to solve a system of nonlinear differential equations for power-law nanofluid flow over a horizontal surface embedded in a non-Darcy porous medium, with convective boundary condition. In Chapter 4, the SQLM is applied to a couple stress nanofluid flow in magneto-porous medium with thermal radiation and chemical reaction. In Chapter 5, the SLLM is used in the model that investigates the entropy generation in a second grade MHD nanofluid flow over a convectively heated stretching sheet with nonlinear thermal radiation and viscous dissipation. In Chapter 6, the BSLLM is applied to the unsteady MHD micropolar nanofluids with homogeneous-heterogeneous chemical reactions over a stretching surface. Finally, in Chapter 7 we present the overall thesis conclusions.

Chapter 2

An unsteady MHD Maxwell nanofluid flow with convective boundary conditions using spectral local linearization method

The focus of this chapter is on unsteady Maxwell flow of a nanofluid over a shrinking surface with both convective and slip boundary conditions. The model is nonlinear; it incorporates relaxation time and captures the salient features of visco-elastic behaviour. An evaluation is given of the impact and significance of Brownian motion and thermophoresis when the nanofluid particle volume fraction flux at the boundary is zero. The transformed equations are solved numerically using the spectral local linearization method (SLLM). An analysis of the residual errors is presented to show the accuracy and convergence of the SLLM.

Research Article

Hloniphile M. Sithole, Sabyasachi Mondal*, Precious Sibanda, and Sandile S. Motsa

An unsteady MHD Maxwell nanofluid flow with convective boundary conditions using spectral local linearization method

Abstract: The main focus of this study is on unsteady Maxwell nanofluid flow over a shrinking surface with convective and slip boundary conditions. The objective is to give an evaluation of the impact and significance of Brownian motion and thermophoresis when the nanofluid particle volume fraction flux at the boundary is zero. The transformed equations are solved numerically using the spectral local linearization method. We present an analysis of the residual errors to show the accuracy and convergence of the spectral local linearization method. We explore the effect of magnetic field and thermophoresis parameters on the heat transfer rate. We show, among other results, that an increase in particle Brownian motion leads to a decrease in the concentration profiles but concentration profiles increase with the increasing value of thermophoresis parameter

*Corresponding Author: Sabyasachi Mondal: Past address: School of Mathematics, Statistics and Computer Science, University of KwaZulu-Natal, Pietermaritzburg-3209, South Africa; Present address: Amity University, Kolkata-700135, West Bengal, India;
Email: sabya.mondal.2007@gmail.com
Hloniphile M. Sithole: School of Mathematics, Statistics and Computer Science, University of KwaZulu-Natal, Pietermaritzburg-3209, South Africa
Precious Sibanda: School of Mathematics, Statistics and Computer Science, University of KwaZulu-Natal, Pietermaritzburg-3209, South Africa
Sandile S. Motsa: School of Mathematics, Statistics and Computer Science, University of KwaZulu-Natal, Pietermaritzburg-3209, South Africa

1 Introduction

There have been only a few studies on Maxwell nanofluid flow for a shrinking sheet in the recent past. However, in general, research on non-Newtonian fluid flow has gained sizeable attention because of the multiplicity of its applications in the biomedical and chemical industries [1]. A non-Newtonian fluid is a fluid whose viscosity varies with the applied stress. The relation between the strain rate and the shear stress is nonlinear, and can be time-dependent [2]. The constitutive equations tend to be highly nonlinear and intricate in comparison with those of a Newtonian fluid. A Maxwell fluid is a viscoelastic material having the properties of elasticity and viscosity [3]. Unlike the Newtonian model, the upper convected Maxwell (UCM) model incorporates relaxation time.

The UCM model has been studied by many researchers, for example, Choi *et al.* [4] gave an analysis of incompressible steady two-dimensional UCM fluid flow in a porous channel. Their study included a consideration of inertia and fluid elasticity. Nandy [5] focused on the unsteady boundary layer flow of a Maxwell nanofluid over a permeable shrinking sheet with a Navier slip condition at the surface. The flow equations were solved using the shooting method. The homotopy analysis method was used by Rashidi *et al.* [6] to find solutions to the conservation equations for heat and mass transfer in a two-dimensional steady magnetohydrodynamic fluid flow in a porous medium [6]. Awais [7] investigated heat absorption and generation in steady flow over a surface stretched linearly in its own plane using the UCM fluid model. A nanofluid is defined as a fluid with suspended solid nanoparticles that are less than $100nm$ in size, and solid volume fraction less than 4%, [8]. Even at low nanoparticle volume concentration, nanofluids have been shown to have improved conductivity and thermal the performance compared to base fluids such as water and oil, [9].

The unsteady Maxwell fluid flow over a stretching surface subject to constructive/destructive chemical reaction was studied by Mukhopadhyay and Bhattacharyya [10].

They showed that for a constructive chemical reaction the concentration field increased but decreased for a destructive chemical reaction [10]. Also, in line with physical expectations, the concentration boundary-layer decreased for a destructive chemical reaction. Nandy *et al.* [11] studied forced convection in an unsteady nanofluid flow past a permeable shrinking sheet subject to heat loss due to thermal radiation. They explored the simultaneous impact of a magnetic field, thermal radiation, and unsteadiness on the heat transfer and flow properties of the fluid. Das *et al.* [12] presented simulated results for heat and mass transfer in an electrically conducting incompressible nanofluid flow near a heated stretching sheet with a convective boundary condition. The impact of an inclined magnetic field in the flow of a fluid with variable thermal conductivity was studied by Hayat et al. [13, 14]. An analysis of the significance of a heat source/ sink and temperature dependent thermal conductivity was given. Qasim and Hayat [15] investigated the impact of heat loss through thermal radiation in unsteady magnetohydrodynamic flow of a micropolar fluid. The influence of Joule heating and thermophoresis in a Maxwell fluid was studied in [16].

Som *et al.* [17] studied Ohmic dissipation and thermal radiation in flow over a stretching sheet embedded in a porous media. The results indicated that fluid injection causes a reduction in heat transfer whereas fluid suction raises the heat transfer coefficient. Hsiao [18] studied conjugate heat transfer with Ohmic dissipation in an incompressible Maxwell fluid close to a stagnation point. Mahapatra *et al.* [19] gave an analysis of stagnation point fluid flow over a stretching surface.

The purpose of this study is to investigate unsteady two-dimensional boundary-layer flow, heat and mass transfer in a Maxwell nanofluid flow over shrinking sheet with both slip and convective boundary conditions. The objective is to extend the study by Nandy [5] to include an evaluation of the impact and significance of thermophoresis and Brownian motion when the nanofluid particle volume fraction at the boundary is not actively controlled. The conservation equations are solved numerically using the spectral local linearization method, see Motsa [20, 21]. To show the accuracy of the numerical scheme, analysis of the residual errors is given for different physical parameter values. The effect of several physical parameters on the fluid properties are shown in tabular and graphical form. Comparison with published work for special cases shows an excellent agreement.

2 Problem formulations

An unsteady laminar boundary layer flow of an incompressible viscous Maxwell nanofluid over a shrinking surface in two dimensions is considered here. The shrinking sheet velocity is $u_w(x, t)$ while the mass transfer velocity is $v_w(x, t)$, t denotes time and x is measured along the sheet. Using the nanofluid model proposed by Buongiorno [22], the conservation equations for mass, momentum, thermal energy and nanoparticles for a Maxwell fluid are:

$$\frac{\partial u}{\partial x} + \frac{\partial v}{\partial y} = 0, \tag{1}$$

$$\frac{\partial u}{\partial t} + u\frac{\partial u}{\partial x} + v\frac{\partial u}{\partial y} = \nu\frac{\partial^2 u}{\partial y^2} - k_0\left(u^2\frac{\partial^2 u}{\partial x^2}\right. \tag{2}$$
$$\left. + 2uv\frac{\partial^2 u}{\partial x \partial y} + v^2\frac{\partial^2 u}{\partial y^2}\right)$$
$$- \frac{\sigma B^2}{\rho_f}\left(u - kv\frac{\partial u}{\partial y}\right),$$

$$\frac{\partial T}{\partial t} + v\frac{\partial T}{\partial y} + u\frac{\partial T}{\partial x} = \alpha\frac{\partial^2 T}{\partial y^2} \tag{3}$$
$$+ \frac{1}{\rho_f c_p}\frac{\partial}{\partial y}\left[\kappa(T)\frac{\partial T}{\partial y}\right]$$
$$+ \frac{\mu}{\rho_f c_p}\left(\frac{\partial u}{\partial y}\right)^2 + \frac{\sigma}{\rho_f c_p}(uB_0 - E_0)^2 + \frac{Q_0}{\rho_f c_p}(T - T_\infty)$$
$$+ \left[\tau D_B\frac{\partial C}{\partial y}\frac{\partial T}{\partial y} + \frac{\tau D_T}{T_\infty}\left(\frac{\partial T}{\partial y}\right)^2\right] + \frac{D_m k_0}{c_s c_p}\frac{\partial^2 C}{\partial y^2}$$
$$- \frac{1}{\rho_f c_p}\frac{\partial q_r}{\partial y},$$

$$\frac{\partial C}{\partial t} + v\frac{\partial C}{\partial y} + u\frac{\partial C}{\partial x} = D_B\frac{\partial^2 C}{\partial y^2} + \frac{D_T}{T_\infty}\frac{\partial^2 T}{\partial y^2} \tag{4}$$
$$+ \frac{D_m k_0}{T_m}\frac{\partial^2 T}{\partial y^2} - k_1(C - C_\infty),$$

where u is the velocity component in the x- direction and v is the velocity component in the y-direction. The kinematic viscosity is ν, the relaxation time of the UCM fluid is k_0, the thermal diffusivity is α, the variable thermal conductivity is $\kappa(T)$ and the chemical reaction parameter is k_1. The Brownian diffusion coefficient is D_B, while the thermophoresis diffusion coefficients is D_T. Here, τ is the effective heat capacity of the nanoparticle material divided by the heat capacity of the ordinary fluid, T is the fluid temperature and C is the nanoparticle volume fraction. The temperature and the nanoparticle concentration at the wall are T_w and C_w, respectively, and T_∞ and C_∞ denote the ambient temperature and concentration respectively.

The velocity slip is proportional to the local shear stress. These equations are subject to the boundary conditions:

$$u = u_w(x, t) + u_{slip}(x, t), \ v = v_w(x, t), \tag{5}$$

$$-k_0\sqrt{1 - \lambda t}\frac{\partial T}{\partial y} = h_f(T_w - T),$$

$$D_B\frac{\partial C}{\partial y} + \frac{D_B}{T_\infty}\frac{\partial T}{\partial y} = 0 \text{ at } y = 0,$$

$$u \to 0, \ T \to T_\infty, \ \frac{\partial u}{\partial y} \to 0, \ C \to C_\infty \text{ as } y \to \infty,$$

where $k_0 = k(1 - \lambda t)$, $u_w(x, t) = -ax(1 - \lambda t)^{-1}$, $u_{slip}(x, t) = \nu N_1 \partial u / \partial y$, $N_1 = N\sqrt{1 - \lambda t}$ is the slip velocity , λ is the unsteadiness parameter and $k_0(> 0)$, $a(> 0)$ are positive constants. This assumption is to allow for the possibility of a similarity solution. We introduce the similarity variables:

$$\eta = y\sqrt{\frac{a}{\nu(1 - \lambda t)}}, \quad \psi = \sqrt{\frac{a\nu}{1 - \lambda t}}xf(\eta), \tag{6}$$

$$T(x, t) = T_\infty + \theta(\eta)(T_w - T_\infty),$$

$$C(x, t) = C_\infty + \phi(\eta)(C_w - C_\infty),$$

where ψ is the stream function, defined by $v = -\partial\psi/\partial x$ and $u = \partial\psi/\partial y$. Equations (1) - (4) are transformed to

$$f''' - f'^2 + ff'' - A\left(\frac{\eta}{2}f'' + f'\right) \tag{7}$$

$$- \beta\left(f^2 f''' - 2ff'f''\right) - M^2 f' - M^2\beta ff'' = 0,$$

$$\frac{1}{Pr_{eff}}\theta'' + \frac{1}{Pr}\left[\theta''(1 + \varepsilon\theta) + \varepsilon\theta'^2\right] + E_c f''^2 \tag{8}$$

$$+ E_c M^2 (f' - E_1)^2 + \left(f - A\frac{\eta}{2}\right)\theta'$$

$$+ D_f\phi'' + He\theta + Nt\theta'^2 + Nb\theta'\phi' = 0,$$

$$\phi'' + Sc\left(f - A\frac{\eta}{2}\right)\phi' + \frac{Nt}{Nb}\theta'' - \gamma Sc\phi + \frac{Nt}{Nb}\theta'' \tag{9}$$

$$+ Sc Sr\theta'' = 0,$$

where the prime denotes derivatives with respect to η. The boundary conditions are

$$f'(0) = -1 + \delta f''(0), f(0) = s, f''(\infty) = 0, f'(\infty) = 0, \tag{10}$$

$$\theta'(0) = -B_i(-\theta(0) + 1), \theta(\infty) = 0,$$

$$Nb\phi'(0) + Nt\theta'(0) = 0, \phi(\infty) = 0,$$

where the parameter $\delta = N\sqrt{av}$ is the non-dimensional velocity slip and $v_w(0, t)$ is the wall mass transfer velocity given by

$$v_w(0, y) = \frac{v_0}{\sqrt{1 - \lambda t}},$$

where v_0 is the constant mass flux velocity. Thus

$$s = -\frac{v_0}{av} = f(0).$$

where wall mass suction occurs when $s > 0$ while wall mass injection occurs when $s < 0$. The non-dimensional parameters in the above equations are the Maxwell parameter $\beta (= k_0 a)$, the unsteadiness parameter $A (= \lambda/a)$, the magnetic field parameter $M \left(= \sqrt{\sigma B_0^2/\rho_f a}\right)$, $He \left(= Q_0/\rho_f c_p\right)$ the heat generation parameter and $Q(= Q_0(1 - \lambda t))$, $Nb \left(= \tau D_B(C_w - C_\infty)/\nu\right)$ is the Brownian motion parameter and $Nt \left(= \tau D_T(T_w - T_\infty)/\nu T_\infty\right)$ is the thermophoresis parameter. The Prandtl number is $Pr (= \nu/\alpha)$, the Schmidt number is $Sc \left(= \nu/D_B\right)$, $Pr_{eff} \left(= Pr/(1 + \frac{4}{3}R)\right)$ is the effective Prandtl number, $B_i \left(= h_f/k_0\sqrt{\frac{\nu}{a}}\right)$ is the Biot number, $\gamma = k_1(C_w - C_\infty)$ is the reaction parameter where $\gamma < 0$ denotes a destructive reaction, $\gamma = 0$ indicates that there is no reaction and $\gamma > 0$ denotes a generative reaction.

Other important physical parameters are the variable thermal conductivity $\kappa(T)$, the Eckert number E_c, the local electromagnetic parameter E_1, the Soret number S_r, the Dufour number D_f and the radiation parameter R. These are defined as

$$\kappa(T) = K_\infty\left(1 + \varepsilon\frac{T - T_\infty}{\Delta T}\right), E_c = \left(\frac{x^2 a^2}{c_p\Delta T(1 - \lambda t)}\right), \tag{11}$$

$$E_1 = \left(\frac{E_0(1 - \lambda t)}{aB_o x}\right),$$

$$S_r = \left(\frac{D_m k_0\Delta T}{T_m\nu\Delta C}\right), D_f = \left(\frac{D_m k_0\Delta C}{c_s c_p\Delta T}\right), \tag{12}$$

$$R = \frac{4\sigma_1 T_\infty^3}{K_1\rho_f c_p\alpha_m},$$

where ε is a small parameter, $\Delta T = T_w - T_\infty$ and the thermal conductivity parameter is K_∞. The important flow attributes, the Nusselt number Nu_x and skin friction coefficient C_f are described by

$$C_f = \frac{\tau_w}{\rho u_w^2(x)}, \quad Nu_x = \frac{xq_w}{k(T_f - T_\infty)}. \tag{13}$$

Here q_w and τ_w are the plate heat flux and the skin friction respectively, defined as

$$q_w = -k\left(\frac{\partial T}{\partial y}\right)_{y=0}, \tau_w = \mu\left(\frac{\partial u}{\partial y}\right)_{y=0}, \tag{14}$$

where μ is the coefficient of viscosity. Equations (13) may be written as

$$Re_x^{\frac{1}{2}}C_f = f''(0), \tag{15}$$

$$Re_x^{-\frac{1}{2}}Nu_x = -\theta'(0), \tag{16}$$

where $Re_x = \frac{u_w(x)x}{\nu}$ is the local Reynolds number. Here, the Sherwood number is zero, due to the assumption of zero mass flux at the surface.

3 Method of solution

The transport equations have been solved using the iterative spectral local linearization method (SLLM), see Motsa [20]. In principle of the SLLM algorithm is to linearize and decouple the system of equations. Motsa *et al.* [21] used the spectral local linearization method to solve the equations that model natural convection in glass-fibre production processes. Shateyi and Marewo [23] used the SLLM to solve equations that models an unsteady MHD flow and heat transfer. Nonetheless, this method has only been used in a limited number of studies, hence its general validation in complex systems remains to be made. For the interested reader, the SLLM algorithm is described in [20].

The differential equations arising from the linearization procedure are solved using a Chebyshev pseudo spectral method. The domain of the problem is transformed to the interval $[-1, 1]$ using the transformation $(b - a)(\tau + 1)/2$. The differentiation matrix D is used to approximate the derivatives $Z_i(\eta)$ of the unknown variables to the matrix vector product,

$$\frac{dZ_i}{d\eta} = \sum_{k=0}^{\bar{N}} D_{lk} Z_i(\tau_k) = DZ_i, \quad l = 0, 1, \ldots, \bar{N}, \quad (17)$$

where the vector function at the collocation points is given by $Z = [z(\tau_0), z(\tau_1), \ldots, z(\tau_N)]^T$, $D = 2D/(b-a)$ with $\bar{N}+1$ collocation points, [20] and

$$Z_j^{(p)} = D^p Z_j. \quad (18)$$

where the superscript in D denotes higher order derivatives.

SLLM Algorithm

The differential equations (7) - (9) may collectively be stated as,

$$\omega_k[F, T, H] = 0, \quad \text{for} \quad k = 1, 2, 3 \quad (19)$$

where ω_1, ω_2 and ω_3 are non-linear operators and F, H, T are given by

$$F = \left\{ f, \frac{\partial f}{\partial \eta}, \frac{\partial^2 f}{\partial \eta^2}, \frac{\partial^3 f}{\partial \eta^3} \right\}, \quad (20)$$

$$T = \left\{ \theta, \frac{\partial \theta}{\partial \eta}, \frac{\partial^2 \theta}{\partial \eta^2} \right\}, \quad (21)$$

$$H = \left\{ \phi, \frac{\partial \phi}{\partial \eta}, \frac{\partial^2 \phi}{\partial \eta^2} \right\}. \quad (22)$$

The system of equations (19) can be simplified and decoupled by linearizing the nonlinear terms. The Chebychev

pseudo-spectral collocation method is utilized to integrate the decoupled system. The simple algorithm is as follows:

1. From the first equation, find F while treating H and T as known functions from initial guesses. This gives F_{r+1}
2. Solve for T in the second equation while treating F and H as known functions, T is known from 1 above and H is known from the initial guess. This gives T_{r+1}
3. Finally, solve for H in the last equation while treating F and T as known functions, T and H are known from 1 and 2 above. We obtain T_{r+1}.
4. Repeat steps 1-3 to find the next iterative solutions.

Using these ideas the nonlinear system of equations (7) - (9) are written as:

$$a_{1,r} f'''_{r+1} + a_{2,r} f''_{r+1} + a_{3,r} f'_{r+1} \quad (23)$$
$$+ a_{4,r} f_{r+1} = a_{5,r},$$
$$b_{1,r} \theta''_{r+1} + b_{2,r} \theta'_{r+1} + b_{3,r} \theta_{r+1} = b_{4,r},$$
$$c_{1,r} \phi''_{r+1} + c_{2,r} \phi'_{r+1} + c_{3,r} \phi_{r+1} = c_{4,r},$$

subject to boundary conditions:

$$f_{r+1}(0) = s, f'_{r+1}(0) \quad (24)$$
$$= -1 + \delta f''_{r+1}(0), f''_{r+1}(\infty) = 0,$$
$$f'_{r+1}(\infty) = 0,$$
$$\theta'_{r+1}(0) = -B_i(1 - \theta_{r+1}(0)), \ \theta_{r+1}(\infty) = 0,$$
$$Nb\phi'_{r+1}(0) + Nt\theta'_{r+1}(0) = 0, \ \phi_{r+1}(\infty) = 0.$$

where

$$a_{1,r} = 1 - \beta f_r^2, a_{2,r} \quad (25)$$
$$= f_r + 2\beta f_r f'_r - A\frac{\eta}{2} - M^2 \beta f_r,$$
$$a_{3,r} = 2\beta f_r f''_r - 2f'_r - A - M^2,$$
$$a_{4,r} = f''_r - 2\beta f_r f'''_r + 2\beta f'_r f''_r - M^2 \beta f''_r,$$
$$a_{5,r} = f_r f''_r - f'^2_r - 2\beta f_r^2 f'''_r + 4\beta f_r f'_r f''_r$$
$$- M^2 \beta f_r f''_r,$$

$$b_{1,r} = \frac{\epsilon}{Pr}\theta_r + \frac{1}{Pr_{eff}} + \frac{1}{Pr}, \quad (26)$$
$$b_{2,r} = \frac{2\epsilon}{Pr}\theta'_r + f_r + Nb\phi'_r + 2Nt\theta'_r - A\frac{\eta}{2},$$
$$b_{3,r} = \frac{\epsilon}{Pr}\theta''_r, b_{4,r} = He, b_{5,r} = \frac{\epsilon}{Pr}\theta''_r \theta_r + \frac{\epsilon}{Pr}\theta'^2_r$$
$$- Ecf''_r - EcM^2 \left(f'_r - E_1\right)^2 - D_f\phi'_r - Nt\theta'^2_r,$$
$$c_{1,r} = Scf_r - ScA\frac{\eta}{2}, c_{2,r} = -\gamma Sc,$$
$$c_{3,r} = -ScS_r\theta''_r - \frac{Nt}{Nb}\theta''_r.$$

Table 1: Comparison of the skin friction coefficient and Nusselt number between the results of present study and reported by Hayat *et al.* [24] when $\beta = 0.2$, $\alpha = 0.3$, $Pr = 1$, $s = 0.5$ and the other parameters are set to zero

Iterations	[24] $-f''(0)$	Current study $-f''(0)$	[24] $-\theta'(0)$	Current study $-\theta'(0)$
1	0.2829900	0.28139017	0.4300000	0.40401296
2	-	0.28149501	-	0.40465707
3	-	0.28149504	-	0.40465726
4	-	0.28149505	-	0.40465726
5	0.2814982	0.28149505	0.4064811	0.40465726
6	-	0.28149505	-	0.40465726
7	-	0.28149505	-	0.40465726
8	-	0.28149505	-	0.40465726
9	-	0.28149505	-	0.40465726
10	0.2814950	0.28149505	0.4047923	0.40465726
20	0.2814950	0.28149505	0.4046587	0.40465726
35	0.2814950	0.28149505	0.4046572	0.40465726
40	0.2814950	0.28149505	0.4046572	0.40465726

The following decoupled matrix system of equations is obtained:

$$\mathbf{A}_1 \mathbf{F}_{r+1} = \mathbf{B}_1 \quad (27)$$
$$\mathbf{A}_2 \mathbf{T}_{r+1} = \mathbf{B}_2$$
$$\mathbf{A}_3 \mathbf{H}_{r+1} = \mathbf{B}_3$$

with corresponding boundary conditions

$$f_{r+1}(\tau_N) = s, f'_{r+1}(\tau_N) = -1 + \delta f''_{r+1}(\tau_N), \quad (28)$$
$$f''_{r+1}(\tau_0) = 0, f'_{r+1}(\tau_0) = 0,$$
$$\theta'_{r+1}(\tau_N) = -B_i(1 - \theta_{r+1}(\tau_N)), \theta_{r+1}(\tau_0) = 0,$$
$$Nb\phi'_{r+1}(\tau_N) + Nt\theta'_{r+1}(\tau_N) = 0, \phi_{r+1}(\tau_0) = 0.$$

where

$$\mathbf{A}_1 = \mathbf{diag}\,[\mathbf{a}_{1,r}]\,\mathbf{D}^3 + \mathbf{diag}\,[\mathbf{a}_{2,r}]\,\mathbf{D}^2 \quad (29)$$
$$+ \mathbf{diag}\,[\mathbf{a}_{3,r}]\,\mathbf{D} + \mathbf{diag}\,[\mathbf{a}_{4,r}]\,, \mathbf{A}_1 = \mathbf{a}_{5,r}$$
$$\mathbf{A}_2 = \mathbf{diag}\,[\mathbf{b}_{1,r}]\,\mathbf{D}^2 + \mathbf{diag}\,[\mathbf{b}_{2,r}]\,\mathbf{D} + \mathbf{diag}\,[\mathbf{b}_{3,r}]$$
$$+ \mathbf{b}_{4,r}\mathbf{I}, \mathbf{A}_2 = \mathbf{c}_{5,r}$$
$$\mathbf{A}_3 = \mathbf{D}^2 + \mathbf{diag}\,[\mathbf{c}_{1,r}]\,\mathbf{D} + \mathbf{c}_{2,r}\mathbf{I}, \quad \mathbf{A}_3 = \mathbf{c}_{3,r}.$$

I is an identity matrix with $(\bar{N} + 1)$ rows and columns, **F**, **H** and **T** are approximate values of f, ϕ and θ calculated at the collocation points. Initial approximations are required to start the iteration process, and these can be selected so as to satisfy the boundary conditions and known flow configuration. For our system, the following guesses were used as suitable initial approximations,

$$f_0(\eta) = \frac{\alpha}{1+\delta}(-e^{-\eta} + 1) + s, g_0(\eta) \quad (30)$$
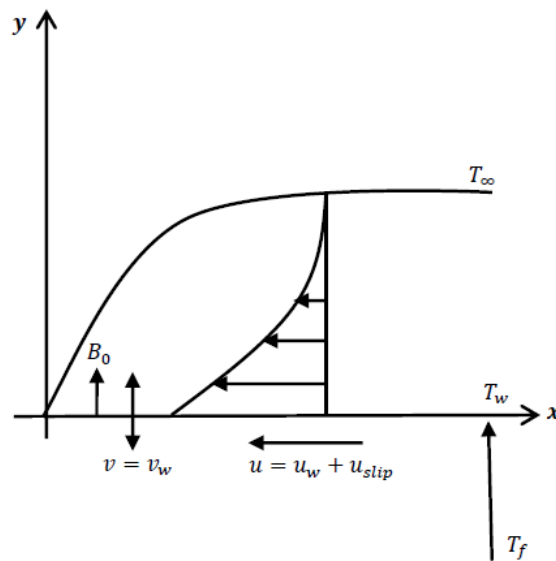
Figure 1: Flow geometry of the problem

$$= \frac{B_i}{1 + B_i}e^{-\eta},$$
$$\theta_0(\eta) = \frac{N_t B_i}{N_b(1 + B_i)}e^{-\eta}.$$

The boundary conditions are inserted in the matrices in (27) and the approximate solutions at each iteration level are obtained by solving (27).
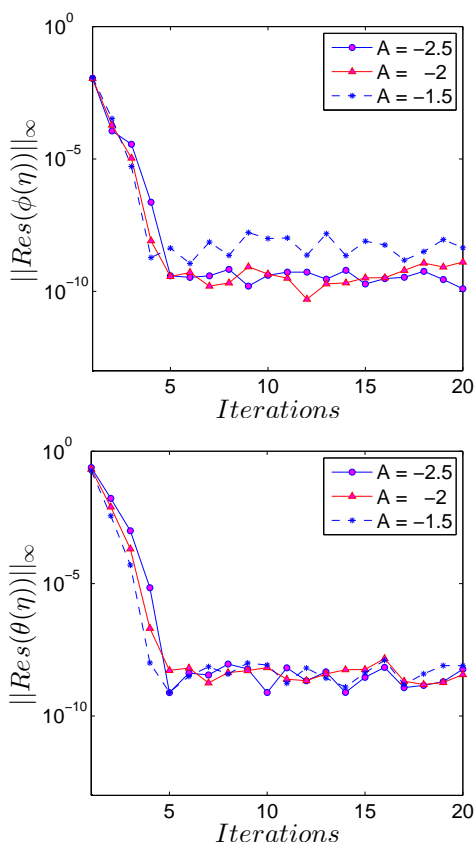
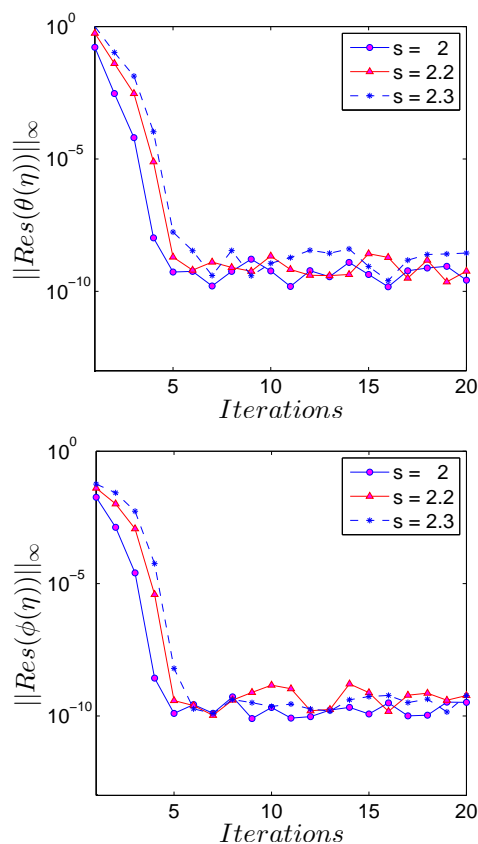**Figure 2:** Residual errors for θ and ϕ when $A = -2.5, -2.0, -1.5$

Figure 3: Residual errors for θ and ϕ when $s = 2, 2.2, 2.3$

Table 2: Computed values of the Nusselt number for different values of Nb, M and Nt

Nb	M	Nt	$|-\theta'(0)|$
0.2			0.06758610
0.4	0.3	0.1	0.06758600
0.8			0.06758579
	0.1		0.09046540
0.2	0.3	0.1	0.08959087
	0.5		0.08728149
		0.05	0.08031901
0.2	0.3	0.07	0.08434208
		0.10	0.09125982

4 Results and discussion

The solutions of the differential equations are given Tables 1 - 2 and Figures 2 - 16. In Table 1 we establish the reliability of the numerical scheme by a comparative analysis of the skin friction coefficient C_f and Nusselt number Nu_x with results reported by Hayat et al. [24] when $\beta = 0.2$, $\alpha = 0.3$, $Pr = 1$ and $s = 0.5$. The other parameters have been set to zero. A good agreement is observed with the previously published work. To gain further insights as to the accuracy and convergence of the method used in this study, we have calculated residual errors as shown in Figures 2 to 4. These are calculated for different values of A, s and β. In general, the solutions have converged with an absolute residual error $||Res|| \approx 10^{-11}$ after five iterations. These results sufficiently demonstrate to the accuracy and convergence of the SLLM.

The numerical computations have been done when $A = -1.0$, $s = 2$, $\delta = 0.25$, $Nb = Nt = 0.1$, $Sc = 0.8$, $Pr = 1.0$, $M = 0.3$, $\varepsilon = 0.1$, $E_c = 0.1$, $E_1 = 1.0$, $D_f = 0.1$, $He = 0.5$, $Sr = 0.1$, $Pr_{eff} = 1.0$, $\gamma = 0.1$, and $Bi = 0.1$. For numerical simulations, the parameter values are chosen from the previous literature on nanofluid flow such as [5, 10, 12, 16, 24] etc. Table 2 shows the Nusselt number for different Nb, M and Nt, the other parameters as stated above. The results show that Nu_x decreases with increas-
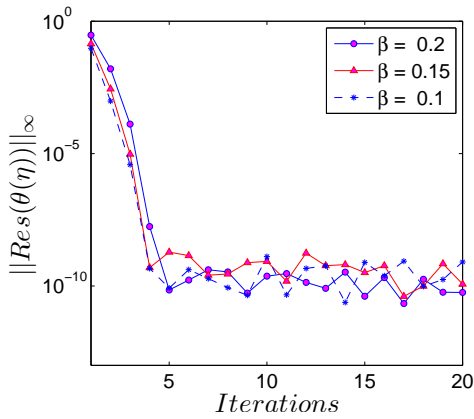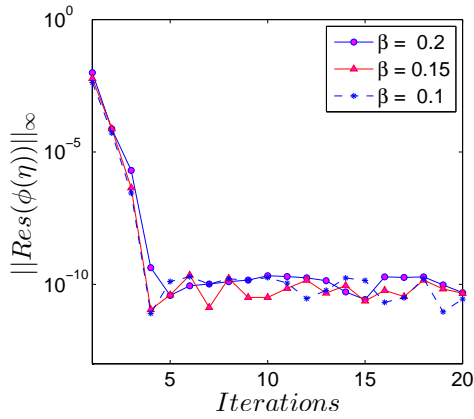
Figure 4: Residual errors for θ and ϕ when $\beta = 0.1, 0.15, 0.2$

Figure 6: Effect of A on the velocity profile $f'(\eta)$

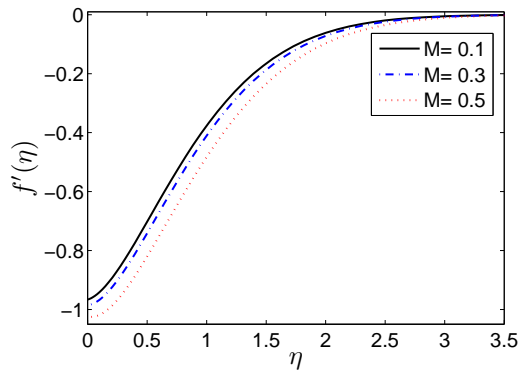**Figure 7:** Effect of β on the velocity profile $f'(\eta)$

Figure 5: Effect of magnetic field parameter M on the velocity profile $f'(\eta)$

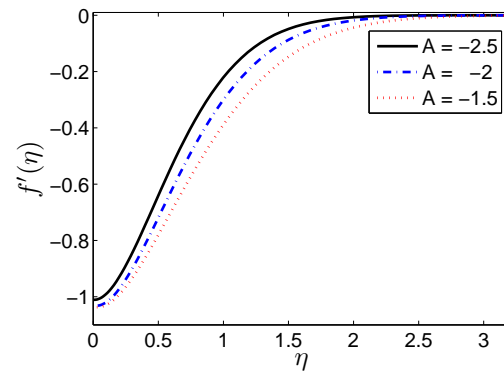ing Nb and M whereas the opposite is observed for increasing values of Nt.
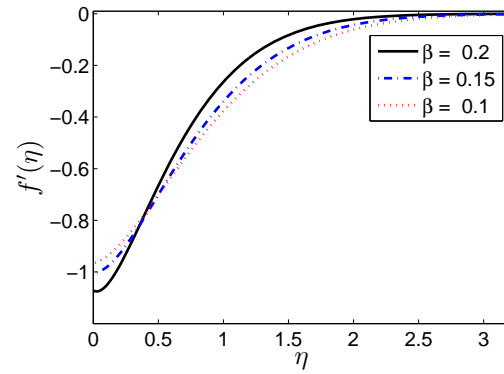
Figure 5 shows that the velocity reduces with increasing magnetic field strength. This is an indication of an increase in the Lorentz force that creates a resistance to the fluid flow near the boundary slowing down the fluid motion. Figure 6 shows that the boundary layer thickness increases as the unsteadiness parameter increases. The velocity profiles decrease with increasing value of A.

Figure 7 shows that as β increases, the boundary layer thickness increases with a cross-over of profiles near the surface. The physical interpretation of this behavior is that an increase in β reduces the fluid in the flow leading to the boundary layer thickness increasing near the surface but a contrary trend is recognized away from the surface.

Figure 8 shows a reduction in the velocity with an increase in the mass suction parameter s. Figure 9 demonstrates the effect of A on the temperature profile. An increase in unsteadiness causes an increase in the solute concentration. Figure 10 shows how the temperature pro-
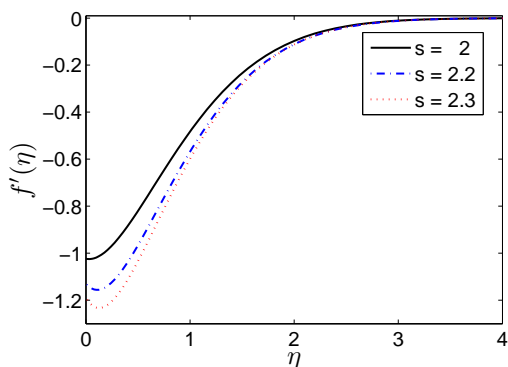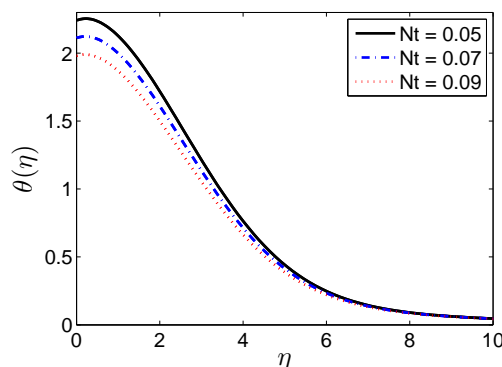
Figure 8: Effect of s on the velocity profile $f'(\eta)$

Figure 9: Effect of A on the temperature profile $\theta(\eta)$

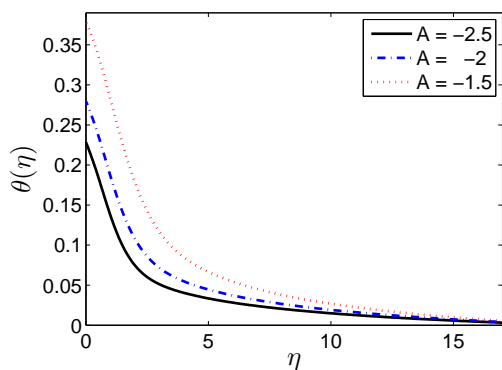**Figure 10:** Effect of β on the temperature profile $\theta(\eta)$
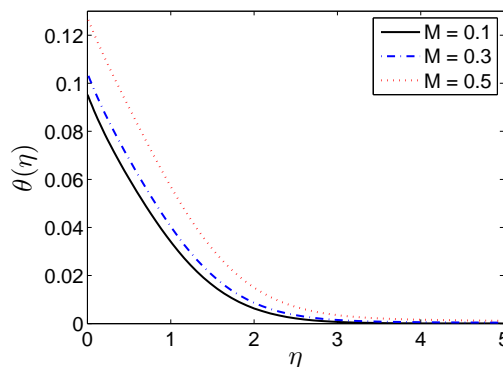

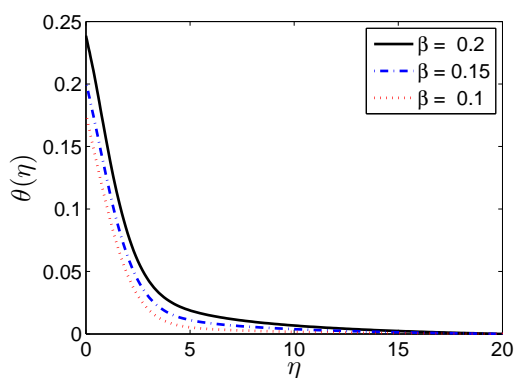**Figure 11:** Effect of Nt on the temperature profile $\theta(\eta)$

Figure 12: Effect of M on the temperature profile $\theta(\eta)$

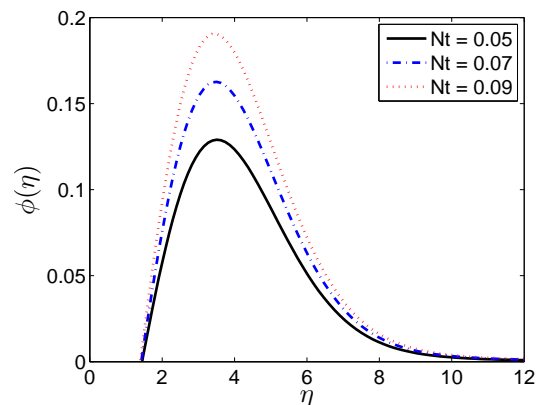files change with respect to variations in the Maxwell parameter β. The temperature profiles increase with increasing β values. This is to be expected since higher Maxwell parameters generally suggest a more solid material able to conduct and retain heat better.

Figure 11 shows the change in temperature profiles with respect to variations in the thermophoresis parameter values. As thermophoresis increases, the temperature profiles decrease near the surface. Figure 12 shows the effect of the magnetic field parameter on $\theta(\eta)$ the temperature profiles. We observe that the temperature profiles increase with increasing values of the magnetic field parameter. The existence of a magnetic field in an electrically conducting fluid produces a body force that decelerates the fluid flow which in turn has the effect of retaining more heat within the boundary layer.
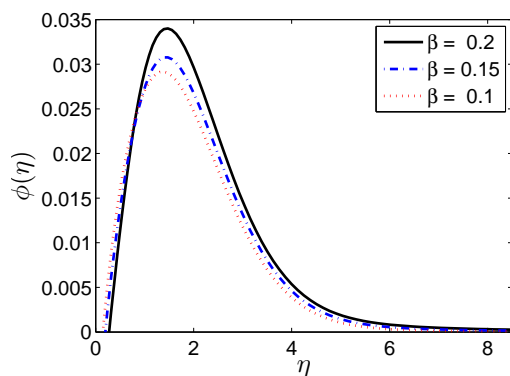
The impact of the unsteadiness parameter, Maxwell parameter, Brownian motion parameter, thermophoresis parameter and the Schmidt number on the concentration profiles is depicted in Figures 13 - 16. In Figures 13 and 14
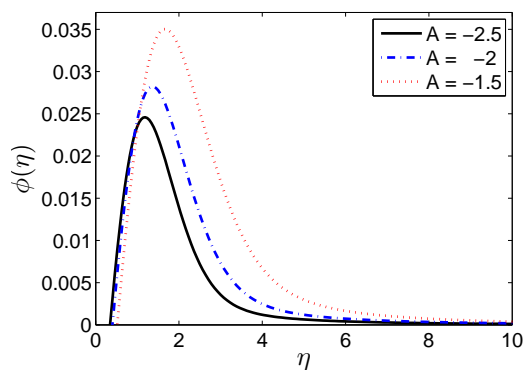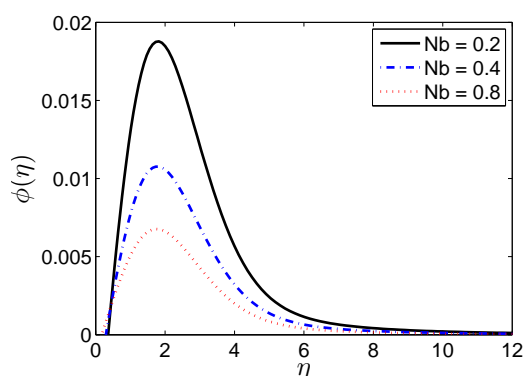
Figure 13: Effect of unsteadiness parameter A on the concentration profile $\phi(\eta)$

Figure 14: Effect of β on the concentration profile $\phi(\eta)$

Figure 15: Effect of Nb on the concentration profile $\phi(\eta)$

Figure 16: Effect of Nt on the concentration profile $\phi(\eta)$

an increase in the unsteadiness parameter and Maxwell parameter causes an increase in the concentration profiles near the surface but the opposite movement is observed far from the surface. Figure 15 shows the impact that the Brownian motion parameter has on the concentration profiles. An increase in the Brownian motion parameter causes a decrease in the concentration profiles. The Brownian motion tends to intensify particle displacement away from the fluid flow regime onto the surface; this phenomenon accounts for a decrease in the concentration of the nanoparticles far from the surface, thus resulting in a decrease in the nanoparticle concentration boundary layer thickness.

Figure 16 depicts the effect of the thermophoresis parameter on the concentration profiles. Thermophoresis is associated with the movement of nanoparticles from a hot to a cold wall, and since it is generated by temperature gradients, this creates a fast flow away from the moving surface. Consequently more fluid is heated away from the surface leading to an increase in the temperature within the thermal boundary layer.

5 Conclusion

In this study, we have investigated unsteady Maxwell nanofluid flow over a shrinking sheet with convective and slip boundary conditions. The conservation equations were solved using an iterative spectral local linearization method. We have given an error analysis to establish the accuracy and convergence of the method. The impact and significance of various physical parameters on the fluid properties has been demonstrated both qualitatively and

quantitatively. The findings can be briefly outlined as follows;

1. The concentration and velocity profiles decrease whereas the temperature profile increases with increasing unsteadiness parameter.
2. Increasing particle Brownian motion leads to a reduction in the concentration profiles but concentration profiles increase with increasing thermophoresis.
3. In terms of heat transfer coefficients, increasing value of particle Brownian motion and magnetic field strength reduces the heat transfer coefficient but the opposite is observed in the case of increased thermophoresis parameter.

Conflict of Interests: The authors declare that there is no conflict of interests regarding the publication of this article.

References

[1] Mushtaq A., Abbasbandy S., Mustafa M., Hayat T., Alsaedi A., et al., Numerical solution for Sakiadis flow of upper-convected Maxwell fluid using Cattaneo-Christov heat flux model, AIP Adv., 2016, 6, 015208.

[2] Sochi T., Flow of non-Newtonian fluids in porous media, J. Polym. Sci. B Polym. Phys., 2010, 48,2437–2767.

[3] Gallegos C., Martínez-Boza F.J., Linear viscoelasticity. Rheology: encyclopedia of life support systems (EOLSS), UNESCO, Eolss, Oxford, 2010, 120–143.

[4] Choi J.J., Rusak Z., Tichy J.A., et al., Maxwell fluid suction flow in a channel, J. Non-Newtonian Fluid Mech., 1999, 85, 165–187.

[5] Nandy S.K., Unsteady flow of Maxwell fluid in the presence of nanoparticles toward a permeable shrinking surface with Navier slip, J. Taiwan Inst. Chem. Eng., 2015, 52, 22–30.

[6] Rashidi M.M., Rostami B., Freidoonimehr N., Abbasbandy S., et al., Free convective heat and mass transfer for MHD fluid flow over a permeable vertical stretching sheet in the presence of the radiation and buoyancy effects, Ain Shams Eng. J., 2014, 5, 901–912.

[7] Awais M., Hayat T., Irum S., Alsaedi A., et al., Heat generation/absorption effects in a boundary layer stretched flow of Maxwell nano fluid: Analytic and numeric solutions, PloS one, 2015, 10, e0129814.

[8] Choi S.U.S., Eastman J.A., Enhancing thermal conductivity of fluids with nanoparticles, ASME, International Mechanical Engineering Congress and Exposition, San Francisco, CA, November 12-17, 1995.

[9] Yu W., France D.M., Routbort J.L., Choi S.U.S., et al., Review and comparison of nano fluid thermal conductivity and heat transfer enhancements, Heat Transfer Eng. 2008, 29, 432–460.

[10] Mukhopadhyay S., Bhattacharyya K., Unsteady flow of a Maxwell fluid over a stretching surface in presence of chemical reaction, J. Egyptian Math. Soc., 2012, 20, 229–234.

[11] Nandy S.K., Sidui S., Mahapatra T.R., et al., Unsteady MHD boundary layer flow and heat transfer of nano fluid over a permeable shrinking sheet in the presence of thermal radiation, Alex. Eng. J., 2014, 53, 929–937.

[12] Das K., Duari P.R., Kundu P.K., et al., Numerical simulation of nano fluid flow with convective boundary condition, J. Egyptian Math. Soc., 2015, 23, 435–439.

[13] Hayat T., Shafiq A., Alsaedi A., Asghar S., et al., Effect of inclined magnetic field in flow of third grade fluid with variable thermal conductivity, AIP Adv., 2015, 5, 087108.

[14] Hayat T., Shehzad S.A., Qasim M., Alsaedi A., et al., Mixed convection flow by a porous sheet with variable thermal conductivity and convective boundary condition, Braz. J. Chem. Eng., 2014, 31, 109–117.

[15] Hayat T., Qasim M., Effects of thermal radiation on unsteady magneto hydrodynamic flow of a micropolar fluid with heat and mass transfer, Z. Naturforsch. A, 2010, 65, 950–960.

[16] Hayat T., Qasim M., Influence of thermal radiation and Joule heating on MHD flow of a Maxwell fluid in the presence of thermo phoresis,Int. J. Heat Mass Trans., 2010, 53, 4780–4788.

[17] Som N.M., Md Arifin N., Md Ali F., Nazar R., et al., Non-darcy flow and heat transfer over a permeable stretching sheet embedded in a porous media with thermal radiation and Ohmic dissipation, Int. J. Theor. Appl. Mech., 2016, 1, 13–18.

[18] Hsiao K.L., Conjugate heat transfer for mixed convection and Maxwell fluid on a stagnation point, Arab. J. Sci. Eng.,2014, 39, 4325–4332.

[19] Mahapatra, T.R., Mondal S., Pal D., et al., Heat transfer due to magneto hydrodynamic stagnation-point flow of a power-law fluid towards a stretching surface in the presence of thermal radiation and suction/injection, ISRN Thermodynamics, 2012, 2012, 1–9.

[20] Motsa S.S., A new spectral local linearization method for nonlinear boundary layer flow problems, J. Appl. Math., 2013, 2013, 1–15.

[21] Motsa S.S., Makukula Z.G., Shateyi S., et al., Spectral local linearisation approach for natural convection boundary layer flow, Math. Prob. Eng., 2013, 2013, 1–7.

[22] Buongiorno J., Convective transport in nano fluids, J. Heat Trans., 2006,128, 240–250.

[23] Shateyi S., Marewo G.T., On a new numerical analysis of the hall effect on MHD flow and heat transfer over an unsteady stretching permeable surface in the presence of thermal radiation and heat source/sink, Boundary Value Prob., 2014, 2014, 1–17.

[24] Hayat T., Shehzad S.A., Qasim M., Obaidat S., et al., Steady flow of Maxwell fluid with convective boundary conditions, Z. Naturforsch. A, 2011, 66, 417–422.

Chapter 3

Non-Darcian nanofluid flow over a horizontal surface embedded in a porous medium

1

   In Chapter 2, we studied the upper convected Maxwell (UCM) non-Newtonian model that incorporates relaxation time. The limitation of the UCM model is that it do not allow for strain dependency and second normal stress difference. To address these limitations, in this chapter the focus is on a complex power-law non-Newtonian nanofluid flow. The complexity of the equations is due to the power terms that arise in the power law model. For this model, the boundary layer nanofluid flow over a horizontal plate embedded in a non-Darcy porous medium is investigated. The nanofluid model incorporates the effects of Brownian motion and thermophoresis, and a mixed convective boundary condition is employed at the surface. The spectral quasilinearization method is used to solve the conservation equations. The impact of specific parameters on the flow behaviour and heat transfer characteristics is discussed.

---

[1] The work in this chapter has been submitted to International Journal of Ambient Energy

Non-Darcian nanofluid flow over a horizontal surface embedded in a porous medium

H. Sithole[a,*], H.Mondal[a], Peri.K. Kameswaran[b], S. Shaw[c], P. Sibanda[a]

[a]*School of Mathematics, Statistics and Computer Science, University of KwaZulu-Natal, Private Bag X01, Scottsville 3209, Pietermaritzburg, South Africa*
[b]*Department of Mathematics, School of Advanced Sciences, VIT University, Vellore 632 014, India*
[c]*Department of Mathematics and Statistical Sciences, Botswana International University of Science and Technology, Private Bag 16, Palapye, Botswana*

Abstract

The boundary layer nanofluid flow over a horizontal plate embedded in a non-Darcy porous medium is investigated in this study. A non-Newtonian power-law fluid is considered as the base fluid. The nanofluid model incorporates the effects of Brownian motion and thermophoresis. A mixed convective boundary condition, which is more useful in practice, is employed at the surface instead of Dirichlet or Neumann boundary conditions. The flow and convective heat transfer have engineering and industrial applications, such as the thermal design of industrial equipment dealing with molten plastics and polymeric liquids, or in nuclear power plants and thermal energy storage processes. The main aim of this study is to use the spectral quasilinearization method to study the effects of non-Newtonian nanofluid flow over a horizontal surface. The objective is to explore both the accuracy and the convergence of the method through the evaluation of residual errors and error norms and to investigate the impact of specific parameters on the flow behavior and heat transfer characteristics.

Keywords: non-Newtonian nanofluid, convective boundary condition, power-law, spectral quasilinearization method

*Corresponding author
Email address:* `sitholeh@ukzn.ac.za` (H. Sithole)

Introduction

A recent innovative technique to enrich heat transfer in fluids has been to suspend nanosized solid particles in a base fluid in such a way that no sedimentation takes place. Such a fluid is called a nanofluid (Choi and Eastman [1]). Several theoretical studies on the characteristics of nanofluids for convective heat transfer, modelling of the equations for convective heat transfer and thermal conductivity exist (Kuznetsov and Nield [2]; Buongiorno [3]; Kameswaran et al. [4]). The boundary layer flow of a nanofluid over a vertical wedge has been discussed by Gorla et al. [5]. Arifin et al. [6] studied both free and mixed convection in a nanofluid flowing past a horizontal flat plate. Chamka et al. [7] investigated non-Darcy natural convection flow in non-Newtonian nanofluid over a cone in a porous medium with uniform heat and volume fraction fluxes. Sudhagar et al. [8] studied nanofluid flow past an isothermal vertical cone.

Many researchers study non-Newtonian nanofluids in an attempt to improve heat and mass transfer for industrial applications ((Nield [9]; Moraveji et al. [10]). Hady et al. [11] have shown the influence of heat generation/absorption and non-Newtonian rheology on natural convection in boundary layer flow adjacent to a vertical cone embedded in a porous medium. Thermal properties of non-Newtonian nanofluids have been discussed by Hojjat et al. [12]. They have performed several experimental studies in this direction. They later extended their work by studying laminar convection subject to a constant wall temperature (Hojjat et al. [13]).

The study of combined free and forced convection in boundary layer flow on a vertical surface embedded in porous media has received a lot of interest, mainly because these processes occur in many industrial applications such as in geothermal energy technology, crude oil extraction, filtration, and underground disposal of chemical and nuclear waste (Cheng [14]; Nield and Bejan [15]; Vafai [16]; Vadasz [17]). Gorla et al. [18] analyzed mixed convection from vertical plate in non-Newtonian fluid saturated porous media. They analyzed the problem of mixed convection in power-law type non-Newtonian fluids with surface mass transfer.

2

In engineering and industrial processes such as cooling or drying, the convective boundary condition is more general and appropriate than assuming constant wall temperature conditions. Shaw et al. [19] studied the influence of the convective boundary condition and nonlinear convection in a Casson fluid flow over a horizontal plate. The convective surface boundary condition for the flow of a nanofluid has been used by many researchers, such as Makinde and Aziz [22] and Yao et al. [23]. Abdel-Wahed and Emam [24] studied boundary layer over a moving surface in a nanofluid with convective boundary conditions. One of their findings was that convective conditions reduce surface heat and mass flux.

The first objective of this study is to investigate MHD mixed convection in nanofluid flow from a horizontal plate. The base fluid is a non-Newtonian power-law fluid. The horizontal surface is embedded in a non-Darcy porous medium. The temperature condition at the boundary is the convective boundary condition. The model equations are solved numerically using a recently developed spectral quasilinearization method. The second objective is to explore the accuracy and convergence of the method through the evaluation of both the residual errors and error norms. To the best of our knowledge, such a study and model has not been reported in the literature.

Mathematical formulation

Consider the steady two-dimensional laminar boundary layer flow over a flat plate embedded in a non-Darcy porous medium that is saturated with a non-Newtonian nanofluid. It is assumed that the free stream moves with constant velocity U_∞. A uniform magnetic field of strength B is imposed normal to the plate. Homogeneity and local thermal equilibrium are assumed. Using the Oberbeck-Boussinesq and the boundary layer flow approximations,

3

the momentum, temperature and concentration equations are written as

$$\frac{\partial u}{\partial x} + \frac{\partial v}{\partial y} = 0, \tag{1}$$

$$\left|\frac{\partial u}{\partial y}\right|^{n-1}\frac{\partial u}{\partial y} + \frac{\partial u|u|}{\partial y} + \frac{\sigma B^2}{\rho_f}\frac{\partial u}{\partial y} = \frac{(1-C_\infty)\rho_f g K\beta}{\mu}\frac{\partial T}{\partial y} - \frac{(\rho_p - \rho_f)gK}{\mu}\frac{\partial C}{\partial y}, \tag{2}$$

$$u\frac{\partial T}{\partial x} + v\frac{\partial T}{\partial y} = \alpha_m\frac{\partial^2 T}{\partial y^2} + \tau D_B\frac{\partial T}{\partial y}\frac{\partial C}{\partial y} + \tau\frac{D_T}{T_\infty}\left(\frac{\partial T}{\partial y}\right)^2, \tag{3}$$

$$u\frac{\partial C}{\partial x} + v\frac{\partial C}{\partial y} = \varepsilon D_B\frac{\partial^2 C}{\partial y^2} + \varepsilon\left(\frac{D_T}{T_\infty}\right)\frac{\partial^2 T}{\partial y^2}, \tag{4}$$

where the velocity components u and v are along the x and y directions, respectively, and n is the power-law index. The fluid is called a pseudoplastic if $n < 1$ and a dilatant if $n > 1$. The fluid is Newtonian for $n = 1$. The gravitational acceleration is denoted by g, σ is the electric conductivity. In addition ρ_f, μ, β and ρ_p represent the base fluid density , the dynamic viscosity, the volumetric volume expansion coefficient of the fluid and density of the nanoparticles, respectively. The permeability of the porous medium is denoted by K. The ratio of the effective heat capacity of the nanoparticle material to the heat capacity of the ordinary fluid is denoted by $\tau = \dfrac{\varepsilon(\rho c)_p}{(\rho c)_f}$. The effective thermal diffusivity of the porous medium is denoted by $\alpha_m = \dfrac{k_m}{(\rho c)_p}$. The parameters ε and k_m are the effective heat capacity and effective thermal conductivity of the porous medium, respectively. The Brownian diffusion coefficient is denoted by D_B while the thermophoretic diffusion coefficient is denoted by D_T. At the surface, the temperature and the nanoparticle concentration are T_w and C_w, respectively, while the ambient temperature and concentration have constant values T_∞ and C_∞, respectively.

The boundary conditions for the flow field are

$$v = 0, \ C = C_w \ \text{ at } y = 0,$$

$$u \to u_\infty, \ C \to C_\infty \ \text{ as } y \to \infty. \tag{5}$$

The bottom surface of the plate is heated by convection from a hot fluid of temperature T_f with heat transfer coefficient h_f. The thermal field is written as

$$-k\frac{\partial T}{\partial y}\bigg|_{y=0} = h_f(T_f - T_w), \quad T|_{y\to\infty} = T_\infty, \tag{6}$$

with thermal conductivity k, such that $T_f > T_w > T_\infty$.

We introduce the following similarity variables:

$$\psi = (\alpha_m U_\infty x)^{1/2} f(\eta), \ \eta = \frac{y}{x}\left(\frac{U_\infty x}{\alpha_m}\right)^{1/2}, \ \theta = \frac{T - T_\infty}{T_f - T_\infty}, \ \phi = \frac{C - C_\infty}{C_w - C_\infty}, \tag{7}$$

with the stream function ψ and velocities defined by $u = \dfrac{\partial \psi}{\partial y}$ and $v = -\dfrac{\partial \psi}{\partial x}$. Here, in dimensionless terms, the stream function is f, temperature is θ and nanoparticle concentration is ϕ. Using the similarity variables, equations (1) to (4) are transformed to

$$f''\left(nf'^{n-1} + 2Gf' + M\right) = \lambda^n \left(\theta' - Nr\phi'\right), \tag{8}$$

$$\theta'' + Nb\,\theta'\phi' + Nt\,\theta'^2 + \frac{1}{2}f\theta' = 0, \tag{9}$$

$$\phi'' + \frac{Le}{2}\,f\phi' + \frac{Nt}{Nb}\theta'' = 0. \tag{10}$$

The transformed boundary conditions are written as

$$f(0) = 0, \ \theta'(0) = -Bi[1 - \theta(0)], \ \phi(0) = 1, \ f'(\infty) = 1, \ \theta(\infty) = 0, \ \phi(\infty) = 0. \tag{11}$$

The non-dimensional parameters in the above equations are

$\lambda = \dfrac{Ra_x}{Pe_x}$ the mixed convection parameter,

$Ra_x = \dfrac{x}{\alpha_m}\left(\dfrac{(1 - \phi_\infty)g\rho\beta K(T_w - T_\infty)}{\mu}\right)^{\frac{1}{n}}$ the Rayleigh number,

$Pe = \dfrac{u_\infty x}{\alpha_m}$ the Peclet number,

$G = \dfrac{\rho bK}{\mu}\left(\dfrac{\alpha}{x}\right)^{2-n} Pe^{2-n}$ the Darcy number where $G = 0$ corresponds to Darcian flow,

$M = \dfrac{\sigma B^2}{\rho}\left(\dfrac{\alpha}{x}\right) Pe^{1-n}$ the magnetic parameter,

$Nr = \dfrac{(\rho_p - \rho_f)(C_w - C_\infty)}{(1 - C_\infty)\rho_f\beta(T_f - T_\infty)}$ the buoyancy ratio,

$Nb = \dfrac{\tau D_B(C_w - C_\infty)}{\alpha_m}$ the Brownian parameter,

$Nt = \dfrac{\tau D_T(T_f - T_\infty)}{\alpha_m T_\infty}$ the thermophoresis parameter, and

$Le = \dfrac{\alpha_m}{\varepsilon D_B}$ the Lewis number.

Following the work by Aziz [20] and Ishak [21], to obtain the similarity solution, we considered the convective heat transfer associated with the hot fluid on the lower surface of the plate to be proportional to $x^{-1/2}$. We define $h_f = cx^{-1/2}$ with constant c and the Biot number is $Bi = \dfrac{c}{k}\sqrt{U_\infty/\alpha_m}$. The local Nusselt number Nu, which represents the dimensionless temperature gradient at the surface, and the local Sherwood number Sh, which represents the dimensionless concentration gradient at the sheet surface, are written as

$$Nu_x/Re_x^{1/2} = -\theta'(0), \tag{12}$$

$$\text{and} \quad Sh_x/Re_x^{1/2} = -\phi'(0), \tag{13}$$

where $Nu_x = \dfrac{q_w x}{k(T_w - T_\infty)}$, $Sh_x = \dfrac{q_m x}{D_B(C_w - C_\infty)}$, and $Re_x = \dfrac{U_\infty x}{\nu}$. Here q_w is the surface heat flux and q_m is the surface mass flux.

Method of solution

The quasilinearization method (QLM), which was originally introduced by Bellman and Kalaba [25], is a generalization of the Newton-Raphson method. The advantage of quasilinearization is that the algorithm is easy to understand and it converges quickly. Tuffuor and Labadie [33] indicate that a disadvantage lies in the instability of the method whenever a poor initial guess is chosen. The nonlinear components of the equations are linearized using the Taylor series, assuming that there is a negligible difference between the values of the unknown function at the current iteration, $r + 1$, and the previous iteration, r. In the spectral quasilinearization method (SQLM), the nonlinear equations are linearized using the QLM and integrated using the Chebyshev spectral collocation method. For further details on the SQLM see Motsa et al. [26].

Applying the quasilinearization scheme to Equations (9)-(10) with the boundary conditions in Equation (11), yields the following iterative schemes:

$$a_{0,r} f''_{r+1} + a_{1,r} f'_{r+1} + a_{2,r} \theta'_{r+1} + a_{3,r} \phi'_{r+1} = R_f, \tag{14}$$

$$b_{0,r} \theta''_{r+1} + b_{1,r} \theta'_{r+1} + b_{2,r} f_{r+1} + b_{3,r} \phi'_{r+1} = R_\theta, \tag{15}$$

$$c_{0,r} \phi''_{r+1} + c_{1,r} \phi'_{r+1} + c_{2,r} f_{r+1} + c_{3,r} \theta''_{r+1} = R_\phi, \tag{16}$$

subject to

$$f_{r+1}(0) = 0, \ f'_{r+1}(\infty) \to 1$$

$$\theta'_{r+1}(0) = -Bi\left[1 - \theta_{r+1}(0)\right], \ \theta_{r+1}(\infty) \to 0$$

$$\phi(0) = 1, \ \phi_{r+1}(\infty) \to 0, \tag{17}$$

where the coefficients in Equations (14)-(16) are obtained as

$$a_{0,r} = n f'^{n-1}_r + M + 2G f'_r,$$

$$a_{1,r} = n(n-1) f''_r f'^{n-2}_r + 2G f''_r,$$

$$a_{2,r} = -\lambda^n, \quad a_{3,r} = \lambda^n Nr, \tag{18}$$

$$b_{0,r} = 1, \quad b_{1,r} = Nb\phi'_r + 2Nt\theta'_r + \frac{1}{2}f_r,$$

$$b_{2,r} = \frac{1}{2}\theta'_r, \quad b_{3,r} = Nb\theta'_r, \tag{19}$$

$$c_{0,r} = 1, \quad c_{1,r} = \frac{1}{2}Le f_r,$$

$$c_{2,r} = \frac{1}{2}\phi'_r, \quad b_{3,r} = \frac{Nt}{Nb}. \tag{20}$$

A Chebyshev pseudospectral method is used to solve Equations (14) to (16). A differentiation matrix D is used to approximate the derivatives of the unknown variables $q(\eta)$ at the collocation points by the matrix vector product

$$\frac{dQ_r^{(1)}}{d\eta}(\eta_j) = \sum_{k=0}^{N} \mathbf{D}_{jk} q(\eta_k) = \mathbf{D}Q_m, \quad j = 0, 1, 2, \ldots, N, \tag{21}$$

where $\mathbf{D} = \frac{2D}{L}$ and $Q = [q(\eta_0), q(\eta_1), q(\eta_2), \ldots, q(\eta_N)]^T$ represent the vector function at the collocation points. The higher order derivatives are given as powers of $\mathbf{D}$, such as

$$Q_r^{(s)} = \mathbf{D}^s Q_r, \tag{22}$$

where s is the order of the derivative.

We choose the Gauss-Lobatto collocation points to discretize the domain $[-1, 1]$ as

$$x_i = \left(\frac{\pi i}{N} \right), \quad i = 0, 1, \ldots, N; \quad -1 \leq x_i \leq 1. \tag{23}$$

Spectral collocation is applied at r using the differentiation matrix $\mathbf{D}$ in order to approximate derivatives of unknown function, to get

$$\mathbf{A}_{11}\mathbf{F}_{r+1} + \mathbf{A}_{12}\mathbf{\Theta}_{r+1} + \mathbf{A}_{13}\mathbf{\Phi}_{r+1} = \mathbf{R}_f,$$

$$\mathbf{A}_{21}\mathbf{F}_{r+1} + \mathbf{A}_{22}\mathbf{\Theta}_{r+1} + \mathbf{A}_{23}\mathbf{\Phi}_{r+1} = \mathbf{R}_\theta,$$

$$\mathbf{A}_{31}\mathbf{F}_{r+1} + \mathbf{A}_{32}\mathbf{\Theta}_{r+1} + \mathbf{A}_{33}\mathbf{\Phi}_{r+1} = \mathbf{R}_\phi, \tag{24}$$

where,

$$\mathbf{A}_{11} = \mathbf{diag}(a_{0,r})\mathbf{D}^2 + \mathbf{diag}(a_{1,r})\mathbf{D}, \; \mathbf{A}_{12} = \mathbf{diag}(a_{2,r})\mathbf{D}, \; \mathbf{A}_{13} = \mathbf{diag}(a_{3,r})\mathbf{D},$$

$$\mathbf{A}_{21} = \mathbf{diag}(b_{2,r})\mathbf{I}, \; \mathbf{A}_{22} = \mathbf{diag}(b_{0,r})\mathbf{D}^2 + \mathbf{diag}(b_{1,r})\mathbf{D}, \; \mathbf{A}_{23} = \mathbf{diag}(b_{3,r})\mathbf{D},$$

$$\mathbf{A}_{31} = \mathbf{diag}(c_{2,r})\mathbf{I}, \; \mathbf{A}_{32} = \mathbf{diag}(c_{3,r})\mathbf{D}^2, \; \mathbf{A}_{33} = \mathbf{diag}(c_{0,r})\mathbf{D}^2 + \mathbf{diag}(c_{1,r})\mathbf{D} \tag{25}$$

where $\mathbf{diag}()$ represents diagonal matrices of order $(N+1) \times (N+1)$, I is an $(N+1) \times (N+1)$ identity matrix, and F, Θ and Φ are the approximate values of f, θ and ϕ, respectively. Initial approximations are required to start the iteration process, and these can be selected as functions that satisfy the boundary conditions, and from known physical considerations of the flow properties. The QLM generally converges swiftly if the initial guess is close to the true solution. For our system, the following initial guesses that satisfy the boundary conditions were used as suitable initial approximations,

$$f_0(\eta) = \eta + e^{-\eta} - 1,$$

$$\theta_0(\eta) = \left(\frac{Bi}{1 + Bi} \right) e^{-\eta},$$

$$\phi_0(\eta) = e^{-\eta}. \tag{26}$$

8

The above equations can be expressed in matrix form as follows

$$
\begin{bmatrix} A_{11} & A_{12} & A_{13} \\ A_{21} & A_{22} & A_{23} \\ A_{31} & A_{32} & A_{33} \end{bmatrix} \begin{bmatrix} F_{r+1} \\ \Theta_{r+1} \\ \Phi_{r+1} \end{bmatrix} = \begin{bmatrix} R_f \\ R_\theta \\ R_\phi \end{bmatrix}. \tag{27}
$$

The boundary conditions are implemented in the matrix and the approximate solutions at each iteration level are obtained by solving equations (27).

Results and Discussion

The system of coupled ordinary differential Equations (8-10) with the boundary conditions (11) are solved using the SQLM. Table 1 gives a comparison between the Nusselt number, $|-\theta'(0)|$ we obtained and the results reported by Chen and Chen [27], Mohammadien and El-Amin [32], Kameswaran and Sibanda [28] and Kairi and RamReddy [31] for various values of the power-law index n.

n	Chen & Chen [27]	Mohammadien & El-Amin [32]	Kameswaran & Sibanda [28]	Kairi & RamReddy [31]	Current study
0.5	-	-	0.37675	0.37768	0.3776634930
1.0	0.4440	0.44390	0.44375	0.4437	0.4439043652
1.5	-	-	0.47635	0.4752	0.4753730016

Table 1: Comparison of results for the Nusselt number $|-\theta'(0)|$ for $G = M = Nb = Nt = Nr = Bi = Le = 0$, $\lambda = 1$ from the current study and results reported by Chen & Chen [27], Mohammadien & El-Amin [32], and Kameswaran & Sibanda [28] and Kairi & RamReddy [31] for various values of the power-law index n.

Table 2 shows the comparison of the Nusselt number $|-\theta'(0)|$ obtained in our study with results reported by Plumb and Huenefeld [29], and Srivinivasacharya and Kumar [30] for various values of the non-Darcy parameter G. From data in both these tables, it is evident that a good agreement with earlier results is achieved with the SQLM method.

G	Srivinivasacharya & Kumar [30]	Plumb & Huenefeld [29]	Current study
0.00	0.443717	0.4439	0.4439043652
0.01	0.442126	0.44232	0.4423159030
0.1	0.429475	0.42969	0.4296890571
1	0.365732	0.36617	0.3661664958
10	0.250634	0.25126	0.2529532882

Table 2: Comparison of results for the Nusselt number $|-\theta'(0)|$ for $M = Nb = Nt = Nr = Bi = Le = 0$, $n = \lambda = 1$ from the current study and reported by Plumb & Huenefeld [29], and Srivinivasacharya & Kumar [30] for various values of the non-Darcy parameter G.

The residual error measures the extent to which a numerical solution approximates the true solution. To gain further insight into the accuracy of the spectral quasilinearization method, we have calculated residual errors as shown in Figures 1(a), 2(a), 3(a) and 4(a). These are calculated for variable values of the power-law index n; mixed convection parameter λ; the non-Darcy parameter G and the Biot number Bi. In most instances, all the solutions have converged with an absolute residual error $||\text{Res}|| \approx 10^{-10}$ after the third iteration. Accurate solutions were achieved with the least number of iterations for the specific values $n = 1$, $\lambda = 2$, $G = 0.5$ and $Bi = 0.1$. For a Darcian flow $G = 0$, the residual error $||\text{Res}|| \approx 10^{-10}$ was obtained after the fifth iteration.

The convergence and stability of the iteration scheme was further evaluated by considering the error norms defined as the difference between the approximate values at successive iterations, i.e,

$$E_f \quad = \max ||\mathbf{F}_{r+1} - \mathbf{F}_r||_\infty, \tag{28}$$

$$E_\theta \quad = \max ||\mathbf{\Theta}_{r+1} - \mathbf{\Theta}_r||_\infty, \tag{29}$$

$$E_\phi \quad = \max ||\mathbf{\Phi}_{r+1} - \mathbf{\Phi}_r||_\infty. \tag{30}$$

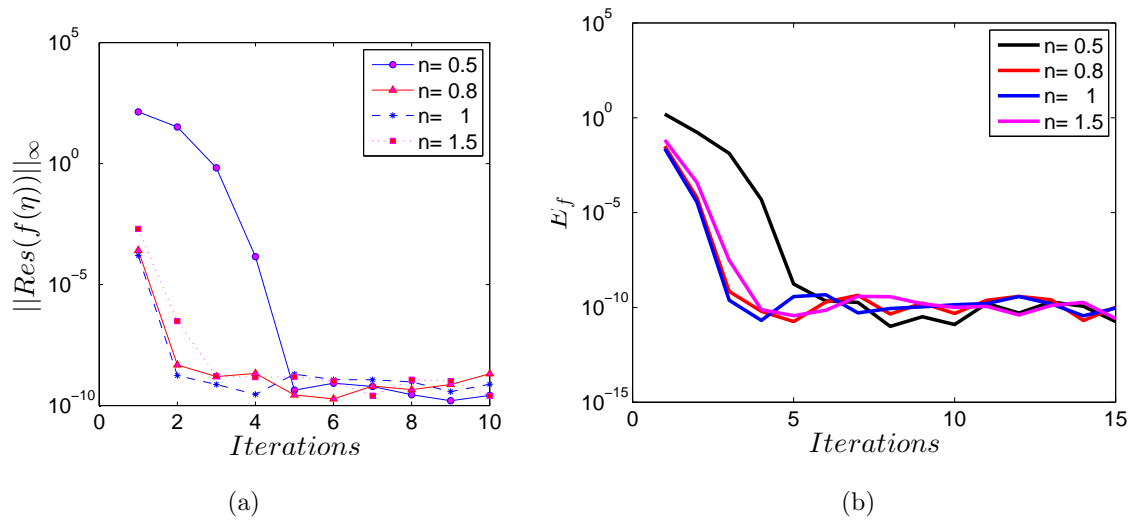Figures 1(b), 2(b), 3(b) and 4(b), show the variation of the solution error norms, E_f and E_θ

10

Figure 1: (a) Residual error $||Res(f(\eta))||_\infty$ against the number of iterations, for different values of the power-law index n. (b) Solution error norm E_f against the number of iterations, for different values of the power-law index n.
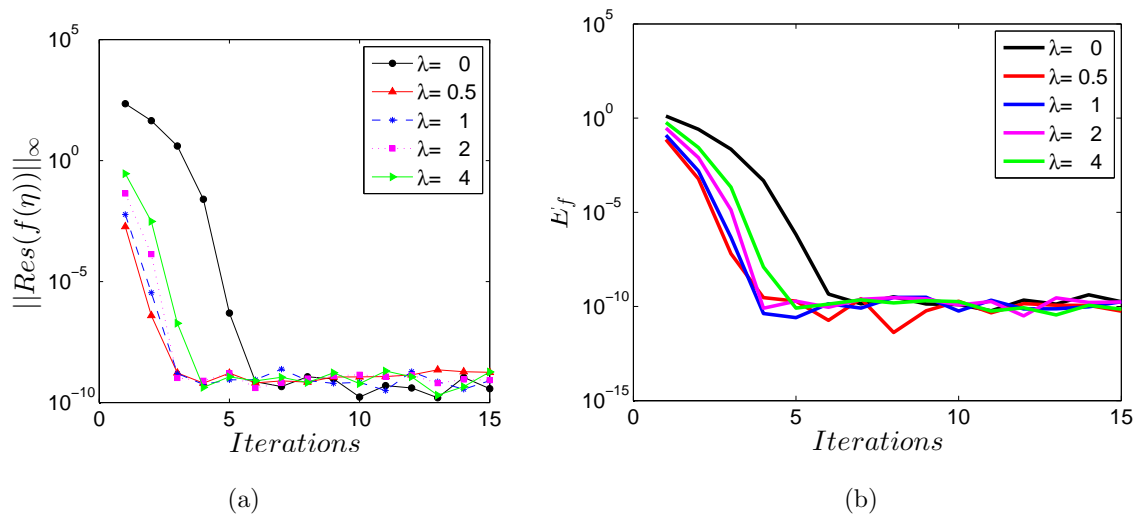

Figure 2: (a) Residual error $||Res(f(\eta))||_\infty$ against the number of iterations, for different values of the mixed convection parameter λ. (b) Solution error norm E_f against the number of iterations, for different values of the mixed convection parameter λ.

11

with the number of iterations for different values of the power-law index n; mixed convection parameter λ; the non-Darcy parameter G and the Biot number Bi. As can be seen in the figures, the error norms decrease to $||\mathrm{E}|| \approx 10^{-11}$ and convergence is reached at the fourth iteration. Convergence solutions were achieved with the least number of iterations for the specific values $n = 1$, $\lambda = 1$, $G = 1$ and $Bi = 4$. It is worth noting, however, that the specific parameter values giving the best accuracy and those giving rise to the best convergence rate were not necessarily the same values.
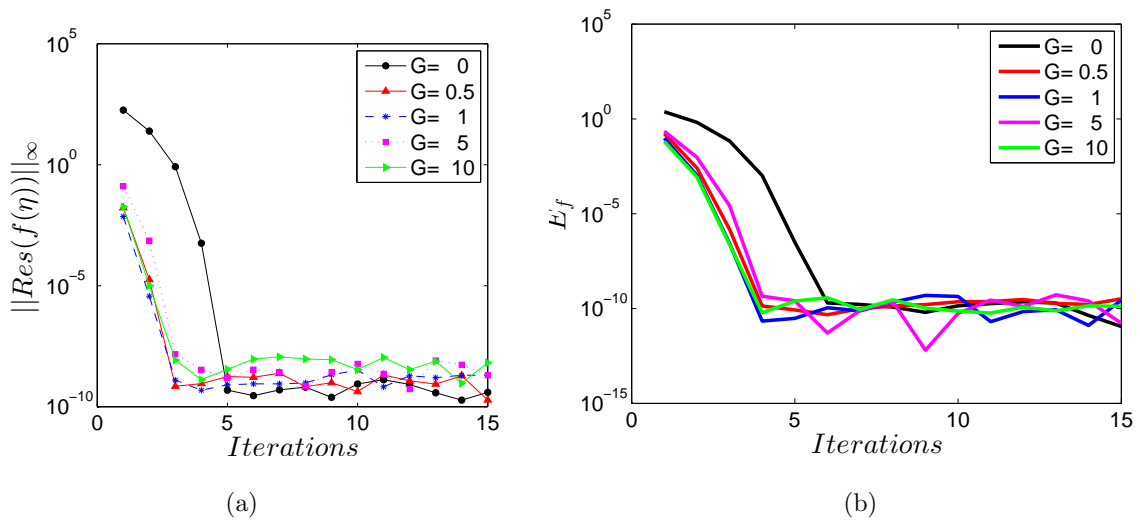

Figure 3: (a) Residual error $||Res(f(\eta))||_\infty$ against the number of iterations, for different values of the non-Darcy parameter G. (b) Solution error norm E_f against the number of iterations, for different values of the non-Darcy parameter G.

Figure 5(a) shows the residual errors against the number of iterations. Figure 5(b) shows the solution error norms E_f, E_θ and E_ϕ against the number of iterations. All the errors are small, showing that the SQLM converges and is accurate. Therefore the results may be trusted.

The fluid velocity for different parameters, specifically the power-law index, non-Darcy number, magnetic parameter, mixed convection, buoyancy ratio and Lewis number, is shown in Figures 6, 7, and 8. From Figure 6(a), it is observed that the velocity of the fluid increases as the fluid nature change from dilatant to pseudoplastic. The maximum streamwise velocity
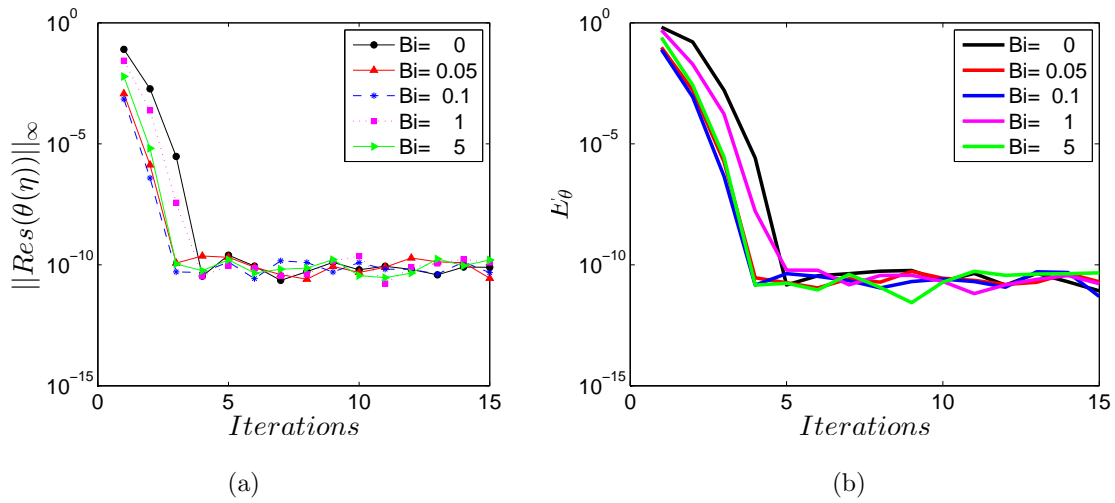
Figure 4: (a) Residual error $||Res(f(\eta))||_\infty$ against the number of iterations, for different values of the Biot number Bi. (b) Solution error norm E_θ against the number of iterations, for different values of the Biot number Bi.
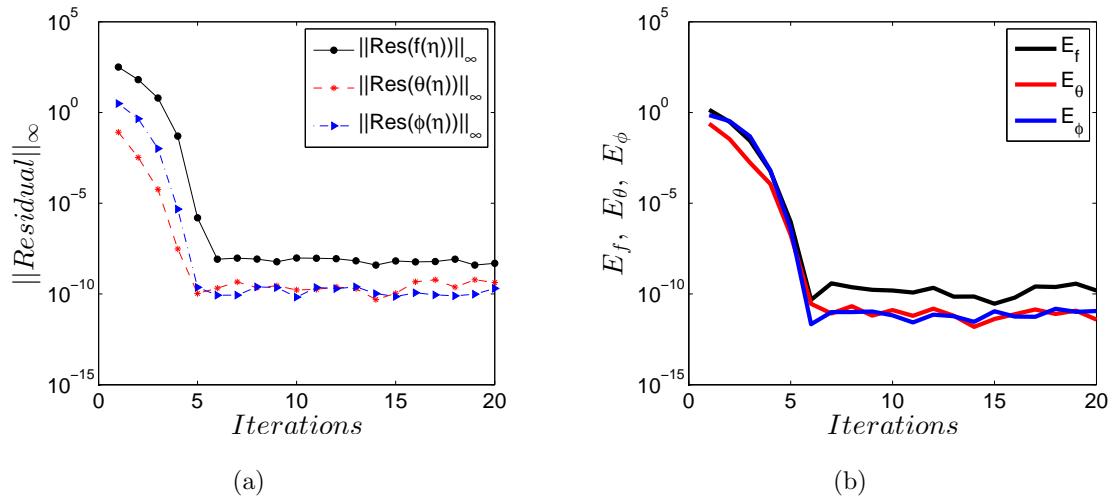

Figure 5: (a) Residual errors $||Res(f(\eta))||_\infty$, $||Res(\theta(\eta))||_\infty$ and $||Res(\phi(\eta))||_\infty$ against the number of iterations. (b) Solution error norms E_f, E_θ and E_ϕ against the number of iterations.

13

is enhanced by the increase in the power index. An increase in the non-Darcy parameter indicates that the porous medium provides increasing resistance to the fluid flow, thereby reducing the flow rate below that which could be achieved without a porous medium. This is observed in Figure 6(b) where, the increase in the non-Darcy parameter leads to a decrease in the fluid velocity profile peaks.
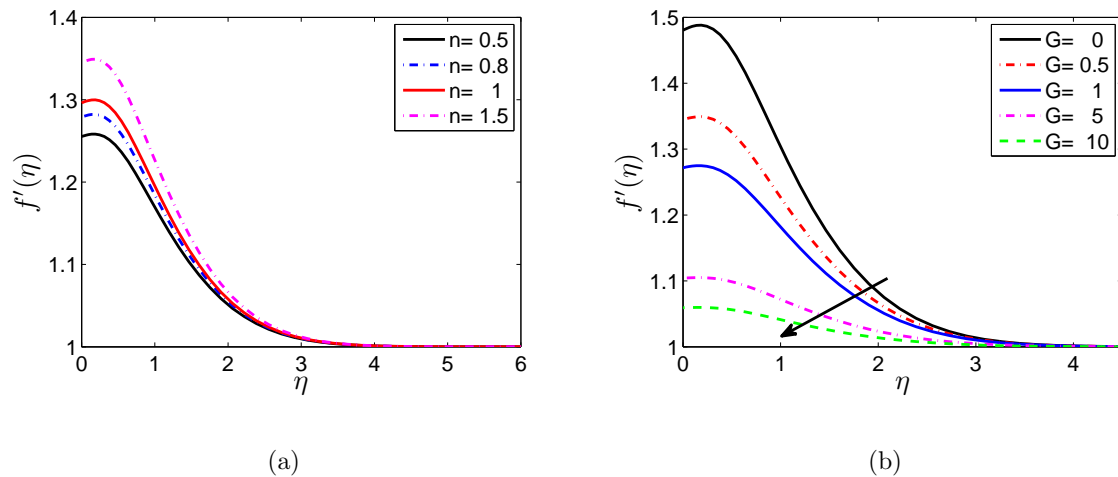

Figure 6: (a) Effect of the power-law index n on the velocity profile $f'(\eta)$ with $G = 0.5$, $M = 1$, $\lambda = 2$, $Nr = 0.2$, $Nb = 0.2$, $Nt = 0.2$, $Bi = 1$, $Le = 10$, and (b) Effect of the non-Darcy parameter G on the velocity profile $f'(\eta)$ with $n = 1.5$, $M = 1$, $\lambda = 2$, $Nr = 0.2$, $Nb = 0.2$, $Nt = 0.2$, $Bi = 1$, $Le = 10$.

The magnetic parameter is directly embedded in the momentum equation and it significantly influences the velocity profiles (see Figure 7(a)). The velocity of the fluid reduces with an increase of the magnetic parameter, and hence the momentum boundary layer thickness is reduced. The reason is that introducing a transverse magnetic field creates a Lorentz drag force which helps to resist the flow and hence reduces the velocity. For $\lambda = 0$, the momentum equation reduces to $f'' = 0$ and this gives a constant velocity, Figure 7(b). The location of the peak velocity shifts away from the plate as λ increases.

Due to opposing buoyancy, the velocity of the fluid increases up to a certain point along the non-dimensional axis and then decreases. Overall, the momentum boundary layer thickness decreases with an increase in the buoyancy ratio (see Figure 8(a)). This is because

14

buoyancy ratio has a tendency to decelerate the fluid flow along the surface. An interesting phenomenon is observed for different Lewis number as shown in Figure 8(b). For Lewis number $Le > 1$, the fluid velocity drops to less than 1 and this fall point decreases with a decrease in the Lewis number. The velocity decreases with increase in the Lewis number, although the influence of the Lewis number on the fluid velocity is fairly marginal.

The Biot number represents the ratio of the internal thermal resistance of a solid to the boundary layer thermal resistance. For $Bi = 0$ the bottom of the plate with hot fluid is totally insulated and the internal thermal resistance of the plate is extremely high which means that no convective heat transfer to the cold fluid on the upper part of the plate takes place. Figure 9 present the velocity and temperature profiles for different values of the Biot number. The velocity of the fluid increases with an increase in the Biot number. This is because the Biot number reduces the plate thermal resistance which enhances the peak fluid velocity.

In Figure 10, the concentration of the nanoparticle is highly influenced by the Brownian parameter and Lewis number. Due to Brownian motion of the nanoparticles, the concentra-
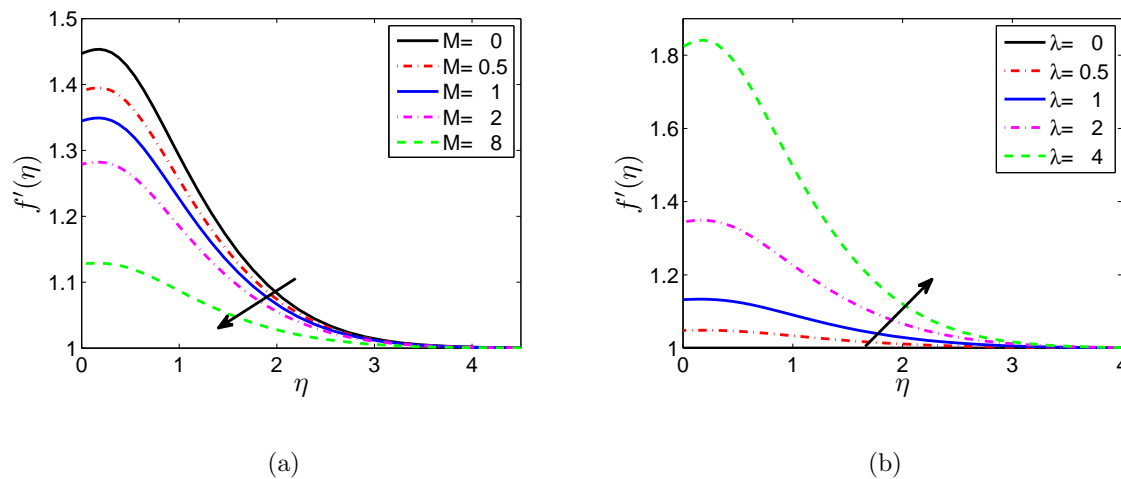

(a)

(b)

Figure 7: (a) Effect of the magnetic parameter M on the velocity profile $f'(\eta)$ with $n = 1.5$, $G = 0.5$, $\lambda = 2$, $Nr = 0.2$, $Nb = 0.2$, $Nt = 0.2$, $Bi = 1$, $Le = 10$, and (b) Effect of the mixed convection parameter λ on the velocity profile $f'(\eta)$ with $n = 1.5$, $G = 0.5$, $M = 1$, $Nr = 0.2$, $Nb = 0.2$, $Nt = 0.2$, $Bi = 1$, $Le = 10$.
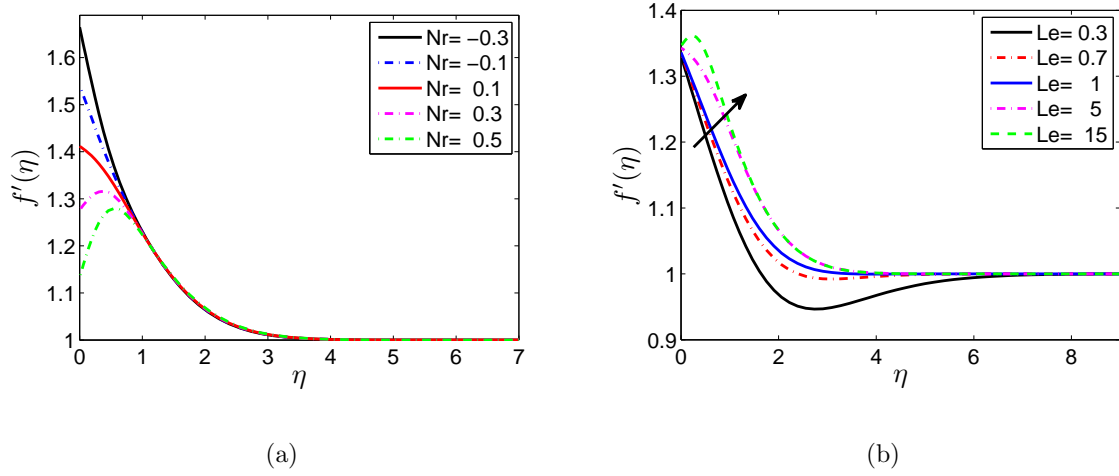
(a)

(b)

Figure 8: (a) Effect of the buoyancy ratio Nr on the velocity profile $f'(\eta)$ with $n = 1.5$, $G = 0.5$, $M = 1$, $\lambda = 2$, $Nb = 0.2$, $Nt = 0.2$, $Bi = 1$, $Le = 10$, and (b) Effect of the Lewis number Le on the velocity profile $f'(\eta)$ with $n = 1.5$, $G = 0.5$, $M = 1$, $\lambda = 2$, $Nb = 0.2$, $Nr = 0.2$, $Nt = 0.2$, $Bi = 1$.
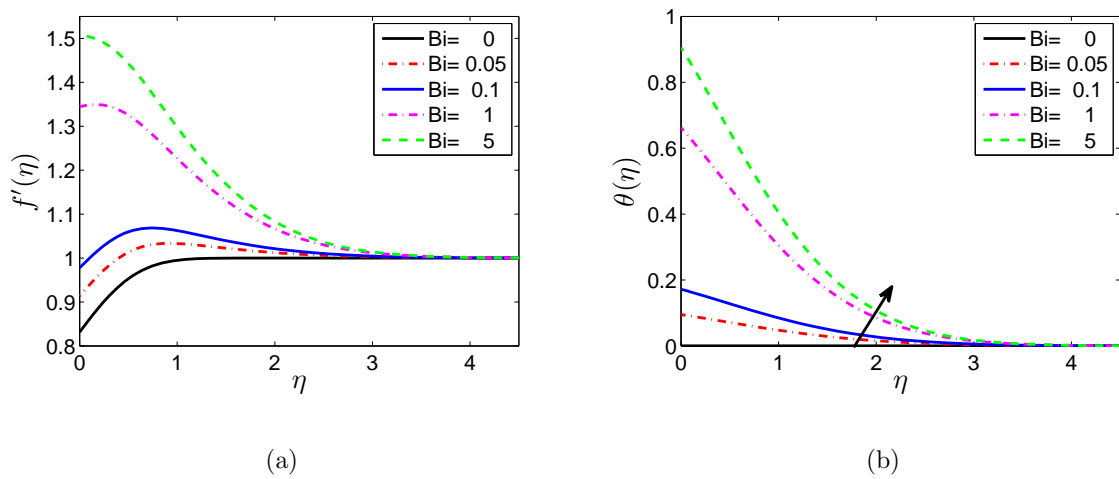

(a)

(b)

Figure 9: (a) Effect of the Biot number Bi on the velocity profile $f'(\eta)$ with $n = 1.5$, $G = 0.5$, $M = 1$, $\lambda = 2$, $Nb = 0.2$, $Nr = 0.2$, $Nt = 0.2$, $Le = 10$, and (b) Effect of the Biot number Bi on the temperature profile $\theta(\eta)$ with $n = 1.5$, $G = 0.5$, $M = 1$, $\lambda = 2$, $Nb = 0.2$, $Nr = 0.2$, $Nt = 0.2$, $Bi = 1$, $Le = 10$.

16

tion in the fluid is not significantly influenced near the surface. In Figure 10(a) it can be observed that the concentration boundary layer thickness decreases with an increase in the Brownian parameter. Figure 10(b) shows that the concentration boundary layer thickness decreases significantly as the Lewis number increases.
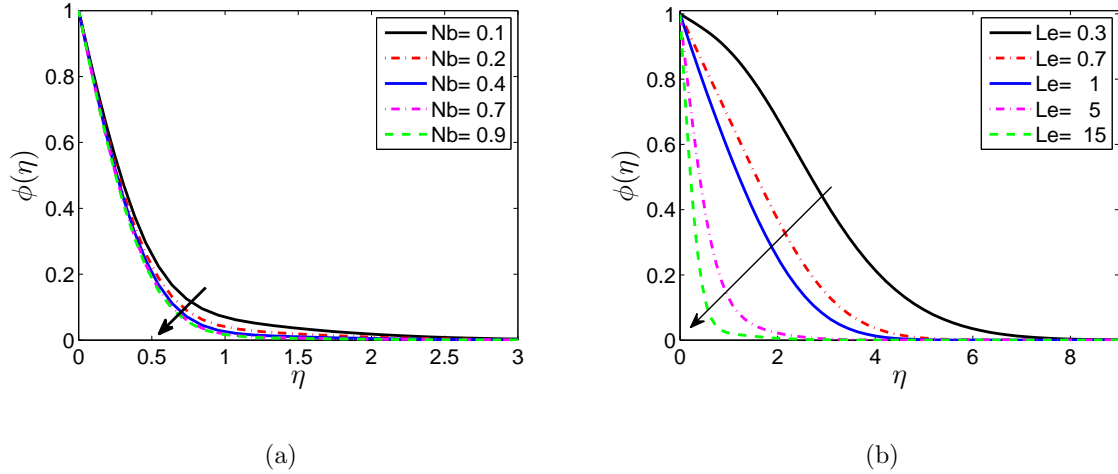

(a)

(b)

Figure 10: (a) Effect of the Brownian parameter Nb on the concentration profile $\phi(\eta)$ with $n = 1.5$, $G = 0.5$, $M = 1$, $\lambda = 2$, $Nr = 0.2$, $Nt = 0.2$, $Bi = 1$, $Le = 10$, and (b) Effect of the Lewis number Le on the concentration profile $\phi(\eta)$ with $n = 1.5$, $G = 0.5$, $M = 1$, $\lambda = 2$, $Nb = 0.2$, $Nr = 0.2$, $Nt = 0.2$, $Bi = 1$.

The Nusselt number is the ratio of convective heat transfer to conductive heat transfer. The Sherwood number is the ratio of convective mass transport to diffusive mass transport. The changes in the Nusselt and Sherwood numbers with various parameters is shown in Figures 11 and 12. Increasing the power-law index tends to increase the velocity and reduce both the thermal and concentration boundary layer thickness. This leads to a reduction in the local Nusselt number and Sherwood numbers. The Nusselt and Sherwood numbers are larger for a dilatant fluid ($n > 1$) compared to pseudoplastic fluid ($n < 1$). The heat transfer rate at the wall reduces with an increase in the non-Darcy parameter G. This observation may be explained by the direct effect of G on the velocity near the wall, which significantly influences the strength of the convection mechanism in transporting heat from the wall as compared to the dispersion mechanism. However, the non-Darcy parameter reduces the

mass transfer rate at the wall. This may indicate a reduction in the velocity near the wall and hence the mass transfer rates by convection.
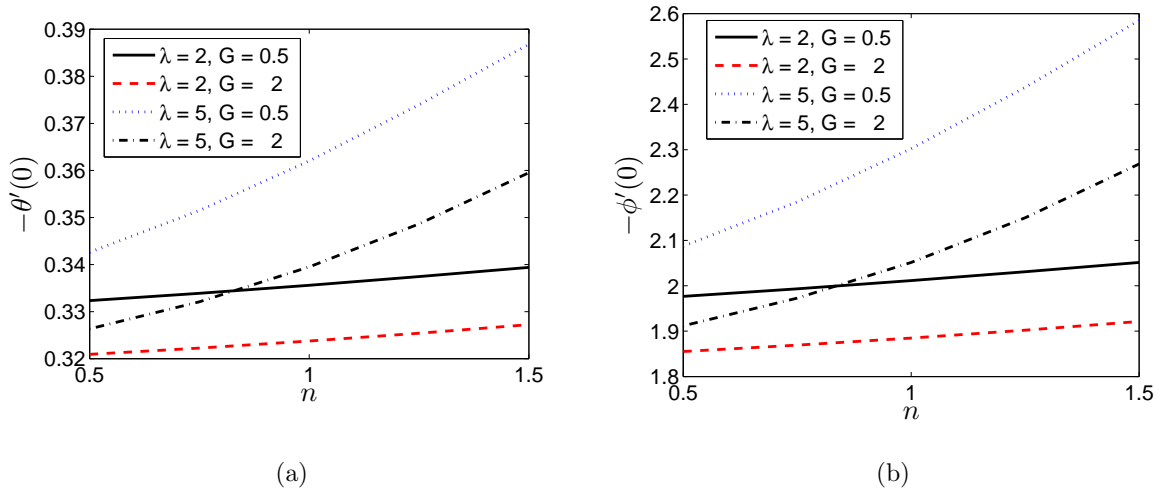

(a)   (b)

Figure 11: (a) Heat transfer rate Nusselt number $-\theta'(0)$ with $M = 1$, $Nb = 0.2$, $Nr = 0.1$, $Nt = 0.2$, $Bi = 1$, $Le = 10$, and (b) Mass transfer rate Sherwood number $\phi'(0)$ as a function of n for different values of λ and G.

The heat and mass transfer rates as functions of Nr for different values of Nt, Nb and Le,are shown in Figure 12. The local Nusselt number and the local Sherwood number are decreasing functions of the buoyancy ratio. As Nb and Nt increase, the value of the local Sherwood number increases, but the increment is not significant. In Figure 12 the heat transfer rate increases with an increase in the Lewis number Le. In Figure 12(b) increasing Le appears to reduce the rate of mass transfer to the wall for the opposing buoyancy. For opposing buoyancy, as Le increases, heat dispersion outweighs mass dispersion and as a result the concentration gradient near the wall becomes smaller, which then reduces the Sherwood number. The opposite is however observed for higher values of Nr, where the mass transfer rate is enhanced. This suggests that, with an increase in Le, mass dispersion decreases, thereby conserving the higher concentration gradients near the surface and enhancing mass transfer by convection.

The heat transfer rate at the wall increases with an increase in the Biot number, as can
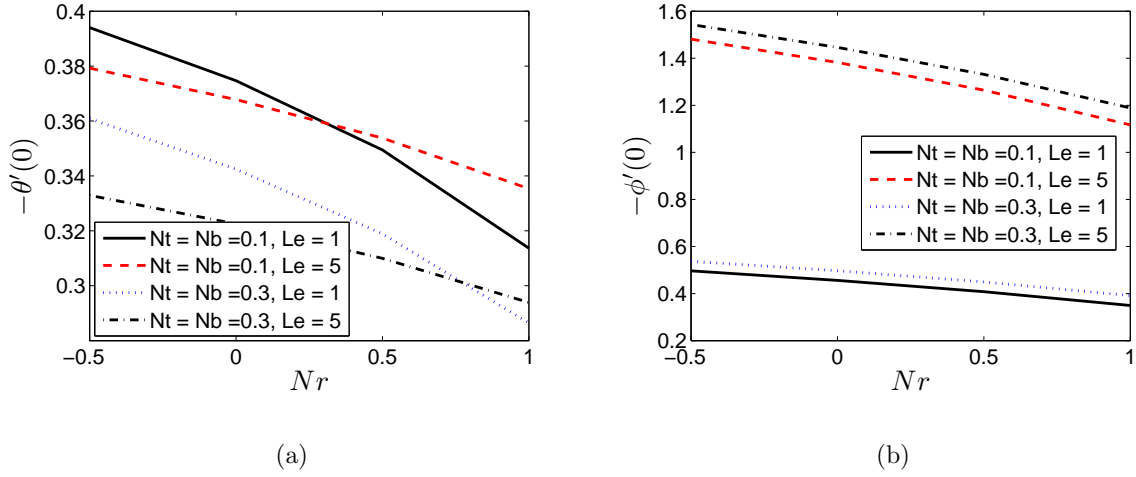
(a)   (b)

Figure 12: (a) Heat transfer rate Nusselt number $-\theta'(0)$ with $M = 1$, $Bi = 1$, $Nr = 0.1$, $\lambda = 2$, $G = 0.5$, $n = 1.5$, and (b) Mass transfer rate Sherwood number $\phi'(0)$ as a function of Nr for different values of Nt, Nb and Le.
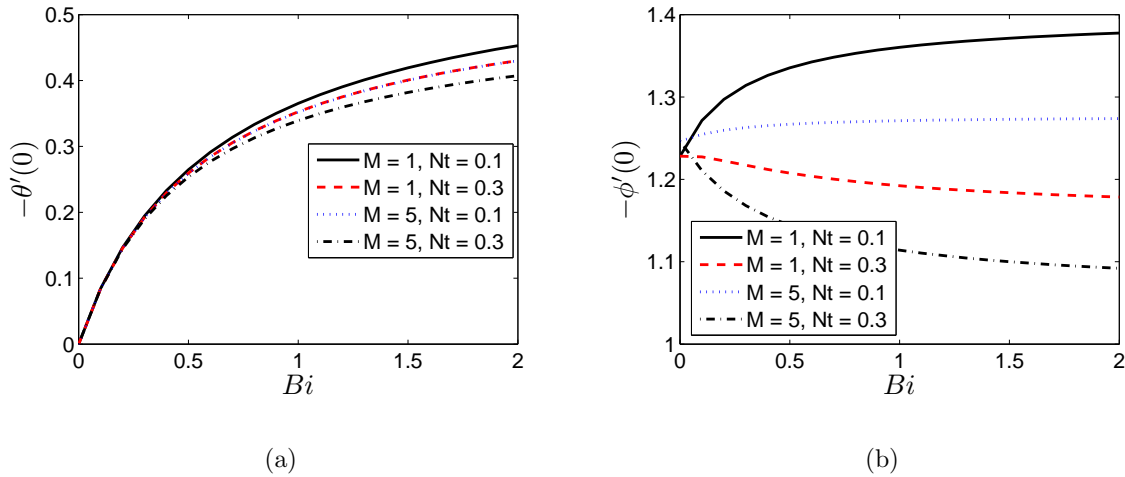

(a)   (b)

Figure 13: (a) Heat transfer rate Nusselt number $-\theta'(0)$ with $Nr = 0.1$, $\lambda = 2$, $G = 0.5$, $n = 1.5$, and (b) Mass transfer rate Sherwood number $\phi'(0)$ as a function of Bi for different values of M and Nt.

19

be seen in Figure 13(a). For $Bi = 0$, no convective heat transfer takes place and the rate of heat transfer at the wall is zero, as expected. The heat transfer and the mass transfer rates decrease with an increase in the magnetic parameter. The mass transfer rate as a function of Bi for different values of M and Nt can be seen in Figure 13(b).

Conclusion

In this study, the boundary layer flow past over a horizontal plate embedded in a porous medium filled with a non-Newtonian nanofluid has been studied. The convective boundary condition was used. The spectral quasilinearization method was used to solve the equations. The accuracy and convergence of the method was established. The following major findings were obtained:

- The accuracy and the convergence of the SQLM is dependent on the choice of parameter values.

- The parameter values giving rise to the best accuracy may not give the best convergence rates.

- Both the heat transfer rate and the mass transfer rate increase with the mixed convection parameter for a dilatant fluid.

- Increasing the Biot number enhances both the velocity and temperature at the surface.

- The heat transfer rate increases with increased values of the Biot number. The mass transfer rate increases with the Biot number for smaller values of the thermophoresis parameter but decreases for bigger values of the thermophoresis parameter.

Acknowledgment

References

[1] Choi, S. U. S., and Eastman, J.A. "Enhancing thermal conductivity of fluids with nanoparticles." 1995 International mechanical engineering congress and exhibition, San Francisco, CA, ASME- Publications-Fed 231 (1995): 99-106.

[2] Kuznetsov, A. V., and Nield, D. A. "Natural convective boundary-layer flow of a nanofluid past a vertical plate." International Journal of Thermal Sciences 49.2 (2010): 243-247.

[3] Buongiorno, J. "Convective transport in nanofluids." Journal of Heat Transfer 128.3 (2006): 240-250.

[4] Kameswaran, P. K., Vasu, B., Murthy, P. V. S. N., and Gorla, R. S. R. "Mixed convection from a wavy surface embedded in a thermally stratified nanofluid saturated porous medium with non-linear Boussinesq approximation." International Communications in Heat and Mass Transfer 77 (2016): 78-86.

[5] Gorla, R. S. R., Chamkha, A. J., and Rashad, A. M. "Mixed convective boundary layer flow over a vertical wedge embedded in a porous medium saturated with a nanofluid: natural convection dominated regime." Nanoscale Research Letters 6.1 (2011): 207.

[6] Arifin, N.M., Nazar, R., and Pop, I. "Free-and mixed-convection flow past a horizontal surface in a nanofluid." Journal of Thermophysics and Heat Transfer, 26.2 (2012):375-382.

[7] Chamkha, A., Abbasbandy, S., and Rashad, A. M. "Non-Darcy natural convection flow for non-Newtonian nanofluid over cone saturated in porous medium with uniform heat and volume fraction fluxes." International Journal of Numerical Methods for Heat & Fluid Flow 25.2 (2015): 422-437.

[8] Sudhagar, P., Kameswaran, P. K., and Kumar, B. R. "Magnetohydrodynamics Mixed Convection Flow of a Nanofluid in an Isothermal Vertical Cone." Journal of Heat Transfer 139.3 (2017): 034503.

[9] Nield, D. A. "A note on the onset of convection in a layer of a porous medium saturated by a non-Newtonian nanofluid of power-law type." Transport in Porous Media 87.1 (2011): 121-123.

[10] Moraveji, M. K., Haddad, S. M. H., and Darabi, M. "Modeling of forced convective heat transfer of a non-Newtonian nanofluid in the horizontal tube under constant heat flux with computational fluid dynamics." International Communications in Heat and Mass Transfer 39.7 (2012): 995-999.

[11] Hady, F. M., Ibrahim, F. S., Abdel-Gaied, S. M., and Eid, M. R. "Effect of heat generation/absorption on natural convective boundary-layer flow from a vertical cone embedded in a porous medium filled with a non-Newtonian nanofluid." International Communications in Heat and Mass Transfer 38. 10 (2011): 1414-1420.

[12] Hojjat, M., Etemad, S. G., Bagheri, R., and Thibault, J. "Thermal conductivity of non-Newtonian nanofluids: Experimental data and modeling using neural network." International Journal of Heat and Mass Transfer 54.5 (2011): 1017-1023.

[13] Hojjat, M., Etemad, S. G., Bagheri, R., and Thibault, J. "Laminar convective heat transfer of non-Newtonian nanofluids with constant wall temperature." Heat and Mass Transfer 47, 2 (2011): 203-209.

[14] Cheng, P. "Heat transfer in geothermal systems." Advances in Heat Transfer 14 (1979): 1-105.

[15] Nield, D. A., and Bejan, A. Convection in Porous Media. Vol. 3. New York: Springer, (2006).

[16] Vafai, K. (Ed), Handbook of Porous Media, Second ed., Taylor & Francis, New York, (2005).

[17] Vadasz, P. (Ed), Emerging topics in heat and mass transfer in porous media: from bioengineering and microelectronics to nanotechnology. Vol. 22. Springer Science & Business Media, Netherlands, (2008).

[18] Gorla, R., Slaouti, A., and Takhar, H. S. "Mixed convection in non-Newtonian fluids along a vertical plate in porous media with surface mass transfer." International Journal of Numerical Methods for Heat & Fluid Flow 7.6 (1997): 598-608.

[19] Shaw, S., Mahanta, G., and Sibanda, P. "Non-linear thermal convection in a Casson fluid flow over a horizontal plate with convective boundary condition." Alexandria Engineering Journal 55.2 (2016): 1295-1304.

[20] Aziz, A., "A similarity solution for laminar thermal boundary layer over a flat plate with a convective surface boundary condition." Communications in Nonlinear Science and Numerical Simulation 14.4 (2009): 1064-1068.

[21] Ishak, A., "Similarity solutions for flow and heat transfer over a permeable surface with convective boundary condition." Applied Mathematics and Computation 217.2 (2010): 837-842.

[22] Makinde, O. D., and Aziz, A. "MHD mixed convection from a vertical plate embedded in a porous medium with a convective boundary condition." International Journal of Thermal Sciences 49.9 (2010): 1813-1820.

[23] Yao, S., Fang, T., and Zhong, Y. "Heat transfer of a generalized stretching/shrinking wall problem with convective boundary conditions." Communications in Nonlinear Science and Numerical Simulation 16.2 (2011): 752-760.

[24] Abdel-Wahed, M. S., and Emam, T. G. "MHD boundary layer behaviour over a moving surface in a nanofluid under the influence of convective boundary conditions." Strojniski vestnik-Journal of Mechanical Engineering 63.2 (2017): 119-128.

[25] Bellman, R. E., and Kalaba, R. E. "Quasilinearization and nonlinear boundary- value problems." Elsevier Publishing Company, New York (1965).

[26] Motsa, S. S., Dlamini, P. G., and Khumalo, M. "Spectral relaxation method and spectral quasilinearization method for solving unsteady boundary layer flow problems," Advances in Mathematical Physics, Article ID 341964, 12 pages, (2014).

[27] Chen, H.-T., and Chen C.o-K. "Free convection flow of non-Newtonian fluids along a vertical plate embedded in a porous medium." ASME. Journal of Heat Transfer 110.1 (1988): 257-260.

[28] Kameswaran, P. K., and Sibanda, P. "Thermal dispersion effects on convective heat and mass transfer in an Ostwald de Waele nanofluid flow in porous media." Boundary Value Problems 2013.1 (2013): 243.

[29] Plumb, O. A., and Huenefeld, J. C. "Non-Darcy natural convection from heated surfaces in saturated porous media." International Journal of Heat and Mass Transfer 24.4 (1981): 765-768.

[30] Srinivasacharya, D., and Kumar, P. V. "Thermal stratification on natural convection over an inclined wavy surface in a nanofluid saturated porous medium." Computational Thermal Sciences: An International Journal 7. (2015): 5-6.

[31] Kairi, R. R., and RamReddy, C. "The effect of melting on mixed convection heat and mass transfer in a non-Newtonian nanofluid saturated in porous medium." Frontiers Heat Mass Transfer 6 (2015): 1-7.

[32] Mohammadien, A. A., and El-Amin, M. F. "Thermal dispersion-radiation effects on non-Darcy natural convection in a fluid saturated porous medium." Transport in Porous Media 40.2 (2000): 153-163.

[33] Tuffuor, S., and Labadie, J. W. "A nonlinear time variant rainfall-runoff model for augmenting monthly data." Water Resources Research 10.6 (1974): 1161-1166.
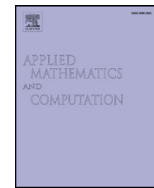
Chapter 4

Numerical simulation of couple stress nanofluid flow in magneto-porous medium with thermal radiation and a chemical reaction

In Chapter 3, we studied the power law model, which has a shear dependent viscosity but without elasticity. In this chapter, we present a study of heat and mass transfer in a couple stress nanofluid flow in a magneto-porous medium with thermal radiation and internal heat generation. The couple stress fluid is the simplest polar fluid theory that displays all the important features and properties of couple stresses in fluids. In the current study, the flow is generated by a stretching surface, and the temperature and concentration distributions are studied subject to nanoparticle Brownian motion and thermophoresis effects. The nonlinear model equations are solved using a spectral quasilinearization method.

Numerical simulation of couple stress nanofluid flow in magneto-porous medium with thermal radiation and a chemical reaction

Hloniphile Sithole, Hiranmoy Mondal*, Sicelo Goqo, Precious Sibanda, Sandile Motsa

School of Mathematics, Statistics and Computer Science, University of KwaZulu Natal, Private Bag X01, Scottsville, Pietermaritzburg 3209, South Africa

ARTICLE INFO

ABSTRACT

We present a study of heat and mass transfer for a couple stress nanofluid flow in a magneto-porous medium with thermal radiation and heat generation. The flow is generated by a stretching surface and the temperature and concentration distributions are studied subject to nanoparticle Brownian motion and thermophoresis effects. The nonlinear model equations have been solved using a spectral quasi-linearization method. The solution method has been used in a limited number of studies in the resent past. Its general reliability for a wider range of problems remains to be determined. Thus in order to determine the accuracy of the solutions, and the convergence of the method, a qualitative presentation of residual errors for different parameters is given. Additionally, for some special flow cases, the current results have been compared with previously published work and found to be in good agreement. A limited parametric study showing the influence of the flow parameters on the fluid properties is given. The numerical analysis of the residual error of PDEs and convergence properties of the method are also discussed. The method is computationally fast and gives very accurate results after only a few iterations using very few grid points in the numerical discretization process. The aim of this manuscript is to pay more attention of residual error analysis with heat and fluid flow on couple stress nanofluids to improve the system performance. Also the fluid temperature in the boundary layer region rise significantly for increasing the values of thermophoresis and Brownian motion parameter. The results show that wall shear stress increases by increasing couple stress parameter.

1. Introduction

Heat and mass transfer processes have been focused of extensive investigation for many decades due to the importance of these processes of physiological flows such as urine transport from kidneys to the bladder and the circulation of blood in small blood vessels. The theory of couple stress fluids, first introduced by Stokes [1] has been widely studied by researchers [2,3]. Couple stresses appear in fluids with very large molecules such as in synovial fluids, for example, Walicki and Walicka

[4] modelled synovial fluids in human joints as couple stress fluids. Examples of studies of the flow of couple stress fluids include Hiremath and Patil [5] who investigated the oscillatory flow of a couple stress fluid through a porous medium while the melting heat transfer in the boundary layer flow of a couple stress fluid over a stretching surface was investigated by Hayat et al. [6].

Nanofluids are recent fluids that offer the promise of significantly enhanced thermophysical properties. Typical base liquids include water, oil or ethylene glycol. The addition of nanoparticles to the base liquids greatly enhances the thermal characteristics of the base liquid. Nanofluids are used in various industrial and technological processes such as in the cooling of electronic devices, transformer cooling, heat exchangers, biomedicine and many other uses. Couple stress nanofluids are useful in MHD power generators, for the removal of blockages in arteries, hyperthermia, cancer tumor treatment, magnetic resonance imaging, etc. Couple stress nanofluid flow occurs in industrial and technological processes such as in hot rolling, wire drawing, glass fiber and paper production, extrusion of polymer fluids and the solidification of liquid crystals. Further recent investigations on nanofluid flows can be quoted through the studies [7,8].

Introducing a magnetic field to the flow of a conducting fluid generally alters the flow field. In general, the magnetic field has a stabilizing effect on the instability, but there are few exceptions. The use of magnetic field to influence heat generation processes in electrically conducting fluids has important engineering applications. For example, in many metallurgical processes such as the drawing of continuous filaments through quiescent fluids, and the annealing and tinning of copper wires, the properties of the end product depends on the rate of cooling. Pal and Mondal [9] studied the effect of MHD and variable viscosity on non-Darcy mixed convective heat transfer over a stretching sheet embedded in a porous medium with non-uniform heat source/sink. Ali et al. [10] analyzed the MHD flow and heat transfer of a couple stress fluid over an oscillatory stretching sheet with heat source/sink in porous medium. Ramesh and Dekavar [11] studied the magnetohydrodynamic peristaltic flow of a couple stress fluid through a homogenous porous media in an asymmetric channel with heat transfer. The flow of a couple stress fluid with variable thermal conductivity was studied by Asad et al. [12]. The MHD flow of an incompressible fluid over a moving surface with a convective boundary condition was studied by Makinde [13]. Sreenadh et al. [14] investigated the flow of a couple stress fluid in a vertical porous layer by applying perturbation method.

Thermal radiation effect plays a significant role in controlling heat transfer processes in polymer processing industries. Additionally, the effect of thermal radiation on flow and heat transfer processes is of major importance in the design of many advanced energy convection systems which operate at high temperatures. Thermal radiation in these systems is usually the result of emission from hot walls and the working fluid. Thermal radiation becomes important when the difference between the surface and the ambient temperature is large. Thus an understanding of radiation heat transfer in a system may assist in achieving productswith desired characteristics. The influence of thermal radiation on hydromagnetic Darcy-Forchheimer mixed convection flow past a stretching sheet embedded in a porous medium was examined by, among others, Pal and Mondal [15].

There is a large number of practical situations in which convection is driven by internal heat sources. This occurs for instance in nuclear heat cores, nuclear disposals, oil extraction and crystal growth. Double diffusive convection in a couple stress fluid with internal heat source was studied by Gaikwad and Kouser [16]. Chamka [17] found solutions for hydromagnetic heat and mass transfer from an inclined plate with internal heat generation or absorption. Hill [18] analyzed double diffusive convection in a porous medium with a concentration based internal heat source. The onset of convection in a porous medium with internal heat generation was investigated by Gasser and Kazimi [19]. Capone et al. [20] analyzed double diffusive penetrative convection with internal heating in an anisotropic porous layer with through flow.

Nagaraju et al. [21] analyzed the effects of thermal radiation, a chemical reaction and heat generation in a nanofluid. Rehman et al. [22] investigated porosity and nano-concentration effects on the stagnation flow of a couple stress fluid over an exponentially stretching surface. Das [23] studied the effects of thermal radiation and chemical reaction on unsteady MHD free convection heat and mass transfer flow of a micropolar fluid past a vertical porous plate in a rotating frame of reference, assuming that the plate is embedded in a uniform porous medium and oscillates in time with a constant frequency in the presence of a transverse magnetic field. Srinivasacharya and Mendu [24] analyzed the flow and heat and mass transfer characteristics of the free convection on a vertical plate with uniform wall temperature and concentration in a micropolar fluid in the presence of a first-order chemical reaction and radiation. Jain et al. [25] studied the effects of radiation and couple stress parameters on unsteady magnetopolar free convection flow with mass transfer and thermal radiation in slip flow regime. The effect of rotation on the onset of double diffusive convection in a Darcy porous medium saturated with a couple stress fluid was studied by Malashetty et al. [26]. The effect of rotation on the onset of double diffusive convection in a horizontal anisotropic porous layer was studied by Malashetty and Heera [27]. Convective instability in either a couple stress fluid layer or couple stress fluid-saturated porous layer heated from below has been investigated in the recent past including the effects of an additional diffusing component (i.e., solute concentration) and external constraints such as magnetic field and /or rotation. Sunil et al. [28] investigated the effect of a magnetic field and rotation on a layer of couple stress fluid heated from below in a porous medium. Sharma and Sharma [29] have investigated the effect of suspended particles on electrically conducting couple stress fluid heated uniformly from below under the influence of uniform rotation and magnetic field.

In this paper, we present a study of the flow of a couple stress nanofluid over a stretching sheet in a magneto-porous medium with thermal radiation and chemical reaction. The model equations are solved using a method that combines the Chebyshev spectral collocation, bivariate Lagrange interpolation polynomials together with spectral quasi-linearization method (SQLM) is used. Residual error estimation is presented to show the high accuracy and fast convergence of the
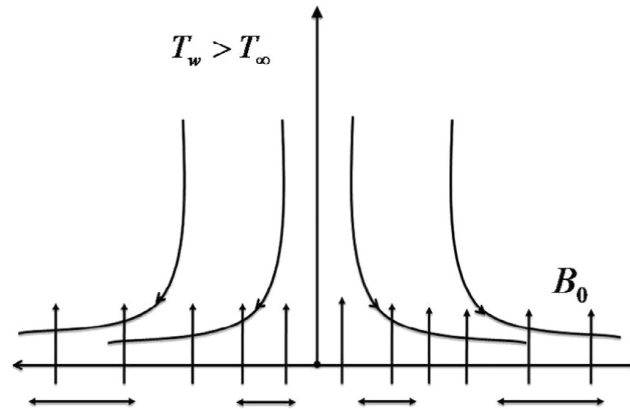
Fig. 1. Physical model and coordinate system.

numerical technique. In fact, the main feature of this study is to introduce the size dependent on classical viscous theory which are synthetic liquids, electro-rheological and Blood.

2. Mathematical formulations

Consider the steady two-dimensional magneto-porous medium flow of an incompressible couple stress nanofluid over a stretching sheet with thermal radiation and heat generation. In a rectangular coordinate system $(\bar{x}, \bar{y})$, the sheet is assumed to coincide with $\bar{y} = 0$ and the flow takes place in the semi-infinite porous space $\bar{y} > 0$ of constant permeability (see Fig. 1). A magnetic field of strength is applied perpendicular to the stretching surface. It is assumed that the sheet is stretched with velocity $u_w = bx$ in which b is the stretching rate. The sheet is maintained at a uniform temperature $T_w > T_\infty$ where T_∞ is the temperature of the ambient fluid. The objective is to determine the velocity, temperature and concentration fields inside the fluid satisfying the boundary conditions at the wall and far from the wall. To this end, we apply the boundary layer approximation to the continuity, momentum, concentration and energy equations to obtain,

$$\frac{\partial u}{\partial \bar{x}} + \frac{\partial v}{\partial \bar{y}} = 0 \tag{1}$$

$$u\frac{\partial u}{\partial \bar{x}} + v\frac{\partial u}{\partial \bar{y}} = \nu\frac{\partial^2 u}{\partial \bar{y}^2} - \frac{\eta_0}{\rho}\frac{\partial^4 u}{\partial \bar{y}^4} - \frac{\sigma B_0^2}{\rho}u - \frac{\nu\phi}{k^*}u + g\beta_t(T - T_\infty) + g\beta_c(C - C_\infty) \tag{2}$$

$$u\frac{\partial T}{\partial \bar{x}} + v\frac{\partial T}{\partial \bar{y}} = \frac{\kappa}{\rho C_p}\frac{\partial^2 T}{\partial \bar{y}^2} - \frac{1}{\rho C_p}\frac{\partial q_r}{\partial \bar{y}} + \frac{Q}{\rho C_p}(T - T_\infty) + \tau\left[D_B\frac{\partial C}{\partial \bar{y}}\cdot\frac{\partial T}{\partial \bar{y}} + \frac{D_T}{T_\infty}\left(\frac{\partial T}{\partial \bar{y}}\right)^2\right] \tag{3}$$

$$u\frac{\partial C}{\partial \bar{x}} + v\frac{\partial C}{\partial \bar{y}} = D_B\frac{\partial^2 C}{\partial \bar{y}^2} + \frac{D_T}{T_\infty}\frac{\partial^2 T}{\partial \bar{y}^2} - R(C - C_\infty) \tag{4}$$

where u and v are the velocity components along the $\bar{x}$ and $\bar{y}$-directions, respectively, ν is the kinematic viscosity, ρ is the density, η_0 is the material constant for the couple stress fluid, σ is electric conductivity, Q is the heat source coefficient, κ is the thermal conductivity, B_0 is the strength of constant applied magnetic field, D_B is the Brownian diffusion coefficient, D_T is the thermophoretic diffusion coefficient, $\tau = \frac{(\rho c)_p}{(\rho c)_f}$ is the ratio of the effective heat capacity of the nanoparticle material to heat capacity of the fluid and C is the volumetric volume expansion coefficient. The flow is subject to the following boundary conditions

$$u = u_w = b\bar{x}, \quad v = 0, \quad \frac{\partial^2 u}{\partial \bar{y}^2} = 0, \quad T = T_w, \quad C = C_w, \quad at \ \ \bar{y} = 0, \tag{5}$$

$$u = 0, \quad \frac{\partial u}{\partial \bar{y}} = 0, \quad T = T_\infty, \quad C = C_\infty \quad at \quad \bar{y} \to \infty \tag{6}$$

Using the Rosseland diffusion approximation, the radiation heat flux is given by $q_r = -\frac{4\sigma^*}{3k^*}\frac{\partial T^4}{\partial y}$ where σ^* is the Stephan Boltzmann constant and k^* is the mean absorption coefficient. The wall temperature excess ratio parameter is $\theta_w = \frac{T_w}{T_\infty}$

where T^4 may be expressed as $T^4 = T_\infty^4 \{1 + (\theta_w - 1)\theta\}^4$. The governing nonlinear partial differential equations are transformed into a system of ordinary differential equations using similarity transformations defined by,

$$y = \sqrt{\frac{b}{\nu}}\bar{y}, \quad u = b\bar{x}f_y(y), \quad v = -\sqrt{\nu b}f(y),$$

$$\theta(y) = \frac{T - T_\infty}{T_w - T_\infty}, \quad H(y) = \frac{C - C_\infty}{C_w - C_\infty}. \tag{7}$$

We obtain a system of non-linear ordinary differential equations with appropriate boundary conditions as follows:

$$kf^v - f''' - ff'' + f'^2 + \beta f' - Gr_t\theta - Gr_cH = 0 \tag{8}$$

$$\left[1 + Nr\{1 + (\theta_w - 1)\theta\}^3\right]\theta'' + 3Nr(\theta_w - 1)\{1 + (\theta_w - 1)\theta\}\theta'^2 + Pr(f\theta' + \lambda\theta) + Pr(Nb\theta'H' + Nt\theta'^2) = 0 \tag{9}$$

$$\frac{1}{Le}\left(H'' + \frac{Nt}{Nb}\theta''\right) + fH' - R_1H = 0 \tag{10}$$

the boundary conditions takes the following forms:

$$f(0) = 0, \quad f'(0) = 1, \quad f'''(0) = 0, \quad \theta(0) = 1, \quad H(0) = 1$$

$$f'(\infty) = 0, \quad f''(\infty) = 0, \quad \theta(\infty) = 0, \quad H(\infty) = 0, \tag{11}$$

where the non-dimensional parameters in the above equations are: $k = (\eta_0 b/\rho\nu^2)$ is the couple stress parameter, $\beta(= \sigma B_0^2/\rho b + \nu\phi/kb)$ is the magneto-porous parameter, $Gr_t(= g\beta(T_w - T_\infty)x^3/\nu^2)$ is the temperature Grashof number, $Gr_c(= g\beta(C_w - C_\infty)x^3/\nu^2)$ is the mass Grashof number, $Nr =$ is the thermal radiation parameter, θ_w is the temperature ratio parameter, $Pr(= \nu/\alpha)$ is the Prandtl number, $\lambda(= Q/c\rho c_p)$ is the heat source $(\lambda > 0)$ or sink $(\lambda < 0)$, $Nb(= \tau D_B(C_w - C_\infty)/\nu)$ is the Brownian motion parameter, $Nt(= \tau D_T(T_w - T_\infty)/\nu T_\infty)$ is the thermophoresis parameter, $Le(= \nu/D_B)$ is the Lewis number, $R_1(= R(C_w - C_\infty))$ is the chemical reaction parameter.

The local Nusselt number, and the local Sherwood numbers are defined by

$$C_f = \frac{\tau_w}{\rho u_w^2}, \quad Nu_x = \frac{\bar{x}q_w}{k(T_w - T_\infty)}, \quad Sh_x = \frac{\bar{x}q_m}{D_B(C_w - C_\infty)}, \tag{12}$$

where

$$\tau_w = \mu\left(\frac{\partial u}{\partial\bar{y}}\right)_{\bar{y}=0} - \frac{\eta_0}{\rho}\left(\frac{\partial^3 u}{\partial\bar{y}^3}\right), \quad q_w = -\left[\left(\frac{16\sigma^*T^3}{3k^*} + k\right)\frac{\partial T}{\partial y}\right]_{\bar{y}=0}$$

$$q_m = -D_B\left(\frac{\partial C}{\partial\bar{y}}\right)_{\bar{y}=0} \tag{13}$$

Using the non-dimensional variables (7) and the relation (12) in (13), we obtain

$$C_f Re_x^{1/2} = f''(0) - kf''''(0),$$

$$Nu_x Re_x^{-1/2} = -(1 + Nr\theta_w^3)\theta'(0)$$

$$Sh_x Re_x^{-1/2} = -H'(0), \tag{14}$$

where $Re_x = \frac{u_w\bar{x}}{\nu}$ is the local Reynolds number.

3. Method of Solution

The spectral quasi-linearization method (SQLM) identifies nonlinear terms which are linearized using Taylor series expansion. The SQLM has been described as being efficient with faster convergence compared to numerical methods such as the Runge–Kutta methods, Motsa et al. [30].

$$F \equiv kf^v - f''' - ff'' + f'^2 + \beta f' - Gr_t\theta - Gr_cH = 0$$

$$\Phi \equiv H'' + \frac{Nt}{Nb}\theta'' + LefH' - LeR_1H = 0$$

$$\Theta \equiv \left[1 + Nr(1 + \theta(\theta_w - 1))^3\right]\theta'' + 3Nr(\theta_w - 1)\theta'^2(1 + \theta(\theta_w - 1))$$

$$+ Pr(f\theta' + \lambda\theta) + Pr(Nb\theta'H' + Nt\theta'^2 = 0) \tag{15}$$

From the system of Eqs. (8)–(10) the nonlinear terms ff', f'^2, θ'^2, $f\theta'$, $\theta\theta''$, $\theta'^2\theta$, fH' and $\theta'H'$ are linearized using Taylor series expansion as

$$ff'' = f_r f''_{r+1} + f''_r f_{r+1} - f_r f''_r \tag{16}$$

$$f'^2 = 2f'_r f'_{r+1} - f'^2_r \tag{17}$$

$$\theta'^2 = 2\theta'_r \theta'_{r+1} - \theta'^2_r \tag{18}$$

$$f\theta' = f_r \theta'_{r+1} + \theta'_r f_{r+1} - f_r \theta'_r \tag{19}$$

$$\theta\theta'' = \theta_r \theta''_{r+1} + \theta''_r \theta_{r+1} - \theta_r \theta''_r \tag{20}$$

$$\theta'^2\theta = 2\theta'_r \theta_r \theta'_{r+1} + \theta'^2_r \theta_{r+1} - 2\theta'^2_r \theta_r \tag{21}$$

$$fH' = f_r H'_{r+1} + H'_r f_{r+1} - f_r H'_r \tag{22}$$

$$\theta'H' = \theta'_r H'_{r+1} + H'_r \theta'_{r+1} - \theta'_r H'_r \tag{23}$$

where the terms containing the subscripts $r+1$ denote the current iteration and terms containing the subscripts r denote previous approximations. Eqs. (16)–(23) are substituted into Eqs. (8)–(10) and the resulting linearized equations are solved as a coupled linear system.

$$
\begin{aligned}
&a_{0,r} f^v_{r+1} + a_{1,r} f^{iv}_{r+1} + a_{2,r} f'''_{r+1} + a_{3,r} f''_{r+1} + a_{4,r} f'_{r+1} + a_{5,r} f_{r+1} + a_{6,r} \theta_{r+1} + a_{5,r} H_{r+1} = R_F,\\
&b_{0,r} \theta''_{r+1} + b_{1,r} \theta'_{r+1} + b_{2,r} \theta_{r+1} + b_{3,r} f_{r+1} + b_{4,r} H'_{r+1} = R_\Theta,\\
&c_{0,r} H''_{r+1} + c_{1,r} H'_{r+1} + c_{2,r} H_{r+1} + c_{3,r} f_{r+1} + c_{4,r} \theta''_{r+1} = R_\Phi,
\end{aligned}
\tag{24}
$$

where

$$a_{0,r} = \frac{\partial F}{\partial f^v} = K, \quad a_{1,r} = \frac{\partial F}{\partial f^{iv}} = 0, \quad a_{2,r} = \frac{\partial F}{\partial f'''} = -1, \quad a_{3,r} = \frac{\partial F}{\partial f''} = -f_r,$$

$$a_{4,r} = \frac{\partial F}{\partial f'} = 2f'_r + \beta, \quad a_{5,r} = \frac{\partial F}{\partial f} = -f''_r, \quad a_{6,r} = \frac{\partial F}{\partial \theta} = -Gr_t, \quad a_{7,r} = \frac{\partial F}{\partial H} = -Gr_c,$$

$$b_{0,r} = \frac{\partial \Theta}{\partial \theta''} = 1 + Nr[1 + \theta_r(\theta_w - 1)]^3, \, b_{1,r} = \frac{\partial \Theta}{\partial \theta'} = 6Nr(\theta_w - 1)\theta'_r[1 + \theta_r(\theta_w - 1)]^2,$$

$$b_{2,r} = \frac{\partial \Theta}{\partial \theta} = 3Nr(\theta_w - 1)\theta''_r[1 + \theta_r(\theta_w - 1)]^2 + 6Nr(\theta_w - 1)^2\theta'^2_r[1 + \theta_r(\theta_w - 1)] + Pr\lambda,$$

$$b_{3,r} = \frac{\partial \Theta}{\partial f} = Pr\theta'_r, \quad b_{4,r} = \frac{\partial \Theta}{\partial H'} = PrNb\theta'_r,$$

$$c_{0,r} = \frac{\partial \Phi}{\partial H''} = 1, \quad c_{1,r} = \frac{\partial \Phi}{\partial H'} = Lef_r, \quad c_{2,r} = \frac{\partial \Phi}{\partial H} = -R_1,$$

$$c_{3,r} = \frac{\partial \Phi}{\partial f} = LeH'_r, \quad c_{4,r} = \frac{\partial \Phi}{\partial \theta''} = \frac{Nt}{Nb}. \tag{25}$$

Spectral collocation is applied using the differentiation matrix **D** to approximate derivatives of the unknown functions, and the new system of equations obtained is solved as a coupled matrix system.

$$
\begin{aligned}
&A_{11}F_{r+1} + A_{12}\Theta_{r+1} + A_{13}\Phi_{r+1} = B_1,\\
&A_{21}F_{r+1} + A_{22}\Theta_{r+1} + A_{23}\Phi_{r+1} = B_2,\\
&A_{31}F_{r+1} + A_{32}\Theta_{r+1} + A_{33}\Phi_{r+1} = B_3.
\end{aligned}
\tag{26}
$$

where

$$A_{11} = \mathbf{diag}[\mathbf{a}_{0,r}]\mathbf{D}^5 + \mathbf{diag}[\mathbf{a}_{1,r}]\mathbf{D}^4 + \mathbf{diag}[\mathbf{a}_{2,r}]\mathbf{D}^3 + \mathbf{diag}[\mathbf{a}_{3,r}]\mathbf{D}^2 + \mathbf{diag}[\mathbf{a}_{4,r}]\mathbf{D} + \mathbf{diag}[\mathbf{a}_{5,r}]\mathbf{I},$$

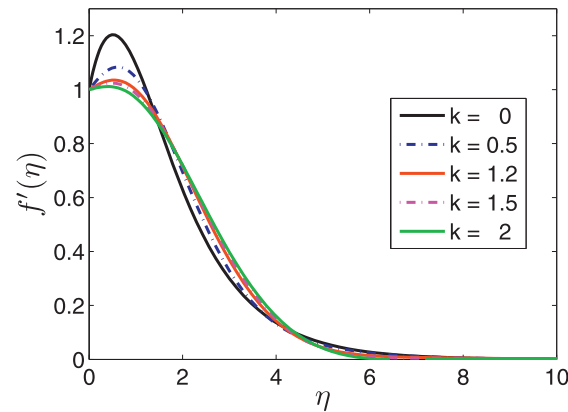$$A_{12} = \mathbf{diag}[\mathbf{a}_{6,r}]\mathbf{I}, \quad A_{13} = \mathbf{diag}[\mathbf{a}_{7,r}]\mathbf{I}$$

Fig. 2. Effect of k on the velocity profile $f'(\eta)$. Parameter values $Gr_t = 0.5$; $Gr_c = 0.3$; $Le = 0.22$; $\beta = 0.5$; $Nr = 0.5$; $\beta = 0.2$; $Pr = 6.8$; $\lambda = 0.2$; $Nb = 0.3$; $\theta_w = 1.2$; $R_1 = 0.5$; and $Nt = 0.3$.
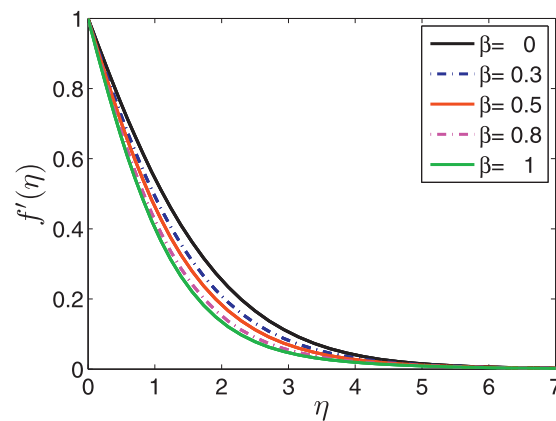

Fig. 3. Effect of β on the velocity profile $f'(\eta)$. Parameter values $k = 0.4$; $Gr_t = 0.1$; $Gr_c = 0.5$; $Le = 0.22$; $\beta = 0.5$; $Nr = 0.5$; $Pr = 6.8$; $\lambda = 0.2$; $Nb = 0.2$; $\theta_w = 1.2$; $R_1 = 0.5$; and $Nt = 0.1$.

$$\mathbf{A_{21}} = \mathbf{diag}[\mathbf{b}_{3,r}], \quad \mathbf{A_{22}} = \mathbf{diag}[\mathbf{b}_{0,r}]\mathbf{D}^2 + \mathbf{diag}[\mathbf{b}_{1,r}]\mathbf{D} + \mathbf{diag}[\mathbf{b}_{2,r}], \quad \mathbf{A_{23}} = \mathbf{diag}[\mathbf{b}_{4,r}]\mathbf{D}$$

$$\mathbf{A_{31}} = \mathbf{diag}[\mathbf{c}_{3,r}], \quad \mathbf{A_{32}} = \mathbf{diag}[\mathbf{b}_{4,r}]\mathbf{D}^2, \quad \mathbf{A_{33}} = \mathbf{diag}[\mathbf{c}_{0,r}]\mathbf{D}^2 + \mathbf{diag}[\mathbf{c}_{1,r}]\mathbf{D} + \mathbf{diag}[\mathbf{c}_{2,r}],$$

$$\mathbf{B}_1 = \mathbf{R}_F, \mathbf{B}_2 = \mathbf{R}_\theta, \mathbf{B}_3 = \mathbf{R}_\phi, \tag{27}$$

The values of the space derivatives at the Chebyshev–Gauss–Lobatto points (η_i) $(i = 0, 1, 2, \ldots, N_\eta)$ are computed as

$$\left. \frac{\partial u}{\partial \eta} \right|_{\eta = \eta_i} = \sum_{j=0}^{N_\eta} u(\eta_j) \frac{dL_j(\eta_i)}{d\eta} \tag{28}$$
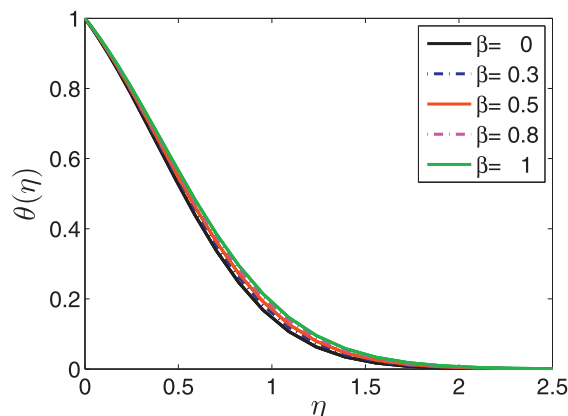
$$= \sum_{j=0}^{N_\eta} u(\eta_j) D_{ij} = \sum_{j=0}^{N_\eta} D_{ij} u(\eta_j), \tag{29}$$

where $D_{ij} = \frac{dL_p(\eta_i)}{d\eta}$, is the standard first derivative Chebyshev differentiation matrix of size $(N_\eta + 1) \times (N_\eta + 1)$. Similarly, for an nth order derivative, we have

$$\left. \frac{\partial^n u}{\partial \eta^n} \right|_{\eta = \eta_i} = \sum_{j=0}^{N_\eta} D_{ij}^n u(\eta_j) = \mathbf{D}^n \mathbf{U}_j, \quad i = 0, 1, 2, \ldots, N_\eta, \tag{30}$$

where the vector $\mathbf{U}_j$ is defined as

$$\mathbf{U}_j = [u_j(\eta_0), u_j(\eta_1), \ldots, u_j(\eta_{N_\eta})]^T. \tag{31}$$

Fig. 4. Effect of β on the temperature profile $\theta'(\eta)$. Parameter values $k = 0.4$; $Gr_t = 0.1$; $Gr_c = 0.5$; $Le = 0.22$; $\beta = 0.5$; $Nr = 0.5$; $Pr = 6.8$; $\lambda = 0.2$; $Nb = 0.2$; $\theta_w = 1.2$; $R_1 = 0.5$; and $Nt = 0.1$.

and the superscript T denotes matrix transpose. In this problem U is replaced with f, θ and H as the unknowns. The boundary conditions are imposed on the individual matrices as shown in the matrix below,

$$
\begin{bmatrix}
D_{1,1} & \dots & D_{1,N+1} & 0 & 0 & \dots & 0 & 0 & 0 & \dots & 0 \\
D_{2,1}^2 & \dots & D_{2,N+1}^2 & 0 & 0 & \dots & 0 & 0 & 0 & \dots & 0 \\
 & A_{11} & & & A_{12} & & & & A_{13} & & \\
D_{N-1,1}^3 & \dots & D_{N-1,N+1}^3 & 0 & 0 & \dots & 0 & 0 & 0 & \dots & 0 \\
D_{N,1} & \dots & D_{N,N+1} & 0 & 0 & \dots & 0 & 0 & 0 & \dots & 0 \\
0 & \dots & 1 & 0 & 0 & \dots & 0 & 0 & 0 & \dots & 0 \\
0 & 0 & 0 & \dots & 0 & 1 & 0 & \dots & 0 & 0 & 0 & \dots & 0 \\
 & A_{21} & & & A_{22} & & & & A_{23} & & \\
0 & 0 & 0 & \dots & 0 & 0 & 0 & \dots & 1 & 0 & 0 & \dots & 0 \\
0 & 0 & 0 & \dots & 0 & 0 & 0 & \dots & 0 & 1 & 0 & \dots & 0 \\
 & A_{31} & & & A_{32} & & & & A_{33} & & \\
0 & 0 & 0 & \dots & 0 & 0 & 0 & \dots & 0 & 0 & 0 & \dots & 1
\end{bmatrix}
\begin{bmatrix}
f_{r+1}(\eta_0) \\
f_{r+1}(\eta_1) \\
\vdots \\
f_{r+1}(\eta_{N-1}) \\
f_{r+1}(\eta_N) \\
f_{r+1}(\eta_{N+1}) \\
\theta_{r+1}(\eta_0) \\
\vdots \\
\theta_{r+1}(\eta_{N+1})) \\
H_{r+1}(\eta_0) \\
\vdots \\
H_{r+1}(\eta_{N+1})
\end{bmatrix}
=
\begin{bmatrix}
0 \\
0 \\
B_1 \\
0 \\
1 \\
0 \\
0 \\
B_2 \\
1 \\
0 \\
B_3 \\
1
\end{bmatrix}
$$

## 4. Results and discussion

The set of nonlinear partial differential equations (8)–(10) with boundary conditions (11) were solved numerically using the SQLM and the significance of the physical parameters is illustrated through graphs. We have compared our Nusselt number results with data in the literature. The results are in good agreement with the literature (see Table 1) with those of Chen [31] and Zaimi [32]. The values of Nusselt number and Sherwood number are tabulated in Table 2 for various values of the thermophoresis parameter Nt. It is found that the local Nusselt number decreases with increases in the thermophoresis parameter Nt and reverse trends are seen for the local Sherwood number. The effects of couple stress parameter, transverse magnetic field, energy enhancement parameters Nb and Nt, Prandtl number, chemical reaction and radiation parameter on the velocity, temperature and concentration profiles are discussed.

In Fig. 2, the effects of the couple stress parameter k on the dimensionless velocity profiles are presented for fixed values of $Gr_t = 0.5$; $Gr_c = 0.3$; $Le = 0.22$; $\beta = 0.5$; $Nr = 0.5$; $\beta = 0.2$; $Pr = 6.8$; $\lambda = 0.2$; $Nb = 0.3$; $\theta_w = 1.2$; $R_1 = 0.5$; and $Nt = 0.3$. As k increases it can be observed that the maximum velocity decreases when $0 < \eta < 2$ and the location of the maximum velocity moves away from the wall. This happens because the power-index is high for couple stress fluid.

Figs. 3–5 show the variation of the velocity and temperature profiles for different values of the magnetic parameter β. Fig. 3 shows that the velocity profiles considerably reduce with an increase in the value of the magnetic field. The presence
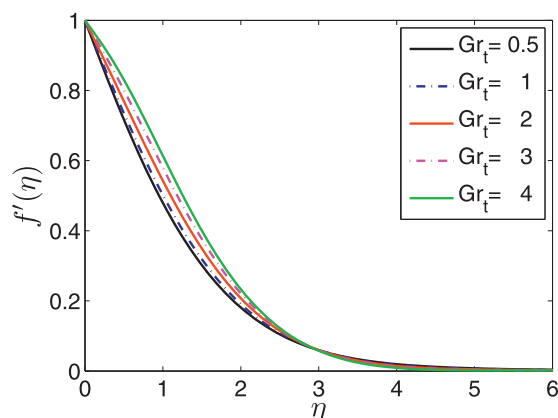
Fig. 5. Residual error for Gr_t on the velocity profile $f'(\eta)$ when $k = 0.5$; $Gr_c = 0.5$; $Le = 0.22$; $\beta = 0.5$; $Nr = 0.5$; $Pr = 6.8$; $\lambda = 0.2$; $Nb = 0.3$; $\theta_w = 1.2$; $R_1 = 0.5$; and $Nt = 0.1$.
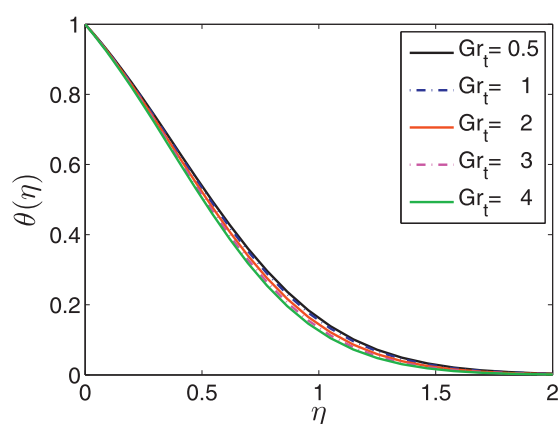
Fig. 6. Effect of Gr_t on the temperature profile $\theta(\eta)$ when $k = 0.5$; $Gr_c = 0.5$; $Le = 0.22$; $\beta = 0.5$; $Nr = 0.5$; $Pr = 6.8$; $\lambda = 0.2$; $Nb = 0.3$; $\theta_w = 1.2$; $R_1 = 0.5$; and $Nt = 0.1$.

Table 1
Comparison of the values of the Nusselt number $Nu_x = \theta'(0)$ with published data for $M = Nb = Nt = \beta = Nr = k = Grt = Grc = 0$, and $\theta_w = 1$ between results of present study and reported by Chen [31] and Zaimi et al. [32] for various values of Pr. For the current study the number of iterations that were required to reach converge was 4 iterations.

Pr	Chen [32]	Zaimi et al.[33]	Current study
0.72	0.46315	0.463145	0.46314490
1	0.58199	0.581977	0.58197671
3	1.16523	1.165246	1.16524595
7	1.89537	1.895403	1.89540326
10	2.30796	2.308004	2.30800394

of the magnetic field produces a Lorentz force which acts in the opposite direction to the fluid motion resulting in a decrease in the fluid velocity and an increase in the fluid temperature as shown in Fig. 4.
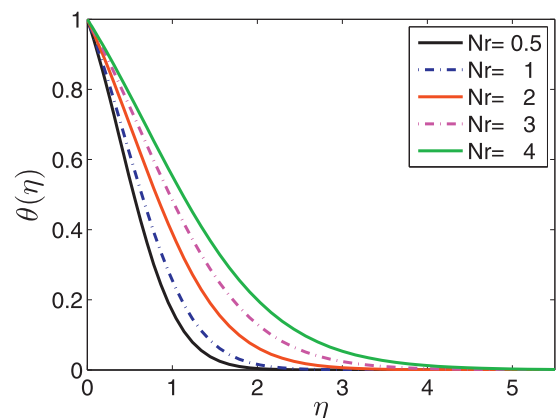
The velocity $f'(\eta)$ and temperature $\theta(\eta)$ profiles for various values of Gr_t are shown in Figs. 5 and 7. It is observed that the effect of increasing the thermal buoyancy parameter Gr_t is to increase the velocity profiles in the momentum boundary layer due to the cooling of the plate by the free convection current. Physically, in the process of cooling the free convection current are carried away from the plate to the free stream and since the free stream is in the upward direction and thus the free stream current induce the velocity to enhance. It is also noted that from Fig. 6 for large value of Gr_t the temperature decreases at the beginning until it achieve peak value and then start decreasing until the value reaches to zero outside of the boundary layer. This is because a large value of Gr_t produces a large buoyancy force, which produces the large kinetic energy.
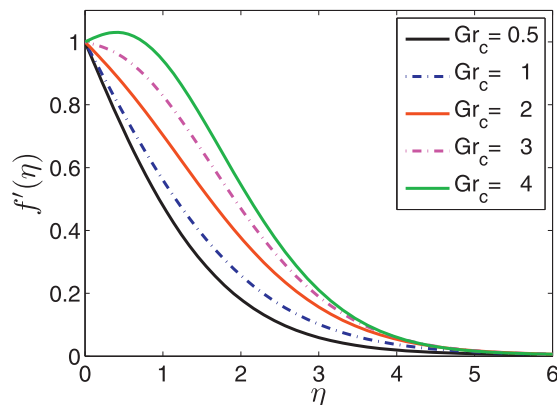
Fig. 7. Effect of Gr_c on the velocity profile $f'(\eta)$ when $k = 0.5$; $Gr_t = 0.5$; $Le = 0.22$; $\beta = 0.5$; $Nr = 0.5$; $Pr = 6.8$; $\lambda = 0.2$; $Nb = 0.3$; $\theta_w = 1.2$; $R_1 = 0.5$; and $Nt = 0.1$.
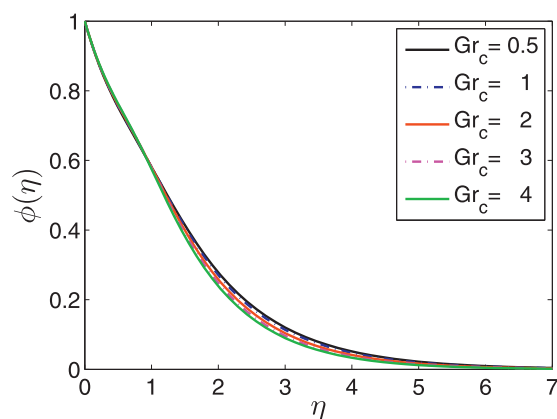

Fig. 8. Effect of Gr_c on the concentration profile $\phi(\eta)$ when $k = 0.5$; $Gr_t = 0.5$; $Le = 0.22$; $\beta = 0.5$; $Nr = 0.5$; $Pr = 6.8$; $\lambda = 0.2$; $Nb = 0.3$; $\theta_w = 1.2$; $R_1 = 0.5$; and $Nt = 0.1$

Fig. 9. Effect of Nr on the temperature profile $\theta(\eta)$ when $k = 0.5$; $Gr_c = 0.3$; $Gr_t = 0.5$; $Le = 0.22$; $\beta = 0.5$; $Pr = 6.8$; $\lambda = 0.2$; $Nt = 0.2$; $Nb = 0.3$ and $R_1 = 0.5$.

Figs. 7–9 show the velocity and concentration profiles for different solutal Grashof numbers Gr_c, for fixed values of $k = 0.5$; $Gr_t = 0.5$; $Le = 0.22$; $\beta = 0.5$; $Nr = 0.5$; $Pr = 6.8$; $\lambda = 0.2$; $Nb = 0.3$; $\theta_w = 1.2$; $R_1 = 0.5$; and $Nt = 0.1$. We observe from Fig. 7 that the velocity profiles increase with an increase in the value of Gr_c. It is also seen from Fig. 8 that the effect of increasing the solutal buoyancy parameter Gr_c is to reduce the concentration profiles throughout the boundary layer.
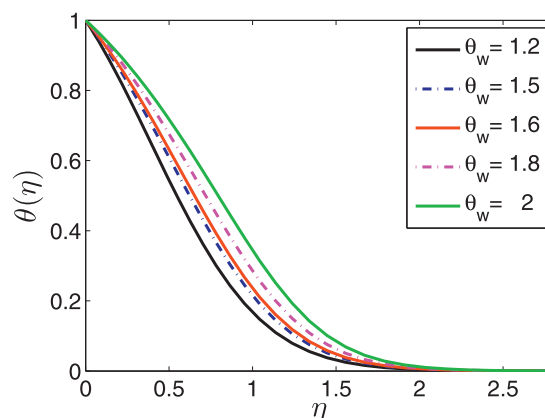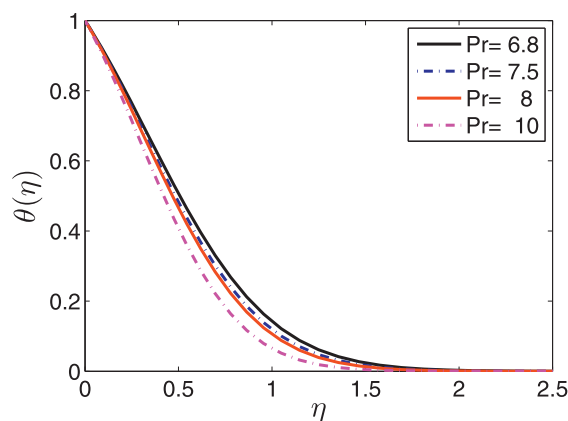
Fig. 10. Effect of θ_w on the temperature profile $\theta(\eta)$ when $k = 0.5$; $Gr_c = 0.3$; $Gr_t = 0.5$; $Le = 0.22$; $\beta = 0.5$; $Nr = 0.5$; $Pr = 6.8$; $\lambda = 0.2$; $Nt = 0.2$; $Nb = 0.3$ and $R_1 = 0.5$.

Fig. 11. Effect of Pr on the temperature profile $\theta(\eta)$. Parameter values $k = 0.2$; $Gr_t = 0.1$; $Gr_c = 0.5$; $Nr = 0.5$; $\beta = 0.5$; $\lambda = 0.2$; $Nb = 0.2$; $Le = 0.22$; $\theta_w = 1.2$; $R_1 = 0.5$; and $Nt = 0.2$.

Table 2
Comparison of the values of the Nusselt number $Nu_x = \theta'(0)$ and Sherwood number $Shr = -\phi'(0)$ with published data for $M = Nb = \beta = Nr = k = Gr_t = Gr_c = 0$, $Nt = 0.1$, $Pr = Le = 10$ and $\theta_w = 1$ between results of present study and reported by Khan and Pop [34] and Zaimi et al. [32] for various values of Nt.

Nt	Khan and Pop [33] Nu_x	Current study Nu_x	Khan and Pop [33] Sh_x	Current study Sh_x
0.1	0.9524	0.95237683	2.1294	2.12939377
0.2	0.6932	0.69317435	2.2740	2.27402146
0.3	0.5201	0.52007904	2.5286	2.52863819
0.4	0.4026	0.40258080	2.7952	2.79516989
0.5	0.3211	0.32105392	3.0351	3.03514402

It is important to note that increasing the thermal radiation parameter Nr leads to an increase in the temperature profiles $\theta(\eta)$ in the boundary layer as seen in Fig. 9. The slope of the temperature distribution curves near the surface show that the heat is always transferred from the surface to the ambient fluid.

Fig. 10 shows that the dimensionless temperature profiles increases as the temperature ratio parameter increases for different values of physical parameters $k = 0.5$; $Gr_c = 0.3$; $Gr_t = 0.5$; $Le = 0.22$; $\beta = 0.5$; $Nr = 0.5$; $Pr = 6.8$; $\lambda = 0.2$; $Nt = 0.2$; $Nb = 0.3$ and $R_1 = 0.5$. This result is expected because as the values of θ_w increases there is an increase in the values of temperature difference $T_w - T_\infty$ and so the temperature of the fluid increase.

Fig. 11 shows the effect of Prandtl numbers on the temperature profiles. It can be seen that the temperature decreases with Pr. The decrease observed in temperature is due to the fact that an increase in Pr leads to low thermal conductivity.

Figs. 12–14 shows temperature and concentration profiles for different values of the thermophoresis parameter Nt for $k = 0.5$; $Gr_c = 0.3$; $Gr_t = 0.5$; $Le = 0.22$; $\beta = 0.5$; $Nr = 0.5$; $Pr = 6.8$; $\lambda = 0.2$; $Nb = 0.3$; $\theta_w = 1.2$ and $R_1 = 0.5$. It is observed that an increase in the thermophoresis parameter Nt leads to increase in the fluid temperature and concentration profiles.
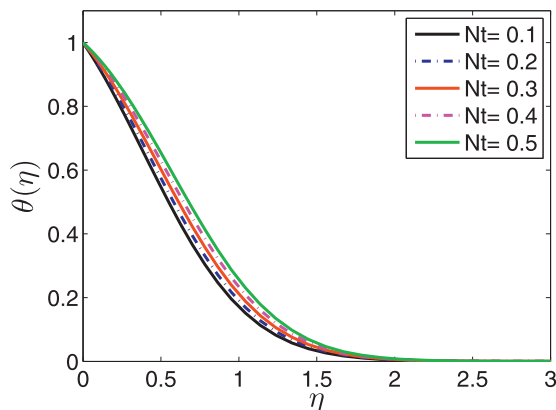
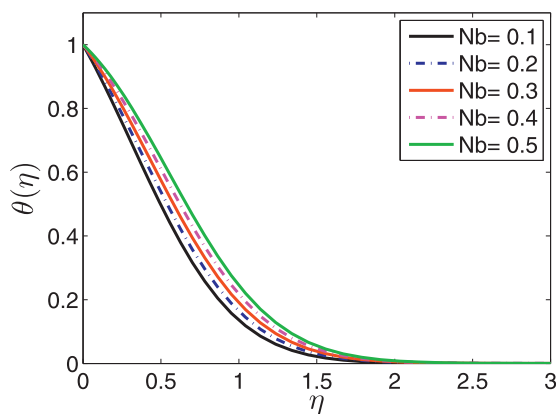**Fig. 12.** Effect of *Nt* on the temperature profile $\theta(\eta)$ when $k = 0.5$; $Gr_c = 0.3$; $Gr_t = 0.5$; $Le = 0.22$; $\beta = 0.5$; $Nr = 0.5$; $Pr = 6.8$; $\lambda = 0.2$; $Nb = 0.3$; $\theta_w = 1.2$ and $R_1 = 0.5$.
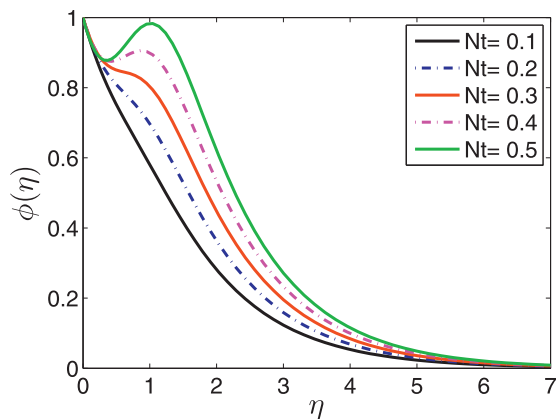
Fig. 13. Effect of *Nt* on the concentration profile $\phi(\eta)$ when $k = 0.5$; $Gr_c = 0.3$; $Gr_t = 0.5$; $Le = 0.22$; $\beta = 0.5$; $Nr = 0.5$; $Pr = 6.8$; $\lambda = 0.2$; $Nb = 0.3$; $\theta_w = 1.2$ and $R_1 = 0.5$.

Fig. 14. Effect of *Nb* on the temperature profile $\theta(\eta)$ when $k = 0.5$; $Gr_c = 0.3$; $Gr_t = 0.5$; $Le = 0.22$; $\beta = 0.5$; $Nr = 0.5$; $Pr = 6.8$; $\lambda = 0.2$; $Nt = 0.2$; $\theta_w = 1.2$ and $R_1 = 0.5$.

We also note that increasing *Nt*, leads to an in increase in temperature and concentration differences between the stretching surface and the ambient fluid.

The effect of the Brownian motion parameter *Nb* on temperature and concentration profiles is shown in Figs. 14–16. The boundary layer profiles for the temperature in case of regular heat transfer fluid increases with the increase in the Brownian motion parameter. This is due to enhanced molecular activity at higher values of *Nb* which increase the fluid temperature but reduce the fluid concentration profiles. The Brownian motion of the nanoparticles can enhance the thermal

Fig. 15. Effect of *Nb* on the concentration profile $\phi(\eta)$ when $k = 0.5$; $Gr_c = 0.3$; $Gr_t = 0.5$; $Le = 0.22$; $\beta = 0.5$; $Nr = 0.5$; $Pr = 6.8$; $\lambda = 0.2$; $Nt = 0.2$; $\theta_w = 1.2$ and $R_1 = 0.5$.
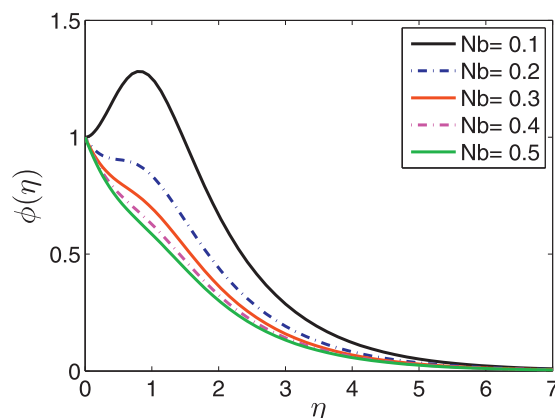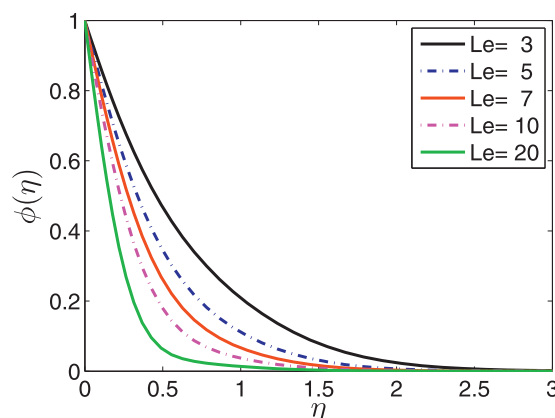

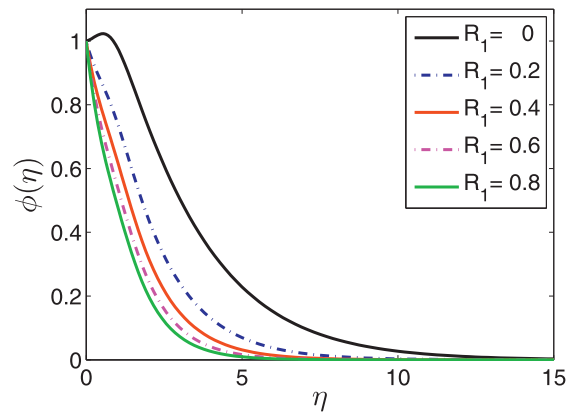
Fig. 16. Effect of *Le* on the concentration profile $\phi(\eta)$. Parameter values $k = 0.5$; $Gr_t = 0.1$; $Gr_c = 0.5$; $Nr = 0.5$; $\beta = 0.5$; $Pr = 6.8$; $\lambda = 0.1$; $Nb = 0.3$; $\theta_w = 1.2$; $R_1 = 0.5$; and $Nt = 0.1$.

conduction via two mechanisms; either a direct effect on nanoparticles that transport heat or indirect contribution due to micro convection of fluid surrounding individual nanoparticles. For small particles, Brownian motion is strong and the parameter *Nb* will have the higher value, the converse in the case of large particle and clearly Brownian motion does exert a significant effect on the temperature.

Fig. 16 shows the nanoparticle concentration profiles for large Lewis numbers and fixed parameters $k = 0.5$; $Gr_t = 0.1$; $Gr_c = 0.5$; $Nr = 0.5$; $\beta = 0.5$; $Pr = 6.8$; $\lambda = 0.1$; $Nb = 0.3$; $\theta_w = 1.2$; $R_1 = 0.5$; and $Nt = 0.1$. It is observed that the nanoparticle concentration distribution decreases with increasing Lewis numbers due to an inverse relationship with the Brownian diffusion coefficient. An increase in the Lewis number leads to a lower Brownian diffusion coefficient.

Fig. 17 shows the influence of the chemical reaction parameter R_1 on the concentration profiles. The chemical reaction parameter increases due to a decrease in the concentration boundary layer of the couple stress fluid. This indicates that the concentration of the diffusing species reduces during a fast reaction.

The residual error or fitting deviation is discussed for different parameters $\beta, Gr_t, Nr, \theta_w, Pr Nt, Nb, Le, R_1$. The residual errors are shown in Fig. 18 to 26 for purposes of determining the accuracy and convergence of the solution method. The residual error in temperature profiles $||Res|| \approx 10^{-8}$ rapidly converges for $0 < iteration < 10$ for magneto-porous parameter $\beta = 0, 0.3$ and thermal Grashof number $Gr_t = 1$. These results sufficiently demonstrate the accuracy and convergence of the method in Figs. 18 and 19. The residual error on the temperature profiles for thermal radiation parameter *Nr*, temperature ratio parameter θ_w and Prandtl number *Pr* rapidly convergent after the iterations $0 < iteration < 5$, $0 < iteration < 7$ and $0 < iteration < 9$ as shown in Figs. 20– 22, respectively. For further insights as to the accuracy and convergence of the method, we have calculated concentration residual errors as shown in Fig. 23–26, respectively. The residual errors rapidly decrease for the different values of $Nt = 0.2, Nb = 0.4, Le = 3$ and $R_1 = 0.4$.

H. Sithole et al./Applied Mathematics and Computation 339 (2018) 820–836

Fig. 17. Effect of R_1 on the concentration profile $\phi(\eta)$ when $k = 0.5$; $Gr_c = 0.3$; $Gr_t = 0.5$; $Le = 0.22$; $\beta = 0.5$; $Nr = 0.5$; $Pr = 6.8$; $\lambda = 0.2$; $Nt = 0.2$; $Nb = 0.3$ and $\theta_w = 1.2$.
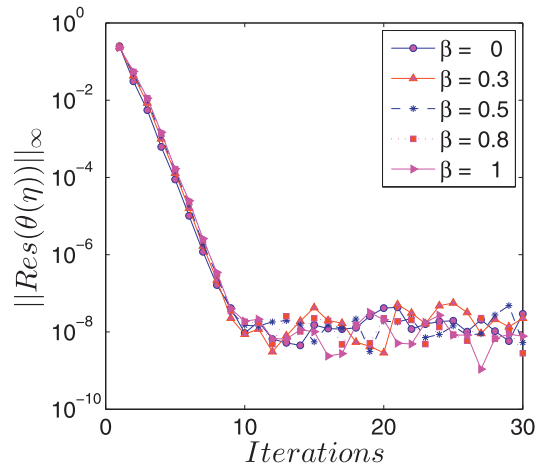
Fig. 18. Residual error for β on the temperature profile $\theta(\eta)$ when $k = 0.4$; $Gr_t = 0.1$; $Gr_c = 0.5$; $Le = 0.22$; $\beta = 0.5$; $Nr = 0.5$; $Pr = 6.8$; $\lambda = 0.2$; $Nb = 0.2$; $\theta_w = 1.2$; $R_1 = 0.5$; and $Nt = 0.1$.
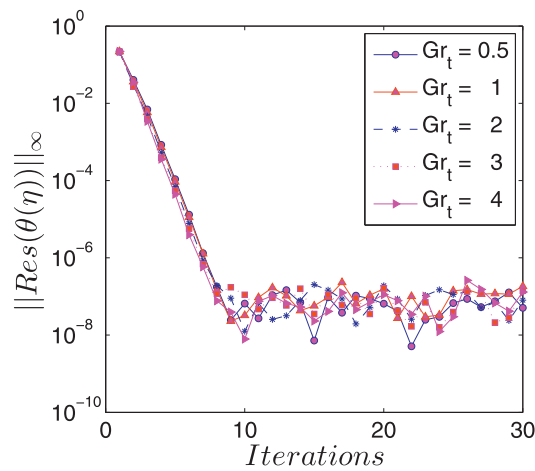
Fig. 19. Residual error for Gr_t on the temperature profile $\theta(\eta)$ when $k = 0.5$; $Gr_c = 0.5$; $Le = 0.22$; $\beta = 0.5$; $Nr = 0.5$; $Pr = 6.8$; $\lambda = 0.2$; $Nb = 0.3$; $\theta_w = 1.2$; $R_1 = 0.5$; and $Nt = 0.1$.

Fig. 20. Residual error for *Nr* on the temperature profile $\theta(\eta)$ when $k = 0.5$; $Gr_c = 0.3$; $Gr_t = 0.5$; $Le = 0.22$; $\beta = 0.5$; $Pr = 6.8$; $\lambda = 0.2$; $Nt = 0.2$; $\theta_w = 1.2$ and $R_1 = 0.5$;

Fig. 21. Residual error for θ_w on the temperature profile $\theta(\eta)$ when $k = 0.5$; $Gr_c = 0.3$; $Gr_t = 0.5$; $Le = 0.22$; $\beta = 0.5$; $Nr = 0.5$; $Pr = 6.8$; $\lambda = 0.2$; $Nt = 0.2$; and $R_1 = 0.5$;
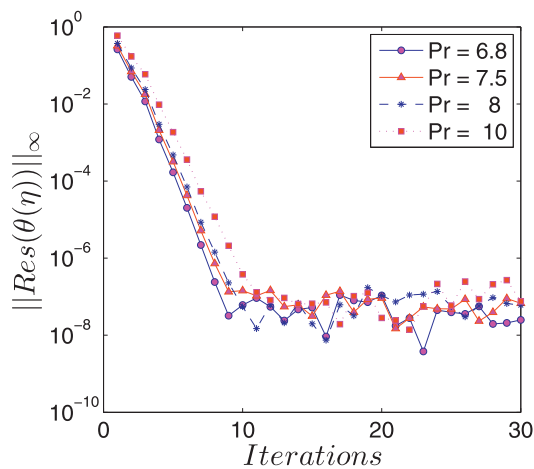
Fig. 22. Residual error for $\theta(\eta)$ when $Pr = 6.8, 7, 8, 10, 12$.
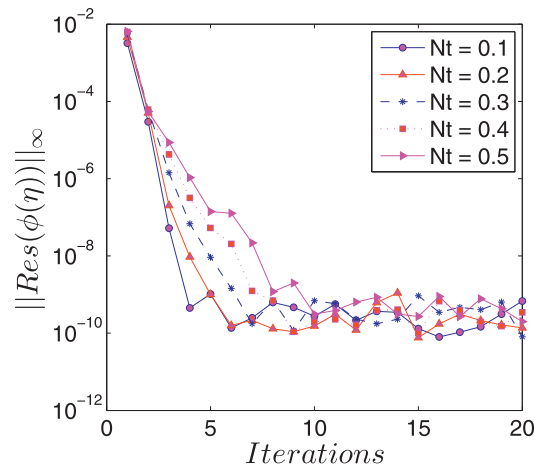
Fig. 23. Residual error for Nt on the concentration profile $\phi(\eta)$ when $k = 0.5$; $Gr_t = 0.5$; $Le = 0.22$; $\beta = 0.5$; $Nr = 0.5$; $Pr = 6.8$; $\lambda = 0.2$; $Nb = 0.3$; $\theta_w = 1.2$; $R_1 = 0.5$; and $Nt = 0.1$.

Fig. 24. Residual error for Nb on the concentration profile $\phi(\eta)$ when $k = 0.5$; $Gr_t = 0.5$; $Le = 0.22$; $\beta = 0.5$; $Nr = 0.5$; $Pr = 6.8$; $\lambda = 0.2$; $Nt = 0.2$; $\theta_w = 1.2$; $R_1 = 0.5$; and $Nt = 0.1$.

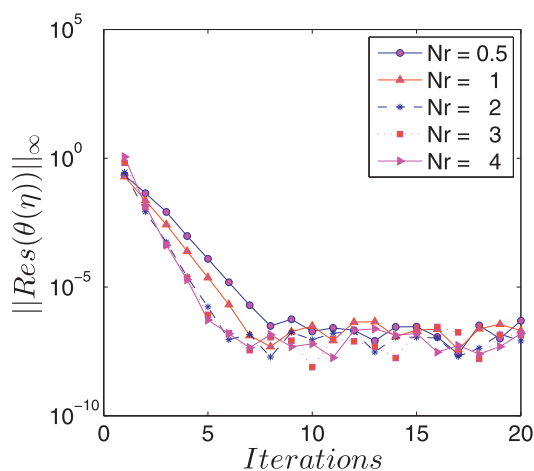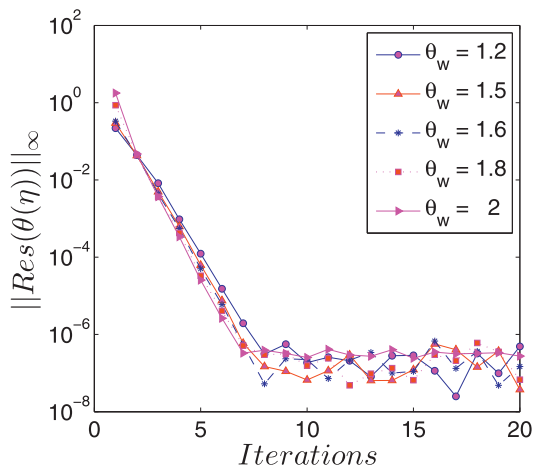**Fig. 25.** Residual error for $\phi(\eta)$ when $Le = 3, 5, 7, 10, 20$.

Fig. 26. Residual error for θ_w on the concentration profile $\phi(\eta)$ when $k = 0.5$; $Gr_c = 0.3$; $Gr_t = 0.5$; $Le = 0.22$; $\beta = 0.5$; $Nr = 0.5$; $Pr = 6.8$; $\lambda = 0.2$; $Nt = 0.2$; $\theta_w = 1.2$ and $\theta_w = 1.2$.
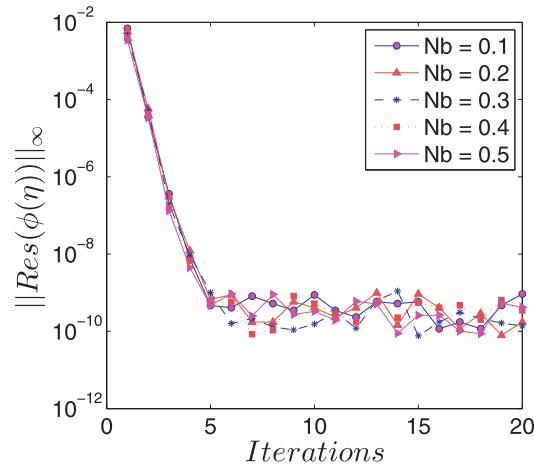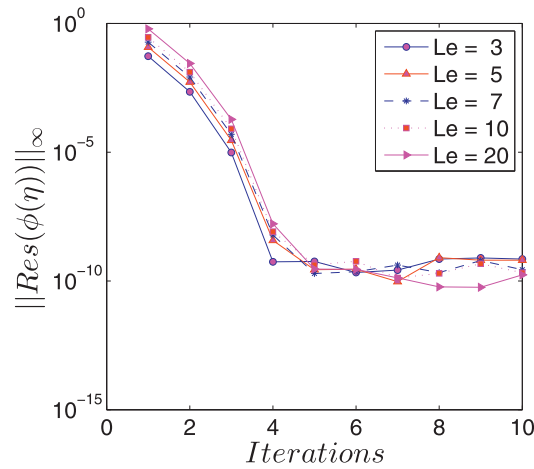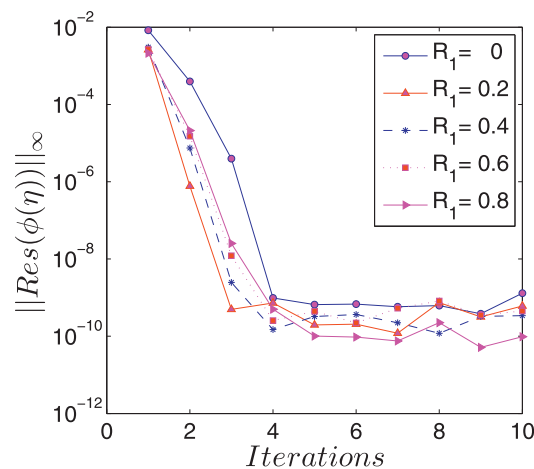
5. Conclusions

A numerical model was developed to study the influence of thermal radiation and couple stress nanofluids on mixed convection along a stretching sheet with magneto-porous medium. Graphical illustrate the flow, heat and mass transfer characteristics and their dependence on some physical parameters. The results in summary have shown that:

(i) The heat transfer characteristics are greatly influenced by an increase in the couple stress parameter.

(ii) The boundary layer flow attains the minimum velocity for higher values of the magneto-porous parameter.

(iii) The buoyancy parameter increases the velocity distribution in the momentum boundary layer.

(iv) Increasing the thermal radiation leads to an increase in the temperature profiles.

(v) Increasing the Prandtl number leads to a decrease in the temperature profiles.

(vi) An increase in the thermophoresis parameter leads to an increase in the fluid temperature and concentration profiles.

(vii) The Brownian motion parameter enhances the temperature in the boundary layer region. Also, increasing the Brownian motion parameter decreases concentration.

(viii) The concentration profiles decrease with an increase in the Lewis number.

(ix) An increase in the reaction rate parameter retards the concentration distribution in the solutal boundary layer.

Acknowledgment

References

[1] V.K. Stokes, Couple stress in fluids, Phys. Fluids 9 (9) (1966) 1709.

[2] S. Islam, C.Y. Zhou, Exact solutions for two dimensional flows of couple stress fluids, Zeitschrift für angewandte Mathematik und Physik 58 (6) (2007) 1035–1048. 2007

[3] S. Islam, C.Y. Zhou, X.J. Ran, Exact solutions for different vorticity functions of couple stress fluids, J. Zhejiang Univ. Sci. A 9 (5) (2008) 672–680.

[4] E. Walicki, A. Walicka, Interia effect in the squeeze film of a couple-stress fluid in biological bearings, Appl. Mech. Eng. 4 (2) (1999) 363–373.

[5] P.S. Hiremath, P.M. Patil, Free convection effects on the oscillatory flow of a couple stress fluid through a porous medium, Acta Mechanica 98 (1) (1993) 143–158.

[6] T. Hayat, M. Mustafa, Z. Iqbal, A. Alsaedi, Stagnation-point flow of couple stress fluid with melting heat transfer, Appl. Math. Mech. 34 (2) (2013) 167–176.

[7] H. Sithole, H. Mondal, P. Sibanda, Entropy generation in a second grade magnetohydrodynamic nanofluid flow over a convectively heated stretching sheet with nonlinear thermal radiation and viscous dissipation, Res. Phys. 9 (2018) 1077–1085.

[8] P. De, H. Mondal, U. K. Bera, Dual solutions of heat and mass transfer of nanofluid over a stretching/shrinking sheet with thermal radiation, Meccanica 51 (1) (2016) 11724.

[9] D. Pal, H. Mondal, Effect of variable viscosity on MHD non-darcy mixed convective heat transfer over a stretching sheet embedded in a porous medium with non-uniform heat source/sink, Commun. Nonlinear Sci. Numer. Simul. 15 (6) (2010) 1553–1564.

[10] N. Ali, S.U. Khan, M. Sajid, Z. Abbas, MHD flow and heat transfer of couple stress fluid over an oscillatory stretching sheet with heat source/sink in porous medium, Alexandria Eng. J. 55 (2016) 915–924.

[11] K. Ramesh, M. Devakar, Magnetohydrodynamic pristaltic transport of couple stress fluid through porous medium in an inclined aymmetric channel with heat transfer, J. Magn. Magn. Mater. 394 (2015) 335–348.

[12] S. Asad, A. Alsaedi, T. Hayat, Flow of couple stress fluid with variable thermal conductivity, Appl. Math. Mech. 37 (3) (2016) 315–324.

[13] O.D. Makinde, On MHD heat and mass transfer over a moving vertical plate with a convective surface boundary condition, Canad. J. Chem. Eng. 88 (6) (2010) 983–990.

[14] S. Sreenadh, S.N. Kishore, A.N.S. Srinivas, R.H. Reddy, MHD free convection flow of couple stress fluid in a vertical porous layer, Adv. Appl. Sci. Res. 2 (6) (2011) 215–222.

[15] D. Pal, H. Mondal, The influence of thermal radiation on hydromagnetic darcy-forchheimer mixed convection flow past a stretching sheet embedded in a porous medium, Meccanica 46 (4) (2011) 739–753.

[16] S.N. Gaikwad, S. Kouser, Double diffusive convection in a couple stress fluid saturated porous layer with internal heat source, Int. J. Heat Mass Transf. 78 (2014) 1254–1264.

[17] A.J. Chamkha, A.R.A. Khaled, Similarity solutions for hydromagnetic simultaneous heat and mass transfer by natural convection from an inclined plate with internal heat generation or absorption, Heat Mass Transf. 37 (2) (2001) 117–123.

[18] A.A. Hill, Double diffusive convection in a porous medium with a concentration based internal heat source, Proc. R. Soc. Lond. A: Math. Phys. Eng. Sci. 461 (2005) 561–574.

[19] R.D. Gasser, M.S. Kazimi, Onset of convection in a porous medium with internal heat generation, ASMEJ. Heat Transf. 98 (1976) 49–54.

[20] F. Capone, M. Gentile, A.A. Hill, Double-diffusive penetrative convection simulated via internal heating in an anisotropic porous layer with throughflow, Int. J. Heat Mass Transf. 54 (7) (2011) 1622–1626.

[21] G. Nagaraju, A. Matta, K. Kaladhar, Effects of chemical reaction and thermal radiation on heat generated stretching sheet in a couple stress fluid flow, Front. Heat Mass Transf. 7 (11) (2016).

[22] A. Rehman, S. Nadeem, M.Y. Malik, Stagnation flow of couple stress nanofluid over an exponentially stretching sheet through a porous medium, J. Power Technol. 93 (2) (2013) 122.

[23] K. Das, Effect of chemical reaction and thermal radiation on heat and mass transfer flow of MHD micropolar fluid in a rotating frame of reference, Int. J. Heat Mass Transf. 54 (15) (2011) 3505–3513.

[24] D. Srinivasacharya, U. Mendu, Thermal radiation and chemical reaction effects on magnetohydrodynamic free convection heat and mass transfer in a micropolar fluid, Turkish J. Eng. Environ. Sci. 38 (2) (2015) 184–196.

[25] N.C. Jain, D. Chaudhary, R.N. Jat, Effects of radiation and couple stress parameters on unsteady magnetopolar free convection flow with mass transfer and thermal radiation in slip flow regime, J. Energy Heat Mass Transf. 32 (4) (2010) 333–346.

[26] M. S. Malashetty, D. Pal, P. Kollur, Double-diffusive convection in a darcy porous medium saturated with a couple-stress fluid, Fluid Dyn. Res. 42 (3) (2010) 035502.

[27] M.S. Malashetty, R. Heera, The effect of rotation on the onset of double diffusive convection in a horizontal anisotropic porous layer, Transp. Porous Media 74 (1) (2008) 105–127.

[28] R.C. Sunil, P.M. Sharma, On a couple stress fluid heated from below in porous medium in the presence of magnetic field and rotation, J. Porous Media 5 (2) (2002) 149–158.

[29] R.C. Sharma, M. Sharma, Effect of suspended particles on couple-stress fluid heated from below in the presence of rotation and magnetic field, Ind. J. Pure Appl. Math. 35 (2004) 973–990.

[30] S.S. Motsa, P.G. Dlamini, M. Khumalo, Spectral relaxation method and spectral quasilinearization method for solving unsteady boundary layer flow problems, Adv. Math. Phys. (2014) 341964.

[31] C. H. Chen, Laminar mixed convection adjacent to vertical, continuously stretching sheets, Heat Mass Transf. 33 (5) (1998) 471–476.

[32] K. Zaimi, A. Ishak, I. Pop, Flow past a permeable stretching/shrinking sheet in a nanofluid using two-phase model, Plos One 9 (11) (2014) 111–743.

[33] W.A. Khan, I. Pop, Boundary-layer flow of a nanofluid past a stretching sheet, Heat Mass Transf. 53 (2010) 2477–2483.

Chapter 5

Entropy generation in a second grade magnetohydrodynamic nanofluid flow over a convectively heated stretching sheet with nonlinear thermal radiation and viscous dissipation

The power law fluid model adopted in Chapter 3 fails to predict the normal stress effects. A second grade fluid model has the essence that allows prediction of the normal stress effects. In this chapter we propose a model that addresses the influence of homogeneous-heterogeneous chemical reactions on a second grade magnetohydrodynamic nanofluid moving over a convectively heated stretching sheet with nonlinear thermal radiation and viscous dissipation. The second grade fluid is assumed to be electrically conducting and is permeated by an applied non-uniform magnetic field. This chapter differs from the previous chapters in that more attention is given to entropy generation analysis during heat and fluid flow, so as to improve the system's performance. The mathematical equations are solved using the spectral local linearization method.

Entropy generation in a second grade magnetohydrodynamic nanofluid flow over a convectively heated stretching sheet with nonlinear thermal radiation and viscous dissipation

Hloniphile Sithole, Hiranmoy Mondal*, Precious Sibanda

School of Mathematics, Statistics and Computer Science, University of KwaZulu-Natal, Private Bag X01, Scottsville, Pietermaritzburg 3209, South Africa

ARTICLE INFO

ABSTRACT

This study addresses entropy generation in magnetohydrodynamic flow of a second grade nanofluid over a convectively heated stretching sheet with nonlinear thermal radiation and viscous dissipation. The second grade fluid is assumed to be electrically conducting and is permeated by an applied non-uniform magnetic field. We further consider the impact on the fluid properties and the Nusselt number of homogeneous-heterogeneous reactions and a convective boundary condition. The mathematical equations are solved using the spectral local linearization method. Computations for skin-friction coefficient and local Nusselt number are carried out and displayed in a table. It is observed that the effects of the thermophoresis parameter is to increase the temperature distributions throughout the boundary layer. The entropy generation is enhanced by larger magnetic parameters and increasing Reynolds number. The aim of this manuscript is to pay more attention of entropy generation analysis with heat and fluid flow on second grade nanofluids to improve the system performance. Also the fluid velocity and temperature in the boundary layer region rise significantly for increasing the values of the second grade nanofluid parameter.

Introduction

Non-Newtonian fluids have various applications in industry and engineering. The fluid model used in this investigation is a subclass of non-Newtonian fluids called a second grade fluid. Second grade fluid flows with constant viscosity over a stretching surface are the subject of considerable attention in many boundary layer studies. This model can describe the normal stress effects in steady flows, shear thinning and shear thickening effects. Non-Newtonian fluids such as second grade nanofluid with both liquid and magnetic properties have varied biomedical applications, like in wound treatment and the elimination of tumors, as well as in heat removal processes.

Das et al. [1] studied the second grade fluid flow passing through a semi-infinite stretching sheet with convective surface heat flux. They provided the exact solutions of the equations for this flow using the Fourier sine transform. Helical flows of a second grade fluid between two coaxial cylinders were investigated by Jamil et al. [2]. The flow was due to the inner cylinder motion. Turkyilmazoglu [3] presented dual and triple solutions of a MHD second grade non-Newtonian fluid with a slip condition. Khan and Pop [4] explored the boundary-layer flow of a nanofluid over a linear stretching surface. The boundary-layer flow of a nanofluid over a linear stretching surface subject to a convective boundary condition was investigated by Makinde and Aziz [5]. Mustafa et al. [6] discussed the stagnation point flow of a nanofluid induced by a linear stretching surface. Akinbobola and Okoya [7] studied a steady two-dimensional non-Newtonian second grade fluid flow under the influence of a temperature dependent viscosity and thermal conductivity, with viscosity varying inversely as linear function of temperature while the thermal conductivity varies directly as linear function of temperature. Erdogan et al. [8] gave an exact solution of an incompressible second-grade fluid flow between two coaxial cylinders with porous walls, assuming that the inner cylinder was rotating with a constant angular velocity and the outer cylinder was at rest. Nadeem et al. [9] examined the boundary layer flow and heat transfer in a second grade fluid flow through a horizontal cylinder.

Cooling capabilities of heat transfer equipment is often constrained because of the low thermal conductivity of conventional heat transfer fluids. It is well known that metals have higher thermal conductivities than fluids. The thermal conductivities of fluids that contain suspended solid metallic particles could be expected to be significantly higher than those of conventional heat transfer fluids. The goal of adding nanoparticles to a fluid is to improve the thermal properties of a fluid using

---

* Corresponding author.
E-mail address: hiranmoymondal@yahoo.co.in (H. Mondal).

the smallest possible concentrations to produce a stable suspension of uniformly dispersed nanoparticles ($< 100\,\text{nm}$) in the base fluid. The suspended nanoparticles enhance the thermal conductivity and heat transfer performance of the base fluids. Nanofluids have a number of engineering and technological applications in heat exchangers. Magnetonanofluids are used in wound treatment and cancer therapy to mention a few examples. A mathematical model describing nanofluid flow that exhibit the characteristics of Brownian motion and thermophoresis was introduced by Buongiorno [10]. Sahoo [11] considered the steady laminar flow and heat transfer in an electrically conducting second-grade fluid over a stretching sheet with partial slip. Zhu et al. [12] studied the effects of the slip condition on the MHD stagnation-point flow over a power-law stretching sheet. Mansur et al. [13] considered the flow and heat transfer in a nanofluid with partial slip boundary conditions.

In the current study, we investigate entropy generation and heat transfer in the flow of a second grade nanofluid. Noghrehabadi et al. [14] considered entropy generation in nanofluid flow over a stretching sheet with heat generation/absorption. Abolbashari et al. [15] studied entropy generation in an unsteady MHD nanofluid flow adjacent to a stretching surface using different types of nanoparticles. Aiboud and Saouli [16] studied entropy generation in viscoelastic MHD flow over a stretching surface. Butt et al. [17] presented the effects of velocity slip on entropy generation in the boundary layer flow over a vertical sheet with convective boundary condition. Irreversibility which is expressed by entropy generation, is due to heat transfer, mass transfer, viscous dissipation, chemical reactions, magnetic field, etc. Magherbi et al. [18] studied entropy generation in convective heat and mass transfer through a square cavity for the case of aiding buoyancy forces. Hidouri et al. [19] studied the influence of the Soret effect on entropy generation in double diffusive convection for the case of a binary perfect gas mixture for both aiding and opposing buoyancy forces through a square cavity. Aracely et al. [20] investigated entropy generation analysis of MHD nanofluid flow in a porous vertical microchannel with nonlinear thermal radiation.

Many chemically reacting systems involve both homogeneous and heterogeneous reactions. Chaudhary and Merkin [21] presented a mathematical model for homogeneous-heterogeneous reactions in stagnation-point boundary-layer flow. Chaudhary and Merkin [22] modeled homogeneous reaction by isothermal cubic kinetics and the heterogeneous reaction by first-order kinetics. The isothermal homogeneous-heterogeneous reactions in boundary layer flow of a viscous fluid flow past a flat plate was studied by Merkin [23]. Khan and Pop [24] studied the effects of homogeneous-heterogeneous reactions on the viscoelastic fluid toward a stretching sheet. Shaw et al. [25] analyzed the influence of permeability, homogeneous and heterogeneous reactions on micropolar fluid along a stretching/shrinking sheet.

The motivation of this study is to investigate entropy generation and the influence of homogeneous-heterogeneous reactions on second grade magnetohydrodynamic nanofluid over a convectively heated stretching sheet with nonlinear thermal radiation and viscous dissipation. To the best of the authors knowledge there are no studies so far on entropy generation in second grade nanofluid over a stretching sheet with homogeneous-heterogeneous reactions. The results of this study may find applications in cooling processes, movement of biological fluids, melt spinning and oceanography. Entropy generation plays a major role in controlling the rate of heat transfer in the proximity of a surface. The mathematical equations are solved using the spectral local linearization method.

Modeling

Consider an incompressible, steady two-dimensional second grade magnetohydrodynamic nanofluid flow over a convectively heated stretching sheet with nonlinear thermal radiation and viscous dissipation with homogeneous–heterogeneous chemical reactions. The flow

field is subject to an external transverse magnetic field of strength B_0. The flow is restricted in the region $y > 0$ with the stagnation point fixed at $x = 0$. The temperature at the surface and in the ambient region is defined as T_w and T_∞ respectively, C_a and C_b are the concentrations of species A and B respectively. In addition the ambient concentration is C_∞. The velocity of the stretching sheet is $U = u_w(x) = cx$, where $c > 0$ represent the stretching rate. This study considers two different types of chemical reactions given by Chaudhary and Merkin [21]; namely a homogeneous (bulk) and a heterogeneous (on sheet) reactions in the boundary layer flow; in the form

$$A + 2B \rightarrow 3B, \text{ rate } = k_1 C_a C_b^2, \tag{1}$$

$$A \rightarrow B, \text{ rate } = k_s C_a. \tag{2}$$

Under these assumptions, the governing boundary layer equations for a second grade fluid flow can be written as:

$$\frac{\partial u}{\partial x} + \frac{\partial v}{\partial y} = 0, \tag{3}$$

$$u\frac{\partial u}{\partial x} + v\frac{\partial u}{\partial y} = \nu\frac{\partial^2 u}{\partial y^2} + \frac{\alpha_1}{\rho}\left[\frac{\partial}{\partial x}\left(u\frac{\partial^2 u}{\partial y^2}\right) - \frac{\partial u}{\partial y}\frac{\partial^2 u}{\partial x \partial y} + v\frac{\partial^3 u}{\partial y^3}\right] - \frac{\sigma B_0^2 u}{\rho}$$
$$+ g\beta_t(T - T_\infty) + g\beta_c C_a, \tag{4}$$

$$u\frac{\partial T}{\partial x} + v\frac{\partial T}{\partial y} = \frac{\kappa}{\rho C_p}\frac{\partial^2 T}{\partial y^2} + \tau\left[D_B\frac{\partial C_b}{\partial y}\frac{\partial T}{\partial y} + \frac{D_T}{T_\infty}\left(\frac{\partial T}{\partial y}\right)^2\right] - \frac{1}{\rho C_p}\frac{\partial q_r}{\partial y}$$
$$+ \frac{\mu}{\rho C_p}\left(\frac{\partial u}{\partial y}\right)^2 + \frac{\alpha_1}{\rho C_p}\frac{\partial u}{\partial y}\left[\frac{\partial}{\partial y}\left(u\frac{\partial u}{\partial x} + v\frac{\partial u}{\partial y}\right)\right] + \frac{\sigma}{\rho C_p}B_0^2 u^2, \tag{5}$$

$$u\frac{\partial C_a}{\partial x} + v\frac{\partial C_a}{\partial y} = D_A\frac{\partial^2 C_a}{\partial y^2} - k_1 C_a C_b^2, \tag{6}$$

$$u\frac{\partial C_b}{\partial x} + v\frac{\partial C_b}{\partial y} = D_B\frac{\partial^2 C_b}{\partial y^2} + \frac{D_T}{T_\infty}\frac{\partial^2 T}{\partial y^2} + k_1 C_a C_b^2, \tag{7}$$

where u and v are velocity components of the nanofluid in the x and y directions, respectively, D_A and D_B are the diffusion species coefficients of A and B respectively, T is the temperature of the nanofluid, g is the acceleration due to gravity, β_{nf} is the coefficient of thermal expansion. The kinematic viscosity is denoted by ν. The Brownian diffusion coefficient is D_B, while the thermophoresis diffusion coefficients is D_T, α_1 is the material parameter, β_t is the thermal expansion coefficient, β_c is the volumetric expansion coefficient, κ is the thermal conductivity of the fluid, q_r is the radiative heat flux and $\tau = \frac{(\rho c_p)_s}{(\rho c_p)_f}$, the effective heat capacity of the nanoparticle material divided by heat capacity of the ordinary fluid. Let $\theta_w = \frac{T_w}{T_\infty}$, so that the temperature is written as $T = T_\infty\{1 + (\theta_w - 1)\theta\}$ (see [26,27]). The boundary conditions for the velocity, temperature and homogeneous-heterogeneous chemical reaction fields are

$$u = u_w, \quad v = v_0, \quad \kappa\frac{\partial T}{\partial y} = h_w(T_w - T), \quad D_A\frac{\partial C_a}{\partial y} = k_s C_a, \quad D_B = \frac{\partial C_b}{\partial y}$$
$$= -k_s C_a \quad \text{at} \quad y = 0, \quad u = 0, \quad \frac{\partial u}{\partial x} \rightarrow 0, \quad T = T_\infty, \quad C_a \rightarrow C_\infty, \quad C_b$$
$$\rightarrow 0 \quad \text{at} \quad y \rightarrow \infty, \tag{8}$$

where v_0 is the suction/injection velocity at the surface of the plate with $v_0 > 0$ for injection, $v_0 < 0$ for suction, and $v_0 = 0$ corresponds to an impermeable plate, h_w is the heat transfer coefficient.

Following Rosseland's approximation to describe the radiative heat flux q_r in the energy equations,

$$q_r = -\frac{4\sigma^\star}{3k^\star}\frac{\partial T^4}{\partial y} \tag{9}$$

where $\sigma^\star$ is the Stefan–Boltzman constant and $k^\star$ is the mean absorption coefficient. Assuming that the temperature differences within the

flow are sufficiently small, T^4 may be expressed as a linear function $T^4 \equiv 4T_\infty^3 - 3T_\infty^4$ and

$$\frac{\partial q_r}{\partial y} = -\frac{16\sigma^\star T_\infty}{3k^\star}\frac{\partial^2 T}{\partial y^2}. \tag{10}$$

The similarity transformations are introduced as:

$$\eta = \sqrt{\frac{c}{\nu}}y, \ u = cxf'(\eta), \ v = -\sqrt{c\nu}f(\eta),$$

$$\theta(\eta) = \frac{T-T_\infty}{T_w - T_\infty}, \ \xi(\eta) = \frac{C_a}{C_\infty}, \ \phi(\eta) = \frac{C_b}{C_\infty}. \tag{11}$$

The system of Eqs. (3)–(7) is transformed to:

$$f''' + ff'' - f'^2 + \lambda_1(2f'f''' - ff^{iv} - f''^2) - Mf' + Gr_t\theta + Gr_c\xi = 0, \tag{12}$$

$$[1 + Nr\{1 + (\theta_w-1)\theta\}^3]\theta'' + 3Nr(\theta_w-1)\{1 + (\theta_w-1)\theta\}^2\theta'^2 + Prf\theta'$$
$$+ Pr(Nb\theta'\phi' + Nt\theta'^2)$$
$$+ PrEc[f''^2 + Mf'^2 + \lambda_1f''(f'f'' - ff''')] = 0, \tag{13}$$

$$\xi'' + Scf\xi' - KSc\xi\phi^2 = 0, \tag{14}$$

$$\frac{1}{\epsilon Sc}\left(\phi'' + \frac{Nt}{Nb}\theta''\right) + f\phi' + K\xi\phi^2 = 0, \tag{15}$$

subject to the boundary conditions

$$f(0) = f_w, \quad f'(0) = 1, \quad \theta'(0) = -\gamma(1-\theta(0)), \quad \xi'(0) = K_s\xi(0), \quad \phi'(0)$$
$$= -\epsilon K_s\xi(0),$$
$$f'(\infty) = 0, \quad f''(\infty) = 0, \quad \theta(\infty) = 0, \quad \xi(\infty) = 1, \quad \phi(\infty) = 0, \tag{16}$$

where a prime refers to differentiation with respect to η, $K_s = \frac{k_s}{D_A\sqrt{\frac{c}{\nu}}}$ and $\epsilon = \frac{D_A}{D_B}$.

In many practical scenarios, the sizes of the diffusion coefficient of the chemical species A and B are expected to be comparable which justifies the assumption that the diffusion coefficient of D_A and D_B are equal. It is assumed that $\epsilon = 1$ which leads to the relationship

$$\xi(\eta) + \phi(\eta) = 1. \tag{17}$$

Consequently, Eqs. (14) and (15) reduce to

$$\xi'' - \frac{Nt}{Nb}\theta'' + Scf\xi' - ScK\xi(1-\xi)^2 = 0, \tag{18}$$

with boundary conditions

$$\xi'(0) = K_s\xi(0), \quad \xi(\infty) = 1. \tag{19}$$

Hence, the system (12)–(15) becomes

$$f''' + ff'' - f'^2 + \lambda_1(2f'f''' - ff^{iv} - f''^2) - Mf' + Gr_t\theta + Gr_c\xi = 0, \tag{20}$$

$$[1 + Nr\{1 + (\theta_w-1)\theta\}^3]\theta'' + 3Nr(\theta_w-1)\{1 + (\theta_w-1)\theta\}^2\theta'^2 + Prf\theta'$$
$$+ Pr(Nb\theta'\phi' + Nt\theta'^2)$$
$$+ PrEc[f''^2 + Mf'^2 + \lambda_1f''(f'f'' - ff''')] = 0, \tag{21}$$

$$\xi'' - \frac{Nt}{Nb}\theta'' + Scf\xi' - ScK\xi(1-\xi)^2 = 0, \tag{22}$$

with the new boundary conditions

$$f(0) = f_w, \quad f'(0) = 1, \quad \theta'(0) = -\gamma(1-\theta(0)), \quad \xi'(0) = K_s\xi(0)$$
$$f'(\infty) = 0, \quad f''(\infty) \to 0, \quad \theta(\infty) = 0, \quad \xi(\infty) = 1. \tag{23}$$

The non-dimensional parameters in the above equations are: $\lambda_1 = \frac{\alpha_1 c}{\rho\nu}$ the second grade fluid parameter, $M = \frac{\sigma B_0^2}{\rho c}$ the Hartman number, $Gr_t = \frac{g\beta_t(T_w-T_\infty)x^3}{\nu^2}$ the temperature Grashof number, $Gr_c = \frac{g\beta_c(C_w-C_\infty)x^3}{\nu^2}$ the mass Grashof number, $Nr = \frac{16T_\infty^3\sigma^\star}{3k^\star\kappa}$ the thermal

radiation parameter, θ_w the temperature ratio parameter, $Pr = \frac{\nu c_p}{\kappa}$ the Prandtl number, $f_w = \frac{v_0}{\sqrt{c\nu}}$ the suction parameter, $\gamma = \frac{h_w}{\kappa\sqrt{\frac{\gamma}{c}}}$ the surface convection parameter, $Nb = \frac{\tau D_B(C_w-C_\infty)}{\nu}$ the Brownian motion parameter, $Nt = \frac{\tau D_T(T_w-T_\infty)}{\nu T_\infty}$ the thermophoresis parameter, K is the homogeneous reaction rate parameter, and K_s is the heterogeneous reaction rate parameter.

The physical quantities of primary interest are the skin friction coefficient, Nusselt number and Sherwood number. The wall shear stress is

$$\tau_w = \left[\mu\frac{\partial u}{\partial y} + \rho\alpha_1\left(2\frac{\partial u}{\partial x}\frac{\partial u}{\partial y} + u\frac{\partial^2 u}{\partial x\partial y}\right)\right]_{y=0}. \tag{24}$$

The local dimensionless skin friction coefficient C_f is given by

$$\frac{1}{2}\sqrt{Re}\,C_f = \{1 + 3\lambda_1 f'(0)\}f''(0). \tag{25}$$

The rate of heat transfer in terms of dimensionless Nusselt number Nu is is given by:

$$Re^{-\frac{1}{2}}Nu = -(1 + Nr)\theta'(0). \tag{26}$$

The rate of mass transfer in terms of dimensionless Sherwood number Sh is given by

$$Re^{-\frac{1}{2}}Sh = -\xi'(0). \tag{27}$$

Method of Solution

In this section, the iterative spectral local linearization method (SLLM) is used to solve the Eqs. (20)–(22) with boundary conditions (23). The SLLM was introduced by Motsa [28]. This method decouples and linearizes systems of equations using a combination of a univariate linearization technique and a spectral collocation discretization. It breaks down a large coupled system of equations into a sequence of smaller systems which can be solved iteratively in a computationally efficient manner using the simple algorithm described below.

SLLM Algorithm

The three coupled differential equations (20)–(22), are described as

$$\omega_j[F, \Theta, H] = 0, \qquad \text{for} \qquad j = 1, 2, 3 \tag{28}$$

where ω_1, ω_2 and ω_3 are non-linear operators representing the nonlinear ODEs (20), (13) and (22) and F, Θ, H are given by

$$F = \left\{f, \frac{\partial f}{\partial\eta}, \frac{\partial^2 f}{\partial\eta^2}, \frac{\partial^3 f}{\partial\eta^3}, \frac{\partial^4 f}{\partial\eta^4}\right\}, \tag{29}$$

$$\Theta = \left\{\theta, \frac{\partial\theta}{\partial\eta}, \frac{\partial^2\theta}{\partial\eta^2}\right\}, \tag{30}$$

$$H = \left\{\xi, \frac{\partial\xi}{\partial\eta}, \frac{\partial^2\xi}{\partial\eta^2}\right\}. \tag{31}$$

The system of Eqs. (34) can be simplified by linearizing nonlinear terms of the same function and its derivative in each of the equations. The system is decoupled and the Chebyshev pseudo-spectral collocation method is used to integrate the decoupled system. The following steps of the algorithm are used,

1. From the first equation, solve for F while treating Θ and H as known functions from initial guesses. The solution F_{r+1} is obtained.
2. Solve for Θ in the second equation while treating F and H as known functions, T is known from the updated solution obtained in 1 above and H is known from the initial guess. The solution Θ_{r+1} is obtained.

3. Finally, solve for H in the last equation while treating F and Θ as known functions, Θ and H are known from the updated solutions of 1 and 2 above. Finally the solution H_{r+1} is obtained.

4. The next iterative solutions are then found by repeating steps 1–3.

The differential equations arising from the linearization procedure are solved using a Chebyshev pseudo spectral method. Consider a system of m nonlinear ordinary differential equations in m unknown functions $Y_i(\eta), i = 1, 2, \ldots, m$ where $\eta \in [a,b]$ is the dependent variable. The domain of the problem is transformed to $[-1,1]$ using the transformation $\frac{1}{2}(b-a)(\iota + 1)$, before applying the spectral method, D_m is the differentiation matrix used to approximate the derivatives of $Y_i(\eta)$ with,

$$\frac{dY_i}{d\eta} = \sum_{k=0}^{\overline{M}} \mathbf{D}_{lk} Y_i(\iota_k) = \mathbf{DY}_i, \quad l = 0, 1, \ldots, \overline{M}. \tag{32}$$

The vector function at the collocation points is given by $Y = [y(\iota_0), y(\iota_1), \ldots, y(\iota_M)]^T, \mathbf{D} = \frac{2D_m}{b-a}$, with $\overline{M} + 1$ collocation points [25]. Powers of $\mathbf{D}$ give higher order derivatives, i.e,

$$Y_j^{(s)} = \mathbf{D}^s \mathbf{Y}_j. \tag{33}$$

where s is the order of the derivative.

Consider

$$\Omega_F = f_r''' + f_r f_r'' - f_r'^2 + \lambda_1 (2f_r' f_r'' - f_r f_r^{iv} - f_r''^2) - Mf_r' + Gr_t\theta_r + Gr_c\xi_r, \tag{34}$$

$$\Omega_\Theta = [1 + Nr\{1 + (\theta_w - 1)\theta_r\}^3]\theta_r'' + 3Nr(\theta_w - 1)\{1 + (\theta_w - 1)\theta_r\}^2\theta_r'^2 Prf_r\theta_r' - Pr(Nb\theta_r'\xi_r' + Nt\theta_r'^2) + PrEc[f_r''^2 + Mf_r'^2 + \lambda_1 f_r'(f_r' f_r'' - f_r f_r''')) \tag{35}$$

$$\Omega_H = \xi_r'' - \frac{Nt}{Nb}\theta_r'' + Scf_r\xi_r' - ScK\xi_r(1-\xi_r)^2. \tag{36}$$

The local linearization scheme corresponding to Eqs. (20)–(22) becomes:

$$\varrho_{0,r}f_{r+1}''' + \varrho_{1,r}f_{r+1}''' + \varrho_{2,r}f_{r+1}'' + \varrho_{3,r}f_{r+1}' + \varrho_{4,r}f_{r+1} = R_f,$$
$$\varpi_{2,r}\theta_{r+1}'' + \varpi_{3,r}\theta_{r+1}' + \varpi_{4,r}\theta_{r+1} = R_\theta,$$
$$\varsigma_{2,r}\xi_{r+1}'' + \varsigma_{3,r}\xi_{r+1}' + \varsigma_{4,r}\xi_{r+1} = R_\xi, \tag{37}$$

subject to boundary conditions:

$$f_{r+1}(0) = f_w, f_{r+1}'(0) = 1, f_{r+1}'(\infty) = 0, f_{r+1}''(\infty) = 0,$$
$$\theta_{r+1}'(0) = -\gamma(1 - \theta_{r+1}(0)), \theta_{r+1}(\infty) = 0,$$
$$\xi_{r+1}'(0) = K_s\xi_{r+1}(0), \xi_{r+1}(\infty) = 1. \tag{38}$$

where the coefficients are

$$\varrho_{0,r} = \frac{\partial\Omega_F}{\partial f_r'''} = -\lambda_1 f_r,$$
$$\varrho_{1,r} = \frac{\partial\Omega_F}{\partial f_r''} = 1 + 2\lambda_1 f_r',$$
$$\varrho_{2,r} = \frac{\partial\Omega_F}{\partial f_r''} = f_r - 2\lambda_1 f_r'',$$
$$\varrho_{3,r} = \frac{\partial\Omega_F}{\partial f_r'} = -2f_r' + 2\lambda_1 f_r''' - M,$$
$$\varrho_{4,r} = \frac{\partial\Omega_F}{\partial f_r} = f_r'' - \lambda_1 f_r''', \tag{39}$$

$$\varpi_{2,r} = \frac{\partial\Omega_\Theta}{\partial\theta_r''} = 1 + Nr\{1 + (\theta_w - 1)\theta_r\}^3,$$
$$\varpi_{3,r} = \frac{\partial\Omega_\Theta}{\partial\theta_r'} = 6Nr(\theta_w - 1)\{1 + (\theta_w - 1)\theta_r\}^2\theta_r' + Prf_r - PrNb\xi_r' + 2Nt\theta_r',$$
$$\varpi_{4,r} = \frac{\partial\Omega_\Theta}{\partial\theta_r} = 3\theta_r''Nr(\theta_w - 1)\{1 + (\theta_w - 1)\theta_r\}^2 + 6Nr(\theta_w - 1)^2\theta_r'^2\{1 + (\theta_w - 1)\theta_r\}, \tag{40}$$

$$\varsigma_{2,r} = \frac{\partial\Omega_H}{\partial\xi_r''} = 1,$$
$$\varsigma_{3,r} = \frac{\partial\Omega_H}{\partial\xi_r'} = Scf_r,$$
$$\varsigma_{4,r} = \frac{\partial\Omega_H}{\partial\xi_r} = -2ScK\xi_r(1-\xi_r) + ScK(1-\xi_r)^2, \tag{41}$$

$$R_f = \varrho_{0,r}f_r''' + \varrho_{1,r}f_r''' + \varpi_{2,r}f_r'' + \varrho_{3,r}f_r' + \varrho_{4,r}f_r - \Omega_F,$$
$$R_\Theta = \varpi_{2,r}\theta_r'' + \varpi_{3,r}\theta_r' + \varpi_{4,r}\theta_r - \Omega_\Theta,$$
$$R_H = \varsigma_{2,r}\xi_r'' + \varsigma_{3,r}\xi_r' + \varsigma_{4,r}\xi_r - \Omega_H. \tag{42}$$

Applying the Chebyshev pseudospectral method to (37), (38), the following decoupled matrix system is obtained:

$$\boldsymbol{\Delta}_1 \mathbf{F}_{r+1} = \mathbf{R}_f$$
$$\boldsymbol{\Delta}_2 \boldsymbol{\Theta}_{r+1} = \mathbf{R}_\theta$$
$$\boldsymbol{\Delta}_3 \mathbf{H}_{r+1} = \mathbf{R}_\xi \tag{43}$$

with corresponding boundary conditions

$$f_{r+1}(\iota_{\overline{M}}) = f_w, \quad \sum_{k=0}^{\overline{M}} \mathbf{D}_{\overline{M}k}f_{r+1}(\iota_k) = 1, \quad \sum_{k=0}^{\overline{M}} \mathbf{D}_{0k}f_{r+1}(\iota_k)$$
$$= 0, \quad \sum_{k=0}^{\overline{M}} \mathbf{D}_{0k}^2 f_{r+1}(\iota_k) = 0,$$

$$\sum_{k=0}^{\overline{M}} \mathbf{D}_{\overline{M}k}\theta_{r+1}(\iota_k) = -\gamma(1 - \theta_{r+1}(\iota_{\overline{M}})), \quad \theta_{r+1}(\iota_0) = 0,$$

$$\sum_{k=0}^{\overline{M}} \mathbf{D}_{\overline{M}k}\xi_{r+1}(\iota_k) = K_s\xi_{r+1}(\iota_{\overline{M}}), \quad \xi_{r+1}(\iota_0) = 1. \tag{44}$$

where

$$\boldsymbol{\Delta}_1 = \mathbf{diag}[\varrho_{0,r}]\mathbf{D}^4 + \mathbf{diag}[\varrho_{1,r}]\mathbf{D}^3 + \mathbf{diag}[\varrho_{2,r}]\mathbf{D}^2 + \mathbf{diag}[\varrho_{3,r}]\mathbf{D} + \mathbf{diag}[\varrho_{4,r}]\mathbf{I},$$
$$\boldsymbol{\Delta}_2 = \mathbf{diag}[\varpi_{2,r}]\mathbf{D}^2 + \mathbf{diag}[\varpi_{3,r}]\mathbf{D} + \mathbf{diag}[\varpi_{4,r}]\mathbf{I},$$
$$\boldsymbol{\Delta}_3 = \mathbf{diag}[\varsigma_{2,r}]\mathbf{D}^2 + \mathbf{diag}[\varsigma_{3,r}]\mathbf{D} + \mathbf{diag}[\varsigma_{4,r}]\mathbf{I}. \tag{45}$$

The matrix $\mathbf{I}$ is an identity matrix with $(\overline{M} + 1)$ rows and columns, $\mathbf{F}$, $\boldsymbol{\Theta}$ and $\mathbf{H}$ are approximate values of f, θ and ξ calculated at the collocation points. Initial guesses are required to start the iteration process. The guesses are selected to satisfy the boundary conditions. The following guesses were used as suitable initial approximations,

$$f_0(\eta) = 1 + f_w - e^{-\eta}, \quad \theta_0(\eta) = \frac{\gamma}{1 + \gamma}e^{-\eta}, \quad \xi_0(\eta) = 1 - \frac{K_s}{1 + K_s}e^{-\eta}. \tag{46}$$

The approximate solutions at each iteration level are obtained by solving (43).

Entropy Generation

Entropy production destroys the available energy in the system of various engineering and industrial processes. So it is important to determine the rate of entropy generation in a system. The volumetric entropy generation of the Newtonian fluid can be written as

$$E_{gen}''' = \frac{k}{T_\infty^2}\left[\left(\frac{\partial T}{\partial y}\right)^2 + \frac{16\sigma^\star T_\infty^3}{3k^\star}\left(\frac{\partial T}{\partial y}\right)^2\right] + \frac{\mu\alpha_1}{T_\infty}\left(u\frac{\partial u}{\partial y}\frac{\partial^2 u}{\partial x\partial y} + v\frac{\partial u}{\partial y}\frac{\partial^2 u}{\partial y^2}\right) + \frac{\mu}{T_\infty}\left(\frac{\partial u}{\partial y}\right)^2 + \frac{\sigma B_0^2}{T_\infty}u^2 + \frac{RD}{C_\infty}\left(\frac{\partial C_a}{\partial y}\right)^2 + \frac{RD}{T_\infty}\frac{\partial T}{\partial y}\frac{\partial C_a}{\partial y}. \tag{47}$$

In Eq. (47), the first term represents irreversibility due to heat transfer with thermal radiation; the second term represents fluid friction irreversibility; the third term is entropy generation due to viscous dissipation; the fourth term is local entropy generation due to the effect of the magnetic field, while the fifth and sixth terms are irreversibility caused by diffusion effect. The characteristic entropy generation rate is

$$E_0''' = \frac{k(T_w - T_\infty)^2}{x^2 T_\infty^2}.$$ (48)

The entropy generation N_G is the ratio between the entropy generation rate E_{gen}''' and the characteristic entropy generation rate E_0''' such that,

$$N_G = \frac{E_{gen}'''}{E_0'''}$$ (49)

$$= Re\left[1 + Nr(1 + \Pi\theta)^3\right]\theta'^2 + \frac{\overline{\alpha_1}ReBr}{\Pi^2}(ff''^2 - ff'f''') + \frac{ReBr}{\Pi^2}(f''^2 + Mf'^2)$$

$$+ \frac{Re\Sigma}{\Pi}\left(\xi'^2 + \frac{\theta'\xi'}{\Pi}\right)$$

where Re, Br, Σ and Π are the Reynold number, Brinkman number, a constant parameter and the temperature difference respectively. These parameters are defined as:

$$Re = \frac{u_w(x)x}{\nu}, \quad Br = \frac{\mu u_w^2(x)}{kT_\infty}, \quad \Sigma = \frac{C_\infty RD}{k}, \quad \Pi = (\theta_w - 1).$$ (50)

Convergence analysis

The system of coupled ordinary differential Eqs. (20)–(22) with the boundary conditions (23) were solved using the SLLM. To check the accuracy of the numerical scheme, both the residual errors and the error norms were evaluated. The residual error measures the extent to which the numerical solution approximates the true solution. The error norm is the difference between approximate values at successive iterations and may be used to evaluate convergence and stability of the iteration scheme.

Fig. 1 shows the residual errors $\|Res(f(\eta))\|_\infty$ and solution error norms E_f against iterations for different values of the second grade nanofluid parameter λ_1. The residual errors after the fifth iteration are of the order of $\|Res(f(\eta))\|_\infty \approx 10^{-9}$. The solution error norm decreases to $E_f \approx 10^{-11}$ at the sixth iteration.

Fig. 2 shows the residual errors $\|Res(\theta(\eta))\|_\infty$ and solution error norms E_θ against iterations for different values of the second grade nanofluid parameter. The residual errors after the fifth iteration are all of order of $\|Res(\theta(\eta))\|_\infty \approx 10^{-10}$. The solution error norm decreases to $E_\theta \approx 10^{-13}$ at the seventh iteration.

Fig. 3 shows the residual errors $\|Res(\xi(\eta))\|_\infty$ and solution error norms E_ξ against iterations for different values of the second grade nanofluid parameter. The residual errors after four iterations ware of the order of $\|Res(\xi(\eta))\|_\infty \approx 10^{-11}$. The solution error norm decreases to $E_\xi \approx 10^{-14}$ at the seventh iteration.

Table 1 shows a comparison of the skin friction coefficient $-f''(0)$ when $f_w = 0.5, \lambda_1 = 0.2$, $M = Nb = Nt = \beta = Nr = K = Gr_t = Gr_c = 0$, and $\theta_w = 1$ between the SLLM results and those reported by Olanrewaju et al. [29]. The results are in good agreement. Increasing the magnetic
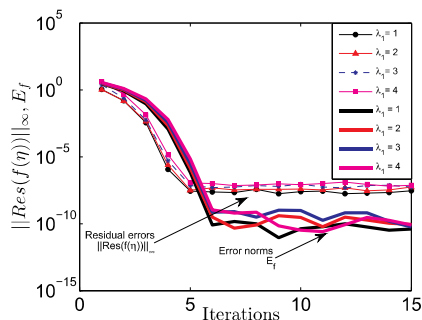

Fig. 1. Residual errors $\|Res(f(\eta))\|_\infty$ and solution error norms E_f against iterations for different values of the second grade nanofluid parameter λ_1.
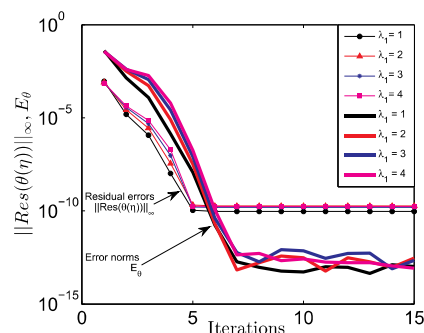
Fig. 2. Residual errors $\|Res(\theta(\eta))\|_\infty$ and solution error norms E_θ against iterations for different values of the second grade nanofluid parameter λ_1.
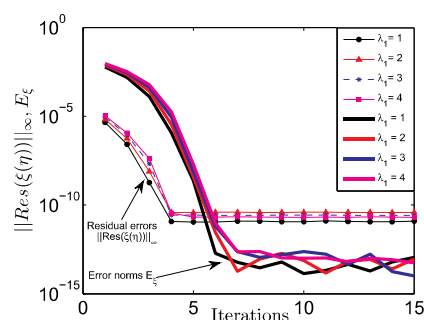
Fig. 3. Residual errors $\|Res(\xi(\eta))\|_\infty$ and solution error norms E_ξ against iterations for different values of the second grade nanofluid parameter λ_1.

Table 1
Comparison of values of skin friction coefficient $-f''(0)$ when $f_w = 0.5$, $\lambda_1 = 0.2$, $\gamma = 0.5$, $Ec = 0.2$, $Pr = 0.71$, $M = Nb = Nt = \beta = Nr = K = Gr_t = Gr_c = 0$ and $\theta_w = 1$.

M	Olanrewaju et al. [29]	Current study
0.7	0.608319	0.60831949
1.2	0.695179	0.69517974
2.2	0.835182	0.83518245

Table 2
Comparison of values of local Nusselt number $-\theta(0)$ when $f_w = 0.5, \lambda_1 = 0.2$, $M = Nb = Nt = \beta = Nr = K = Gr_t = Gr_c = 0$ and $\theta_w = 1$.

γ	Pr	Olanrewaju et al. [29]	Hayat et al. [30]	Current study
0.1	0.7	0.083016	0.082916	0.08273795
0.5		0.250178	0.250173	0.24976956
1		0.334552	0.334452	0.33407505
2		0.410235	0.402237	0.40190279
0.5	0.5	0.214368	0.214365	0.21441547
	0.7	0.250142	0.250132	0.24976956
	1	0.289161	0.288561	0.28782508
	2	0.356176	0.356172	0.35519994

field exerts retarding force on the flow which tends to increase the skin friction coefficient within the boundary layer, this can be seen from Table 1.

Table 2 shows a comparison of the heat transfer at the wall $-\theta(0)$ when $f_w = 0.5, \lambda_1 = 0.2$, $M = Nb = Nt = \beta = Nr = K = Gr_t = Gr_c = 0$, and $\theta_w = 1$, between the SLLM results and those reported by Olanrewaju et al. [29] and Hayat et al. [30].

H. Sithole et al.
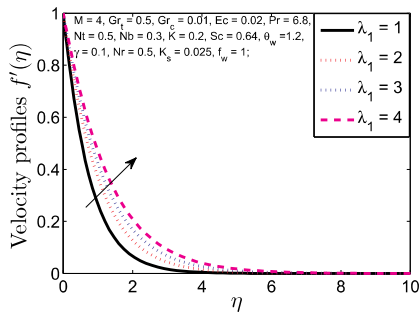
Fig. 4. Velocity profiles for different values of the second grade nanofluid parameter λ_1.

Fig. 5. Velocity profiles for different values of temperature Grashof number Gr_t.

Fig. 6. Velocity profiles for different values of solutal Grashof number Gr_c.

Fig. 7. Temperature profiles for different values of second grade nanofluid parameter λ_1.
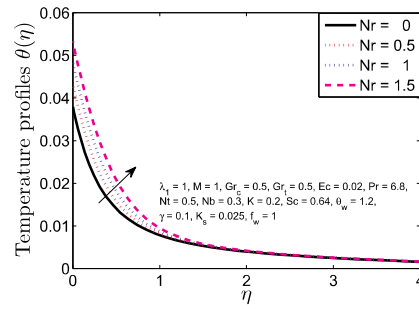
Fig. 8. Temperature profiles for different values of thermal radiation parameter *Nr*.
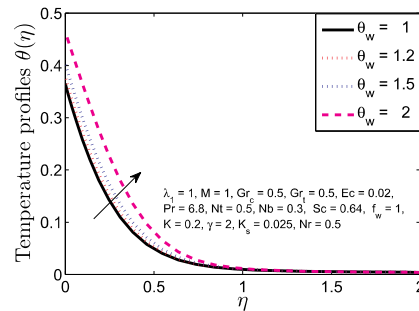
Fig. 9. Temperature profiles for different values of temperature ratio parameter θ_w.
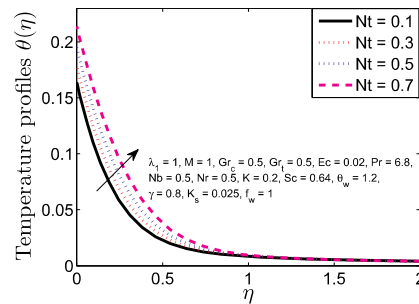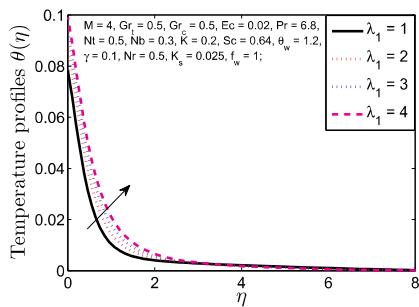
Fig. 10. Temperature profiles for different values of thermophoresis parameter *Nt*.
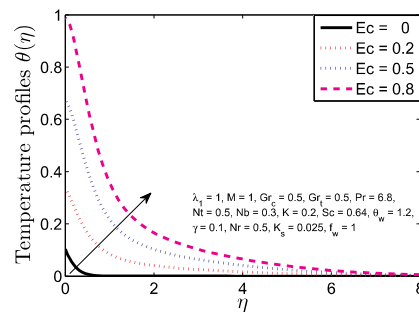
Fig. 11. Temperature profiles for different values of Eckert number *Ec*.
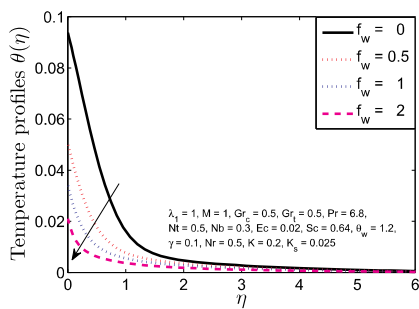
Fig. 12. Temperature profiles for different values of injection parameter f_w.

Fig. 13. Concentration profiles for different values of thermophoresis parameter Nt.

Fig. 14. Concentration profiles for different strength of the homogenous reaction K.

Fig. 15. Concentration profiles for different strength of the heterogenous reaction K_s.
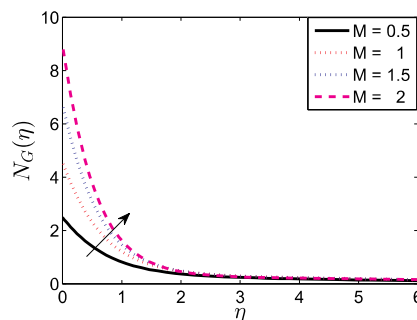
Fig. 16. Entropy profile for various values of M.
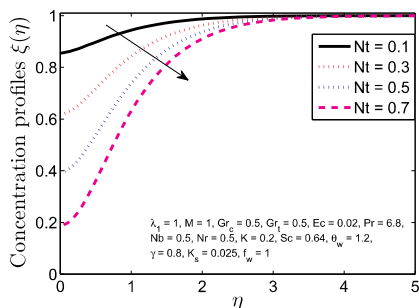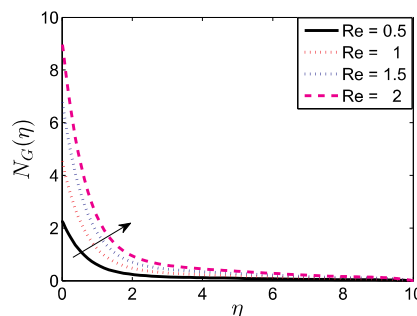
Fig. 17. Entropy profile for various values of Re.
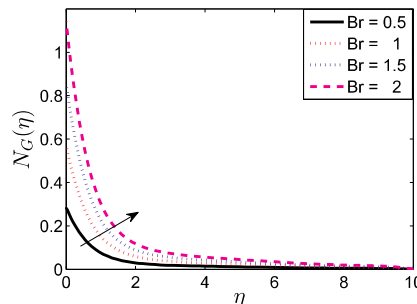
Fig. 18. Entropy profile for various values of Br.
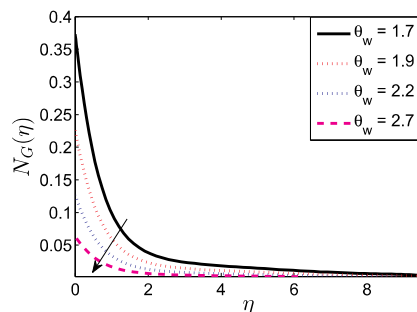
Fig. 19. Entropy profile for various values of θ_w.

Discussion

Velocity field

Fig. 4 shows the velocity profiles for different values of second grade nanofluid parameter $\lambda_1 = 1,2,3,4$. It is observed that the transverse velocity component increases with the second grade nanofluid parameter. Fig. 5 shows that the horizontal velocity profiles increases with the increase in the thermal Grashof number Gr_t and, the peak is observed near the stretching sheet which exponentially decreases from the stretching surface. Fig. 6 shows the velocity profiles for various values

of the solutal buoyancy force given by the solutal Grashof number Gr_c. We note that the effect of increasing Gr_c is to increase the velocity profiles.

Temperature profile

Figs. 7 illustrates the effect of the second grade nanofluid parameter on the temperature profiles when other parameters are kept fixed. It is observed that an increase in the second grade nanofluid parameter leads to an increase in the temperature profiles. The variations of temperature profiles with η are depicted in Fig. 8 for various values of Nr. It is important to note that increase in Nr leads to an increase in the temperature profiles in the thermal boundary layer. It is also observed that the slope of the temperature distribution near the surface when there is radiation is always negative and thus the heat is always transferred from the surface to the ambient fluid which increases the thermal boundary layer. Fig. 9 shows that the temperature profiles $\theta(\eta)$ increases as the temperature ratio parameter θ_w increases for different values of physical parameters. These results are expected because as θ_w increases there is an increase in the temperature difference $T_w - T_\infty$ and so the temperature of the fluid increases. Fig. 10 shows the effect of the thermophoresis parameter on the temperature profiles. It is noted that as the thermophoresis parameter increases, the temperature profiles also increase. Fig. 11 shows temperature profiles for different values of the Eckert number Ec. The effect of Eckert number is to increase the temperature distribution in flow region. Variations of temperature profiles for different values of the suction or injection parameter f_w in the boundary layer are shown in Fig. 12. It is seen that suction has a tendency to reduce the thickness of the boundary layer resulting in a decrease in the fluid temperature profiles.

Concentration field

The effect of the thermophoretic parameters Nt on concentration field are shown in Fig. 13. It is observed that the effect of increasing the thermophoretic parameters is to reduce the concentration profiles. Thus, it can be noted that the concentration profiles as well as the thickness of solutal boundary layer decrease with the increase in the thermophoretic parameter Nt. The changes in the concentration profile $\xi(\eta)$ with increasing homogeneous parameter K and the stretching heterogeneous parameter K_s are depicted in Figs. 14 and 15. The boundary conditions at the wall ($y = 0$) and far from the sheet (streamline y → ∞) are satisfied. The concentration profiles decrease negligibly with K and K_s. This effect occurs only in the vicinity of the wall.

Entropy generation profile

Fig. 16 shows the effect of the magnetic parameter M on the entropy generation number $N_G(\eta)$. An increase in M results in an increase in $N_G(\eta)$. In the neighborhood of the sheet, M has significant impact on $N_G(\eta)$, whereas at regions far from the sheet, M only have a slight effect on $N_G(\eta)$. The magnetic parameter tends to increase the resistance to the fluid motion, consequently the temperature increases, resulting in an increase in the entropy generation. Fig. 17 relates entropy generation number $N_G(\eta)$ to the Reynolds number Re. It is noted that an increase in Re leads to a significant increase in entropy generation, in the vicinity of the sheet. As Re increases, entropy generation caused by the heat transfer dominates through diffusion in the neighborhood of the stretching sheet. Consequently, entropy generation increases due to the contribution of heat transfer. Moreover, when Re increases, the inertia forces are enhanced, hence, the values of the viscous forces decrease. Fig. 18 displays entropy generation with the Brinkman number, which represents a measure of the significance of the heat produced by viscous heating to heat transported by molecular conduction. An increase in Br tends to increase $N_G(\eta)$ especially in the vicinity of the sheet. Viscous

dissipation prevails through the heat transported via the molecular conduction in the neighborhood of the sheet. In the vicinity of the sheet, essential heat generation occurs over the boundary layer which increases the degree of disorder of the system. Fig. 19 shows the changes in the entropy generation number $N_G(\eta)$ with the temperature ratio parameter θ_w. It can be observed that in the neighborhood of the sheet, $N_G(\eta)$ decreases with increasing θ_w.

Conclusion

Entropy generation and the effect of homogeneous-heterogeneous reactions on second grade magnetohydrodynamic nanofluid flow over a convectively heated stretching sheet with nonlinear thermal radiation and viscous dissipation has been investigated. The major outcomes of this study are:

- Enhancement occur in the momentum and thermal boundary layer thicknesses when the second grade nanofluid parameter increases.
- The thermophoresis parameter acts to increase the temperature profiles.
- The solute concentration at the surface decrease with the strength of the homogeneous and heterogeneous reactions.
- Entropy generation is enhanced by the Hartmann, Reynolds and Brinkmann numbers.
- The entropy generation number decreases with the increase of temperature difference ratio parameter.

Acknowledgments

References

[1] Das K, Sharma RP, Sarkar A. Heat and mass transfer of a second grade magneto-hydrodynamic fluid over a convectively heated stretching sheet. J Comput Des Engg 2016;3:330–6.

[2] Jamila M, Rauf A, Fetecau C, Khan NA. Helical flows of second grade fluid due to constantly accelerated shear stresses. Commun Nonlinear Sci Numer Simul 2011;16:1959–69.

[3] Turkyilmazoglu M. Dual and triple solutions for MHD slip flow of non-Newtonian fluid over a shrinking surface. Comput Fluids 2011;70:53–8.

[4] Khan WA, Pop I. Boundary-layer flow of a nanofluid past a stretching sheet. Int J Heat Mass Transf 2010;53:2477–83.

[5] Makinde OD, Aziz A. Boundary layer flow of a nanofluid past a stretching sheet with a convective boundary condition. Int J Therm Sci 2011;50:1326–32.

[6] Mustafa M, Hayat T, Pop I, Asghar S, Obaidat S. Stagnation-point flow of a nanofluid towards a stretching sheet. Int J Heat Mass Transf 2011;54:5588–94.

[7] Akinbobola TE, Okoya SS. The flow of second grade fluid over a stretching sheet with variable thermal conductivity and viscosity in the presence of heat source/sink. J Nigerian Mathe Soc 2015;34(3):331–42.

[8] Erdogan ME, Imrak CE. Steady flow of a second-grade fluid in an annulus with porous walls. Mathe Prob Engg 2008. Article ID 867906.

[9] Nadeem S, Rehman A, Lee C, Lee J. Boundary layer flow of second grade fluid in a cylinder with heat transfer. Math Prob Engg 2012. Article ID 640289.

[10] Buongiorno J. Convective transport in nanofluids. J Heat Transf 2006;128(3):240–50.

[11] Sahoo B. Effects of slip, viscous dissipation and Joule heating on the MHD flow and heat transfer of a second grade fluid past a radially stretching sheet. Appl Math Mech 2010;31(2):159–73.

[12] Zhu J, Zheng LC, Zhang ZG. Effects of slip condition on MHD stagnation-point flow over a power-law stretching sheet. Appl Math Mech 2010;31(4):439–48.

[13] Mansur S, Ishak A, Pop I. Flow and heat transfer of nanofluid past stretching/shrinking sheet with partial slip boundary conditions. Appl Math Mech 2014;35(11):1401–10.

[14] Noghrehabadi A, Saffarian MR, Pourrajab R, Ghalambaz M. Entropy analysis for nanofluid flow over a stretching sheet in the presence of heat generation/absorption and partial slip. J Mech Sci Technol 2013;27(3):927–37.

[15] Abolbashari MH, Freidoonimehr N, Nazari F, Rashidi MM. Entropy analysis for an unsteady MHD flow past a stretching permeable surface in nano-fluid. Powder Technol 2014;267:256–67.

[16] Aiboud S, Saouli S. Entropy analysis for viscoelastic magnetohydrodynamic flow over a stretching surface. Int J Nonlinear Mech 2010;45:482–9.

[17] Butt AS, Munawar S, Ali A, Mehmood A. Entropy generation in hydrodynamic slip

flow over a vertical plate with convective boundary. J Mech Sci Technol 2012;26(9):2977–84.

[18] Magherbi M, Abbassi H, Hidouri N, Ben Brahim A. Second law analysis in convective heat and mass transfer. Entropy 2006;8:1–17.

[19] Hidouri N, Magherbi M, Abbassi H, Ben Brahim A. Entropy generation in double diffusive in presence of Soret effect. Prog Comput Fluid Dyn 2007;5:237–46.

[20] Aracely L, Guillermo I, Joel P, Joel M, Orlando L. Entropy generation analysis of MHD nanofluid flow in a porous vertical microchannel with nonlinear thermal radiation, slip flow and convective-radiative boundary conditions. Int J Heat and Mass Transf 2017;107:982–94.

[21] Chaudhary MA, Merkin JH. A simple isothermal model for homogeneous-heterogeneous reactions in boundary-layer flow. I Equal diffusivities. Fluid Dyn Res 1995;16(6):311–33.

[22] Chaudhary MA, Merkin JH. A simple isothermal model for homogeneous-heterogeneous reactions in boundary-layer flow. II Different diffusivities for reactant and autocatalyst. Fluid Dyn Res 1995;16(6):335–59.

[23] Merkin JH. A model for isothermal homogeneous-heterogeneous reactions in boundary-layer flow. Math Comput Modell 1996;24(8):125–36.

[24] Khan WA, Pop IM. Effects of homogeneous-heterogeneous reactions on the viscoelastic fluid toward a stretching sheet. J Heat Transf 2012;134(6):064506.

[25] Shaw S, Kameswaran PK, Sibanda P. Homogeneous-heterogeneous reactions in micropolar fluid flow from a permeable stretching or shrinking sheet in a porous medium. Boundary Value Probl 2013;1:77.

[26] Pal D, Mondal H. MHD non-Darcian mixed convection heat and mass transfer over a non-linear stretching sheet with Soret-Dufour effects and chemical reaction. Int Commun Heat and Mass Transf 2011;38:463–7.

[27] De P, Mondal H, Bera UK. Dual solutions of heat and mass transfer of nanofluid over a stretching/shrinking sheet with thermal radiation. Meccanica 2016;51(1):117–24.

[28] Motsa SS. A new spectral local linearization method for nonlinear boundary layer flow problems. J Appl Math 2013:1–15.

[29] Olanrewaju MA, Gbadeyan JA, Idowu AS. Flow and heat transfer analysis of a second grade fluid with newtonian heating in the presence of elastic deformation in a porous medium. Pacific J Sci Technol 2016;17(1).

[30] Hayat T, Shehzad SA, Qasim M, Obaidat S. Flow of a second grade fluid with convective boundary conditions. Therm Sci 2011;15(2):253–61.

Chapter 6

Bivariate Spectral Local Linearization Method (BSLLM) for Unsteady MHD Micropolar Nanofluids with Homogeneous–Heterogeneous Chemical Reactions Over a Stretching Surface

The work in this chapter extends from that in the previous chapters in the sense that we now consider an unsteady flow in which the fluid properties vary with both time and space. We consider a micropolar fluid that contain rotating micro components. We explore the characteristics of homogeneous–heterogeneous reactions in unsteady two-dimensional MHD flow of a micropolar nanofluid over a stretching surface. The homogeneous–heterogeneous chemical reactions have cubic autocatalytic kinetics and first order kinetics. The bivariate spectral local linearization method, which has not been used for a micropolar non-Newtonian nanofluid flow before, is used to solve the model equations. The method is applied independently in time and space directions. We show the accuracy of bivariate spectral local linearization method for the fluid flow configuration under study.

ORIGINAL PAPER

CrossMark

Bivariate Spectral Local Linearisation Method (BSLLM) for Unsteady MHD Micropolar-Nanofluids with Homogeneous–Heterogeneous Chemical Reactions Over a Stretching Surface

Hloniphile Sithole[1] · Hiranmoy Mondal[1] · Vusi Mpendulo Magagula[2] · Precious Sibanda[1] · S. Motsa[1,2]

Abstract

A mathematical model of MHD micropolar-nanofluid flow deformed by a stretchable surface is presented with a homogeneous–heterogeneous reactions given by isothermal cubic auto-catalator kinetics and first order kinetics. We assumed the existence of an induced magnetic field. The basic microrotation flow and heat mass transfer nonlinear equations are solved using the bivariate spectral local linearisation method. An analysis of the accuracy of the method is given using residual errors, and the influence of certain variables on the fluid properties are discussed. The results show, that the concentration distribution is reduced by an increase in the homogeneous reaction parameter while it increases with the Schmidt number. The rate of heat transfer is enhanced by larger values of the Prandtl number and the thermophoresis parameter.

Keywords Nanofluids · Homogeneous–heterogeneous reactions · Micropolar fluid · Thermophoresis · Brownian motion

List of Symbols

C_a, C_b	Concentration of homogeneous–heterogeneous reactions species
C_{fx}, Nu_x, Sh_x	Local skin friction, Nusselt and Sherwood number
C_∞	Species concentration far away from the wall
T_∞	Temperature of the fluid far away from the wall
C_p	Specific heat at constant pressure
D_B	Mass diffusivity
f	Dimensionless stream function
Ha	Hartmann number

Hiranmoy Mondal
hiranmoymondal@yahoo.co.in

1   School of Mathematics, Statistics and Computer Science, University of KwaZulu-Natal, Private Bag X01, Scottsville, Pietermaritzburg 3209, South Africa

2   Department of Mathematics, Faculty of Science and Engineering, University of Swaziland, Private Bag 4, Matsapha, Swaziland

Springer

86

12   Page 2 of 14   Int. J. Appl. Comput. Math   (2019) 5:12

K	Material parameter
K_s	Heterogeneous reaction parameter
k_1^*	Thermal conductivity of the fluid
N	Angular velocity
Q_0	Heat generation coefficient
Pr	Prandtl number
D_B	Brownian diffusion coefficient
D_T	Thermophoretic diffusion coefficient
N_b	Brownian motion parameter
N_t	Thermophoresis parameter
Sc_A	Scidth number
u, v	Velocity component

Greek Symbols

ψ	Stream function
λ	Homogeneous reaction rate parameter
ρ	Density of the fluid
μ	Dynamic viscosity of the fluid
ν	Kinematic viscosity
ξ, η	Transformed variables
ϵ	Ratio of the diffusion coefficient

Subscripts

C	Concentration
T	Temperature
w	Conditions at the wall
∞	Free stream condition

Introduction

Mixed convection due to homogeneous–heterogeneous chemical reactions deformed a stretching surface arises in many applications, such as in the production of plastic, polythene, paper, polymer extrusion, cooling of elastic sheets, and other areas in, science and engineering technology. The flow of a non-Newtonian fluid has applications in many areas including the biosciences, the manufacture and use of paints and liquid crystals. In this study the non-Newtonian fluids that are of particular interest are micropolar fluids with suspended nanoparticles and subject to an applied magnetic field. An excellent review of micropolar fluids and their applications was presented by Kumari et al. [1], Pal and Chatterjee [2]. There is also an extensive literature on MHD fluid flows by Sithole et al. [3].

The effect of MHD heat and mass transfer subject to viscous dissipation in a micropolar nanofluid through a porous medium is investigated by Ishak et al. [4], Muthuraj and Srinivas [5], Shercliff [6] and Pal and Mondal [7]. The flow of electrically conducting micropolar nanofluid over a moving vertical surface with non-consistent heat source/sink investigated by Sarkar and Kundu [8].

Kameswaran et al. [9] and Ravikiran and Radhakrishnamacharya [10] studied the effect of combined homogeneous and heterogeneous chemical reactions on the peristaltic motion of a micropolar fluid through a porous medium with wall effects and a slip boundary condition. The effects of homogeneous–heterogeneous reactions and nonlinear density temperature

87

Int. J. Appl. Comput. Math   (2019) 5:12   Page 3 of 14   12

variation in a micropolar fluid flow with convective boundary condition was analyzed by RamReddy and Pradeepa [11] and Sachin et al. [12]. From the literature it would appear that nonlinear convection in unsteady MHD micropolar nanofluids flow with homogeneous–heterogeneous reactions has not been fully investigated. The current study investigates this problem.

Based on the above observations, the aim of the study is to explore the characteristics of homogeneous–heterogeneous reactions in unsteady two-dimensional MHD flow of a micropolar nanofluid over a stretching surface. The transformed conservation nonlinear equations are solved by efficient bivariate spectral local linearisation method [13]. This manuscript also investigates the micropolar-based nanofluids to be utilized with homogeneous–heterogeneous chemical reactions. The analysis discusses the validity of the continuum assumption for micropolar-based nanofluids, temperature response of the particles inside of the fluid (see Refs. [14–16]).

Formulation

Assuming an unsteady two-dimensional micropolar nano fluid flow deformed by implementing stretchable surface having homogeneous–heterogeneous chemical reactions. The flow of the micropolar fluid is restricted to ($y > 0$) and the stagnation point is fixed at $x = 0$. The wall and ambient temperature are T_w and T_∞ respectively, C_a and C_b the concentrations of homogeneous and heterogeneous species A and B respectively (see Khan et al. [17], Hayat et al. [18]). The equationstake the forms:

$$A + 2B \rightarrow 3B, \quad \text{rate} = k_1 C_a C_b^2, \tag{1}$$

$$A \rightarrow B, \quad \text{rate} = k_s C_a \tag{2}$$
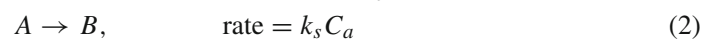
where k_1 and k_2 are the rate constants. Using these assumptions, and the usual boundary layer approximation, the system of equations for the viscoelastic nanofluid is given by:

$$\frac{\partial u}{\partial x} + \frac{\partial v}{\partial y} = 0, \tag{3}$$

$$\frac{\partial u}{\partial t} + u\frac{\partial u}{\partial x} + v\frac{\partial u}{\partial y} = U_e\frac{dU_e}{dx} + \left(\frac{\mu + k_1^*}{\rho}\right)\left(\frac{\partial^2 u}{\partial x^2} + \frac{\partial^2 u}{\partial y^2}\right)$$
$$+ \frac{k_1^*}{\rho}\frac{\partial N}{\partial y} - \frac{\sigma B_0^2}{\rho}(u - U_e) \tag{4}$$

$$\rho_j\left(\frac{\partial N}{\partial t} + u\frac{\partial N}{\partial x} + v\frac{\partial N}{\partial y}\right) = \gamma\frac{\partial^2 N}{\partial y^2} - k_1^*\left(2N + \frac{\partial u}{\partial y}\right) \tag{5}$$

$$\frac{\partial T}{\partial t} + u\frac{\partial T}{\partial x} + v\frac{\partial T}{\partial y} = \frac{\kappa}{\rho C_p}\left(\frac{\partial^2 T}{\partial x^2} + \frac{\partial^2 T}{\partial y^2}\right) + \tau D_B\left(\frac{\partial C_b}{\partial x}.\frac{\partial T}{\partial x} + \frac{\partial C_b}{\partial y}.\frac{\partial T}{\partial y}\right)$$
$$+ \tau\frac{D_T}{T_\infty}\left[\left(\frac{\partial T}{\partial x}\right)^2 + \left(\frac{\partial T}{\partial y}\right)^2\right] + \frac{Q_0}{\rho C_p}(T - T_\infty), \tag{6}$$

$$\frac{\partial C_a}{\partial t} + u\frac{\partial C_a}{\partial x} + v\frac{\partial C_a}{\partial y} = D_A\left(\frac{\partial^2 C_a}{\partial x^2} + \frac{\partial^2 C_a}{\partial y^2}\right)$$
$$+ \frac{D_T}{T_\infty}\left(\frac{\partial^2 T}{\partial x^2} + \frac{\partial^2 T}{\partial y^2}\right) - k_1 C_a C_b^2, \tag{7}$$

88

12   Page 4 of 14   Int. J. Appl. Comput. Math   (2019) 5:12

$$\frac{\partial C_b}{\partial t} + u\frac{\partial C_b}{\partial x} + v\frac{\partial C_b}{\partial y} = D_B\left(\frac{\partial^2 C_b}{\partial x^2} + \frac{\partial^2 C_b}{\partial y^2}\right)$$

$$+ \frac{D_T}{T_\infty}\left(\frac{\partial^2 T}{\partial x^2} + \frac{\partial^2 T}{\partial y^2}\right) + k_1 C_a C_b^2, \tag{8}$$

where t is the time, u and v are the velocity in the x- and y-directions respectively, $v = (\mu/\rho)$ is the kinematic viscosity, ρ is the density, k_1^* is the vortex viscosity, N angular velocity of the microroration, σ is the electrical conductivity, j is the microinertia density and γ is the spin gradient viscosity. Moreover, Q_0 is the volumetric rate of heat generation, $\tau = (\rho c)_p/(\rho c)_f$ is ratio between the effective heat capacity of the nanofluid and the heat capacity of the base fluid, D_B and D_T are the Brownian motion coefficient thermophoretic diffusion coefficient respectively. The convenient conditions for this problem are:

$$u = u_w = ax, \ v = 0, \ N = -n\frac{\partial u}{\partial y},$$

$$T = T_w(x), \ D_A\frac{\partial C_a}{\partial y} = k_s C_a, \ D_B = \frac{\partial C_b}{\partial y} = -k_s C_a \ \text{as} \ y = 0,$$

$$u \to 0, \ N \to 0, \ T \to T_\infty, \ C_a \to C_\infty, \ C_b \to 0 \ \text{as} \ y \to \infty. \tag{9}$$

To reduce the equations above to a more convenient form, we introduce the non-dimensional variables:

$$\psi = (av)^{1/2}\xi^{1/2}xf(\xi, \eta), \ \eta = \left(\frac{a}{v}\right)^{1/2}\xi^{-1/2}y, \ \xi = 1 - e^\zeta, \ \zeta = at,$$

$$N = \left(\frac{a}{v}\right)^{1/2}\xi^{-1/2}axh(\xi, \eta), \ \theta(\xi, \eta) = \frac{T - T_\infty}{T_w - T_\infty}, \tag{10}$$

$$g(\xi, \eta) = \frac{C_a}{C_\infty}, \ \phi(\xi, \eta) = \frac{C_b}{C_\infty}$$

where $0 \leq \xi \leq 1$, and ψ is the stream function which is defined in the usual form as $u = \frac{\partial \psi}{\partial y}$, $v = -\frac{\partial \psi}{\partial x}$. The nonlinear equations and boundary conditions are reduced to

$$(1 + K)f''' + Kh' + \frac{1}{2}\eta(1 - \xi)f'' + \xi(ff'' - f'^2 - Ha^2(f' - 1))$$

$$= \xi(1 - \xi)\frac{\partial f'}{\partial \xi}, \tag{11}$$

$$\left(1 + \frac{K}{2}\right)h'' + \frac{1}{2}(1 - \xi)(h + \eta h') + \xi(fh' - f'h - K(2h + f''))$$

$$= \xi(1 - \xi)\frac{\partial h}{\partial \xi}, \tag{12}$$

$$\frac{1}{Pr}\theta'' + N_b\theta'\phi' + N_t\theta'^2 + \xi(f\theta' + \delta\theta) + \frac{1}{2}\eta(1 - \xi)\theta'$$

$$= \xi(1 - \xi)\frac{\partial \theta}{\partial \xi}, \tag{13}$$

$$\frac{1}{S_{CA}}\left(g'' + \frac{N_t}{N_b}\theta''\right) + \xi fg' - \lambda\xi g\phi^2 + \frac{1}{2}\eta(1 - \xi)g'$$

$$= \xi(1 - \xi)\frac{\partial g}{\partial \xi}, \tag{14}$$

89

Int. J. Appl. Comput. Math   (2019) 5:12   Page 5 of 14   12

$$\frac{1}{\epsilon S_{CA}}\left(\phi'' + \frac{N_t}{N_b}\theta''\right) + \xi f\phi' + \xi\lambda g\phi^2 + \frac{1}{2}(1-\xi)\eta\phi'$$

$$= \xi(1-\xi)\frac{\partial\phi}{\partial\xi}. \tag{15}$$

The appropriate boundary conditions are:

$$f(\xi,0) = 0, \quad f'(\xi,0) = 1, \quad h(\xi,0) = -nf''(\xi,0), \quad \theta(\xi,0) = 1,$$
$$g'(\xi,0) = K_s g(\xi,0), \quad \phi'(\xi,0) = -K_s g(\xi,0) \quad \text{at} \quad \eta \to 0 \tag{16}$$
$$f'(\xi,\infty) = 1, \quad h(\xi,\infty) = 0, \quad \theta(\xi,\infty) = 0, \quad g(\xi,\infty) = 1,$$
$$\phi(\xi,\infty) = 0, \quad \text{at} \quad \eta \to \infty \tag{17}$$

where K is the material parameter, Ha is the Hartmann number, λ is the homogeneous reaction rate parameter, ϵ is the ratio of the diffusion coefficient, K_s heterogeneous reaction rate parameter.

The diffusion co-efficient D_A and D_B are considered of comparable size which leads to assume $D_A = D_B$, that is $\epsilon = 1$. Hence,

$$g(\xi,\eta) + \phi(\xi,\eta) = 1. \tag{18}$$

Thus, Eqs. (14) and (15) reduce to single equation

$$\frac{1}{S_{CA}}\left(g'' + \frac{N_t}{N_b}\theta''\right) + \xi fg' - \lambda\xi g(1-g)^2 + \frac{1}{2}\eta(1-\xi)g' = \xi(1-\xi)\frac{\partial g}{\partial\xi} \tag{19}$$

The local skin friction coefficient C_{f_x}, the local Nusselt number Nu_x and the local Sherwood number Sh_x are the most significant physical quantities. These can be written as:

$$C_f = \frac{\tau_w}{\rho u_w^2(x)}, \tag{20}$$

where

$$\tau_w = \left((\mu + k_1^*)\frac{\partial u}{\partial y} + k_1^* N\right)_{y=0}. \tag{21}$$

Thus

$$C_{f_x} Re^{1/2} = \xi^{-1/2}\left(1 + (1-n)K\right)f''(\xi,0), \tag{22}$$

where $Re = \frac{u_w(x)x}{\nu}$ is the local Reynolds number. The Nusselt number is

$$Nu_x = \frac{xh_w}{\kappa(T_w - T_\infty)}, \tag{23}$$

where h_w is the surface heat flux, which can been written as:

$$h_w = -\kappa\left(\frac{\partial T}{\partial y}\right)_{y=0}. \tag{24}$$

Equation (23) becomes as

$$Nu_x Re^{-1/2} = -\xi^{-1/2}\theta'(\xi,0). \tag{25}$$

Finally, the Sherwood number is

$$Sh_x = \frac{xh_m}{\rho D_B(C_w - C_\infty)}, \tag{26}$$

where h_m represents the surface mass flux, which can be obtained from

$$h_m = -\rho D_B \left(\frac{\partial C}{\partial y}\right)_{y=0}, \tag{27}$$

hence, Eq. (26) becomes as

$$Sh_x Re^{-1/2} = -\xi^{-1/2}\phi'(\xi, 0). \tag{28}$$

Methods of Solution

In this section we introduce the bivariate spectral local linearisation method (BSLLM)(see Ref. [13]) for approximating solutions of system of the nonlinear partial differential equations. Consider a system of n nonlinear partial differential equations of the form,

$$\Omega_1 [S_1, S_2, \ldots, S_n] = 0, \tag{29}$$

$$\Omega_2 [S_1, S_2, \ldots, S_n] = 0, \tag{30}$$

$$\vdots$$

$$\Omega_n [S_1, S_2, \ldots, S_n] = 0, \tag{31}$$

where

$$S_1 = \left\{ g_1, \frac{\partial g_1}{\partial \eta}, \frac{\partial^2 g_1}{\partial x^2}, \ldots, \frac{\partial^p g_1}{\partial \eta^p}, \frac{\partial g_1}{\partial \zeta}, \frac{\partial}{\partial \zeta}\left(\frac{\partial g_1}{\partial \eta}\right) \right\}, \tag{32}$$

$$S_2 = \left\{ g_2, \frac{\partial g_2}{\partial \eta}, \frac{\partial^2 g_2}{\partial \eta^2}, \ldots, \frac{\partial^p g_2}{\partial \eta^p}, \frac{\partial g_2}{\partial \zeta}, \frac{\partial}{\partial \zeta}\left(\frac{\partial g_2}{\partial \eta}\right) \right\}, \tag{33}$$

$$\vdots$$

$$S_n = \left\{ g_n, \frac{\partial g_n}{\partial \eta}, \frac{\partial^2 g_n}{\partial \eta^2}, \ldots, \frac{\partial^p g_n}{\partial \eta^p}, \frac{\partial g_n}{\partial \zeta}, \frac{\partial}{\partial \zeta}\left(\frac{\partial g_n}{\partial \eta}\right) \right\} \tag{34}$$

where $g_k(\eta, \zeta)$ and Ω_k for $k = 1, 2, \ldots, n$ are non-linear operators containing spatial and time derivatives of $g_k(\eta, \zeta)$. We assume that the solution may be approximated by a bivariate Lagrange interpolating polynomial of the form

$$g_k(\eta, \zeta) \approx \sum_{i=0}^{N_\eta} \sum_{j=0}^{N_\zeta} g_k(\eta_i, \zeta_j)\mathcal{L}_i(\eta)\mathcal{L}_j(\zeta), \tag{35}$$

for $k = 1, 2, \ldots, n$. The polynomial interpolates $g_k(\eta, \zeta)$ at selected points (η_i, ζ_j) in both the η and ζ directions, for $i = 0, 1, 2, \ldots, N_\eta$ and $j = 0, 1, 2, \ldots, N_\zeta$. These selected grid points are given by

$$\{\eta_i\} = \left\{ \cos\left(\frac{\pi i}{N_\eta}\right) \right\}_{i=0}^{N_\eta}, \quad \{\zeta_j\} = \left\{ \cos\left(\frac{\pi j}{N_\zeta}\right) \right\}_{j=0}^{N_\zeta} \tag{36}$$

91

Int. J. Appl. Comput. Math   (2019) 5:12   Page 7 of 14   12

are the Chebyshev–Gauss–Lobatto points. The function $\mathcal{L}_i(\eta)$ is the characteristic Lagrange cardinal polynomial based on the Chebyshev–Gauss–Lobatto grid points

$$\mathcal{L}_i(\eta) = \prod_{\substack{i=0 \\ i \neq k}}^{N_\eta} \frac{\eta - \eta_k}{\eta_i - \eta_k}, \tag{37}$$

where

$$\mathcal{L}_i(\eta_k) = \delta_{ik} = \begin{cases} 0 & \text{if } i \neq k \\ 1 & \text{if } i = k. \end{cases} \tag{38}$$

Applying the quasilinearisation method independently to each equation, we get

$$\sum_{s=0}^{p} \alpha_{s,r}^{(1)}(\eta, \zeta) g_{1,r+1}^{(s)} + \beta_r^{(1)}(\eta, \zeta) \frac{\partial g_{1,r+1}^{(0)}}{\partial \zeta} + \gamma_r^{(1)}(\eta, \zeta) \frac{\partial g_{1,r+1}^{(1)}}{\partial \zeta} = R_1(\eta, \zeta), \tag{39}$$

$$\sum_{s=0}^{p} \alpha_{s,r}^{(2)}(\eta, \zeta) g_{2,r+1}^{(s)} + \beta_r^{(2)}(\eta, \zeta) \frac{\partial g_{2,r+1}^{(0)}}{\partial \zeta} + \gamma_r^{(2)}(\eta, \zeta) \frac{\partial g_{2,r+1}^{(1)}}{\partial \zeta} = R_2(\eta, \zeta), \tag{40}$$

$$\vdots$$

$$\sum_{s=0}^{p} \alpha_{s,r}^{(n)}(\eta, \zeta) g_{n,r+1}^{(s)} + \beta_r^{(n)}(\eta, \zeta) \frac{\partial g_{n,r+1}^{(0)}}{\partial \zeta} + \gamma_r^{(n)}(\eta, \zeta) \frac{\partial g_{n,r+1}^{(1)}}{\partial \zeta} = R_n(\eta, \zeta), \tag{41}$$

where $\alpha_{s,r}^{(k)}(\eta, \zeta)$, $\beta_r^{(k)}(\eta, \zeta)$ and $\gamma_r^{(k)}(\eta, \zeta)$ are variable coefficients of $g_{k,r+1}^{(s)}$, $\frac{\partial g_{k,r+1}^{(0)}}{\partial \zeta}$, and $\frac{\partial g_{k,r+1}^{(1)}}{\partial \zeta}$, respectively, for $k = 1, 2, \ldots, n$ and $s = 0, 1, 2, \ldots, p$. These coefficients correspond to the kth equation, for $k = 1, 2, \ldots, n$. Since constant p denotes the order of differentiation, then

$$\alpha_{s,r}^{(k)}(\eta, \zeta) = \frac{\partial \Omega_k}{\partial g_{k,r}^{(s)}}, \tag{42}$$

$$\beta_r^{(k)}(\eta, \zeta) = \frac{\partial \Omega_k}{\partial \left(\frac{\partial g_{k,r}^{(0)}}{\partial \zeta} \right)}, \tag{43}$$

$$\gamma_r^{(k)}(\eta, \zeta) = \frac{\partial \Omega_k}{\partial \left(\frac{\partial g_{k,r}^{(1)}}{\partial \zeta} \right)}. \tag{44}$$

$$R_k(\eta, \zeta) = \sum_{s=0}^{p} \alpha_{s,r}^{(k)}(\eta, \zeta) g_{k,r}^{(s)} + \beta_r^{(k)}(\eta, \zeta) \frac{\partial g_{k,r}^{(0)}}{\partial \zeta} + \gamma_r^{(k)}(\eta, \zeta) \frac{\partial g_{k,r}^{(1)}}{\partial \zeta}) - \Omega_k. \tag{45}$$

Equations (39), (40), and (41) are evaluated at the Chebyshev–Gauss–Lobbatto grid points ζ_j ($j = 0, 1, \ldots, N_\zeta$) and η_i ($i = 0, 1, \ldots, N_\eta$). Substituting Eq. (35) and its derivatives into Eqs. (39), (40), and (41) yields

$$A_{1,1} \mathbf{G}_{1,i} + \boldsymbol{\beta}_r^{(1)} \sum_{j=0}^{N_\zeta} d_{i,j} \mathbf{G}_{1,j} + \boldsymbol{\gamma}_r^{(1)} \sum_{j=0}^{N_\zeta} d_{i,j} \mathbf{DG}_{1,j} = \mathbf{R}_{1,i}, \tag{46}$$

92

12   Page 8 of 14   Int. J. Appl. Comput. Math   (2019) 5:12

$$A_{2,2}\mathbf{G}_{2,i} + \boldsymbol{\beta}_r^{(2)} \sum_{j=0}^{N_\zeta} d_{i,j}\mathbf{G}_{2,j} + \boldsymbol{\gamma}_r^{(2)} \sum_{j=0}^{N_\zeta} d_{i,j}\mathbf{DG}_{2,j} = \mathbf{R}_{2,i}, \tag{47}$$

$$\vdots$$

$$A_{n,n}\mathbf{G}_{n,i} + \boldsymbol{\beta}_r^{(n)} \sum_{j=0}^{N_\zeta} d_{i,j}\mathbf{G}_{n,j} + \boldsymbol{\gamma}_r^{(n)} \sum_{j=0}^{N_\zeta} d_{i,j}\mathbf{DG}_{n,j} = \mathbf{R}_{n,i}, \tag{48}$$

where

$$A_{1,1} = \sum_{s=0}^{p} \boldsymbol{\alpha}_{s,r}^{(1)}\mathbf{D}^{(s)}, \quad A_{2,2} = \sum_{s=0}^{p} \boldsymbol{\alpha}_{s,r}^{(2)}\mathbf{D}^{(s)}, \quad \ldots, \quad A_{n,n} = \sum_{s=0}^{p} \boldsymbol{\alpha}_{s,r}^{(n)}\mathbf{D}^{(s)}. \tag{49}$$

The diagonal matrices of the corresponding variable coefficients are given by

$$\boldsymbol{\alpha}_{s,r}^{(k)} = \begin{bmatrix} \alpha_{s,r}^{(k)}(\eta_0, \zeta_j) & & & \\ & \alpha_{s,r}^{(k)}(\eta_1, \zeta_j) & & \\ & & \ddots & \\ & & & \alpha_{s,r}^{(k)}(\eta_{N_\eta}, \zeta_j) \end{bmatrix}, \tag{50}$$

$$\boldsymbol{\beta}_r^{(k)} = \begin{bmatrix} \beta_r^{(k)}(\eta_0, \zeta_j) & & & \\ & \beta_r^{(k)}(\eta_1, \zeta_j) & & \\ & & \ddots & \\ & & & \beta_r^{(k)}(\eta_{N_\eta}, \zeta_j) \end{bmatrix}, \tag{51}$$

$$\boldsymbol{\gamma}_r^{(k)} = \begin{bmatrix} \gamma_r^{(k)}(\eta_0, \zeta_j) & & & \\ & \gamma_r^{(k)}(\eta_1, \zeta_j) & & \\ & & \ddots & \\ & & & \gamma_r^{(k)}(\eta_{N_\eta}, \zeta_j) \end{bmatrix}. \tag{52}$$

Imposing boundary conditions for $i = 0, 1, \cdots, N_\zeta - 1$, Eqs. (46), (47), and (48) can be expressed as the following $N_\zeta(N_\eta + 1) \times N_\zeta(N_\eta + 1)$ matrix system

$$\begin{bmatrix} B_{0,0}^{(k)} & B_{0,1}^{(k)} & \cdots & B_{0,N_\zeta-1}^{(k)} \\ B_{1,0}^{(k)} & B_{1,1}^{(k)} & \cdots & B_{1,N_\zeta-1}^{(k)} \\ \vdots & \vdots & \ddots & \vdots \\ B_{N_\zeta-1,0}^{(k)} & B_{N_\zeta-1,1}^{(k)} & \cdots & B_{N_\zeta-1,N_\zeta-1}^{(k)} \end{bmatrix} \begin{bmatrix} \mathbf{G}_{k,0} \\ \mathbf{G}_{k,1} \\ \vdots \\ \mathbf{G}_{k,N_\zeta-1} \end{bmatrix} = \begin{bmatrix} \mathcal{R}_{k,0} \\ \mathcal{R}_{k,1} \\ \vdots \\ \mathcal{R}_{k,N_\zeta-1} \end{bmatrix}, \tag{53}$$

where

$$B_{(i,i)}^{(k)} = \sum_{s=0}^{p} \boldsymbol{\alpha}_{s,r}^{(k)}\mathbf{D}^{(s)} + \boldsymbol{\beta}_r^{(k)}d_{i,i}\mathbf{I} + \boldsymbol{\gamma}_r^{(k)}d_{i,i}\mathbf{D}, \quad \text{for } k = 1, 2, \ldots, n, \text{ when } i = j,$$
$$B_{(i,j)}^{(k)} = \boldsymbol{\beta}_r^{(k)}d_{i,j}\mathbf{I} + \boldsymbol{\gamma}_r^{(k)}d_{i,j}\mathbf{D}, \quad \text{for } k = 1, 2, \ldots, n, \text{ when } i \neq j. \tag{54}$$

The vector $\mathcal{R}_{k,i}$ is defined as

$$\mathcal{R}_{k,i} = \mathbf{R}_{k,i} - \left(\boldsymbol{\beta}_r^{(k)}d_{i,N_\zeta}\mathbf{I} + \boldsymbol{\gamma}_r^{(k)}d_{i,N_\zeta}\mathbf{D}\right)\mathbf{G}_{k,N_\zeta}$$

93

Int. J. Appl. Comput. Math   (2019) 5:12   Page 9 of 14   12

for $i = 0, 1, \cdots, N_\zeta - 1$ and $k = 1, 2, \ldots, n$. The vector $\mathbf{G}_{k,N_\zeta}$ corresponds to the initial boundary condition which is always prescribed.

Since the highest order of differentiation for Eqs. (11)–(15) is $p = 3$ and $n = 5$, applying the BSLLM method to the equations, we get

$$A_{1,1}\mathbf{G}_{1,i} + \boldsymbol{\beta}_r^{(1)} \sum_{j=0}^{N_\zeta} d_{i,j}\mathbf{G}_{1,j} + \boldsymbol{\gamma}_r^{(1)} \sum_{j=0}^{N_\zeta} d_{i,j}\mathbf{DG}_{1,j} = \mathbf{R}_{1,i}, \tag{55}$$

$$A_{2,2}\mathbf{G}_{2,i} + \boldsymbol{\beta}_r^{(2)} \sum_{j=0}^{N_\zeta} d_{i,j}\mathbf{G}_{2,j} + \boldsymbol{\gamma}_r^{(2)} \sum_{j=0}^{N_\zeta} d_{i,j}\mathbf{DG}_{2,j} = \mathbf{R}_{2,i}, \tag{56}$$

$$A_{3,3}\mathbf{G}_{3,i} + \boldsymbol{\beta}_r^{(3)} \sum_{j=0}^{N_\zeta} d_{i,j}\mathbf{G}_{3,j} + \boldsymbol{\gamma}_r^{(3)} \sum_{j=0}^{N_\zeta} d_{i,j}\mathbf{DG}_{3,j} = \mathbf{R}_{3,i}, \tag{57}$$

$$A_{4,4}\mathbf{G}_{4,i} + \boldsymbol{\beta}_r^{(4)} \sum_{j=0}^{N_\zeta} d_{i,j}\mathbf{G}_{4,j} + \boldsymbol{\gamma}_r^{(4)} \sum_{j=0}^{N_\zeta} d_{i,j}\mathbf{DG}_{4,j} = \mathbf{R}_{4,i}, \tag{58}$$

$$A_{5,5}\mathbf{G}_{5,i} + \boldsymbol{\beta}_r^{(5)} \sum_{j=0}^{N_\zeta} d_{i,j}\mathbf{G}_{5,j} + \boldsymbol{\gamma}_r^{(5)} \sum_{j=0}^{N_\zeta} d_{i,j}\mathbf{DG}_{5,j} = \mathbf{R}_{5,i}, \tag{59}$$

where

$$A_{1,1} = \sum_{s=0}^{3} \boldsymbol{\alpha}_{s,r}^{(1)}\mathbf{D}^{(s)}, \qquad A_{2,2} = \sum_{s=0}^{3} \boldsymbol{\alpha}_{s,r}^{(2)}\mathbf{D}^{(s)}, \qquad A_{3,3} = \sum_{s=0}^{3} \boldsymbol{\alpha}_{s,r}^{(3)}\mathbf{D}^{(s)}, \tag{60}$$

$$A_{4,4} = \sum_{s=0}^{3} \boldsymbol{\alpha}_{s,r}^{(4)}\mathbf{D}^{(s)}, \qquad A_{5,5} = \sum_{s=0}^{3} \boldsymbol{\alpha}_{s,r}^{(5)}\mathbf{D}^{(s)}. \tag{61}$$

The coefficients for $s = 0, 1, 2, 3$ are given by:

$$\alpha_{s,r}^{(1)} = \frac{\partial \Omega_1}{\partial g_{1,r}^{(s)}}, \quad \alpha_{s,r}^{(2)} = \frac{\partial \Omega_2}{\partial g_{2,r}^{(s)}}, \quad \alpha_{s,r}^{(3)} = \frac{\partial \Omega_3}{\partial g_{3,r}^{(s)}}, \quad \beta_r^{(1)} = \frac{\partial \Omega_1}{\partial \left(\frac{\partial g_{1,r}^{(0)}}{\partial \zeta}\right)}, \quad \beta_r^{(2)} = \frac{\partial \Omega_2}{\partial \left(\frac{\partial g_{2,r}^{(0)}}{\partial \zeta}\right)},$$

$$\beta_r^{(3)} = \frac{\partial \Omega_3}{\partial \left(\frac{\partial g_{3,r}^{(0)}}{\partial \zeta}\right)}, \quad \gamma_r^{(1)} = \frac{\partial \Omega_1}{\partial \left(\frac{\partial g_{1,r}^{(1)}}{\partial \zeta}\right)}, \quad \gamma_r^{(2)} = \frac{\partial \Omega_2}{\partial \left(\frac{\partial g_{2,r}^{(1)}}{\partial \zeta}\right)}, \quad \gamma_r^{(3)} = \frac{\partial \Omega_3}{\partial \left(\frac{\partial g_{3,r}^{(1)}}{\partial \zeta}\right)}.$$

The right hand side for $k = 1, 2, 3, 4, 5$ is given by

$$R_{k,i} = \sum_{s=0}^{3} \alpha_{s,r}^{(k)}(\eta, \zeta)g_{k,r}^{(s)} + \beta_r^{(k)}(\eta, \zeta)\frac{\partial g_{k,r}^{(0)}}{\partial \zeta} + \gamma_r^{(k)}(\eta, \zeta)\frac{\partial g_{k,r}^{(1)}}{\partial \zeta}) - \Omega_k. \tag{62}$$

The equations can be expressed as a matrix system in Eq. (53) and the entries of the matrix are given by Eq. (54).

94

12   Page 10 of 14   Int. J. Appl. Comput. Math   (2019) 5:12

Results and Discussion

The numerical solutions of the Eqs. (11)–(15) together with the boundary conditions (16) are presented. $N_t = 10$ and $N_x = 60$ collocation points were used in the ξ and η domains respectively. By considering the error norms between two successive iterations, the convergence and stability of the iteration scheme was evaluated. We define the error norms as,

$$E_f = \max_{0 \leq i \leq N_t} ||\mathbf{F}_{r+1,i} - \mathbf{F}_{r,i}||_\infty, \tag{63}$$

Figure 1 depicts the change in the error terms E_f, E_h, E_θ, E_g, and E_ϕ with the number of iterations. The errors E_f, E_h, E_θ, E_g, and E_ϕ decrease rapidly with an increase in the number of iterations. It is evident that the BSLLM is converging and the size of the error is less than 10^{-10} to 10^{-14} after 5 iterations. Furthermore, the accuracy of the BSLLM is estimated by considering the residual errors. We define the residual error functions as,

$$Res_q = \max_{0 \leq i \leq N_t} ||\delta_q [\mathbf{F}_i, \ \mathbf{H}_i, \ \boldsymbol{\Theta}_i, \ \mathbf{G}_i, \ \boldsymbol{\Phi}_i] ||_\infty, \tag{64}$$

where q stands for δ_f, δ_h, δ_θ, δ_g, and δ_ϕ represent the corresponding nonlinear PDEs. The maximum infinity norm is considered over all collocation points ξ_i. Figure 2 gives the residual errors $||Res_f||_\infty$, $||Res_h||_\infty$, $||Res_\theta||_\infty$, $||Res_g||_\infty$, and $||Res_\phi||_\infty$ against the number of iterations. Residual errors decrease significantly with the increase in the number of iterations.

Fig. 1 Error norms E_f, E_h, E_θ, E_g, and E_ϕ against the number of iterations
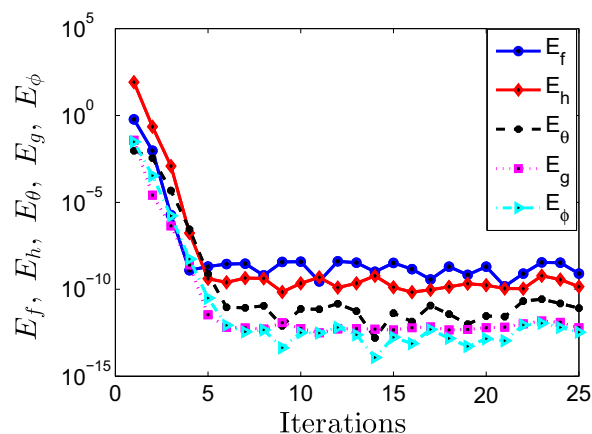
Fig. 2 Residual errors $||Res_f||_\infty$, $||Res_h||_\infty$, $||Res_\theta||_\infty$, $||Res_g||_\infty$, and $||Res_\phi||_\infty$ against the number of iterations

95

Int. J. Appl. Comput. Math   (2019) 5:12   Page 11 of 14   12
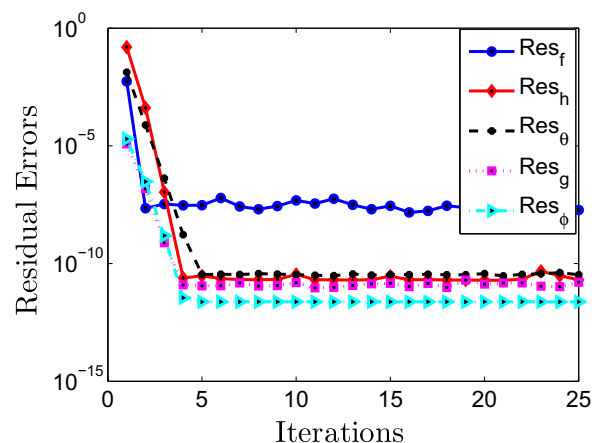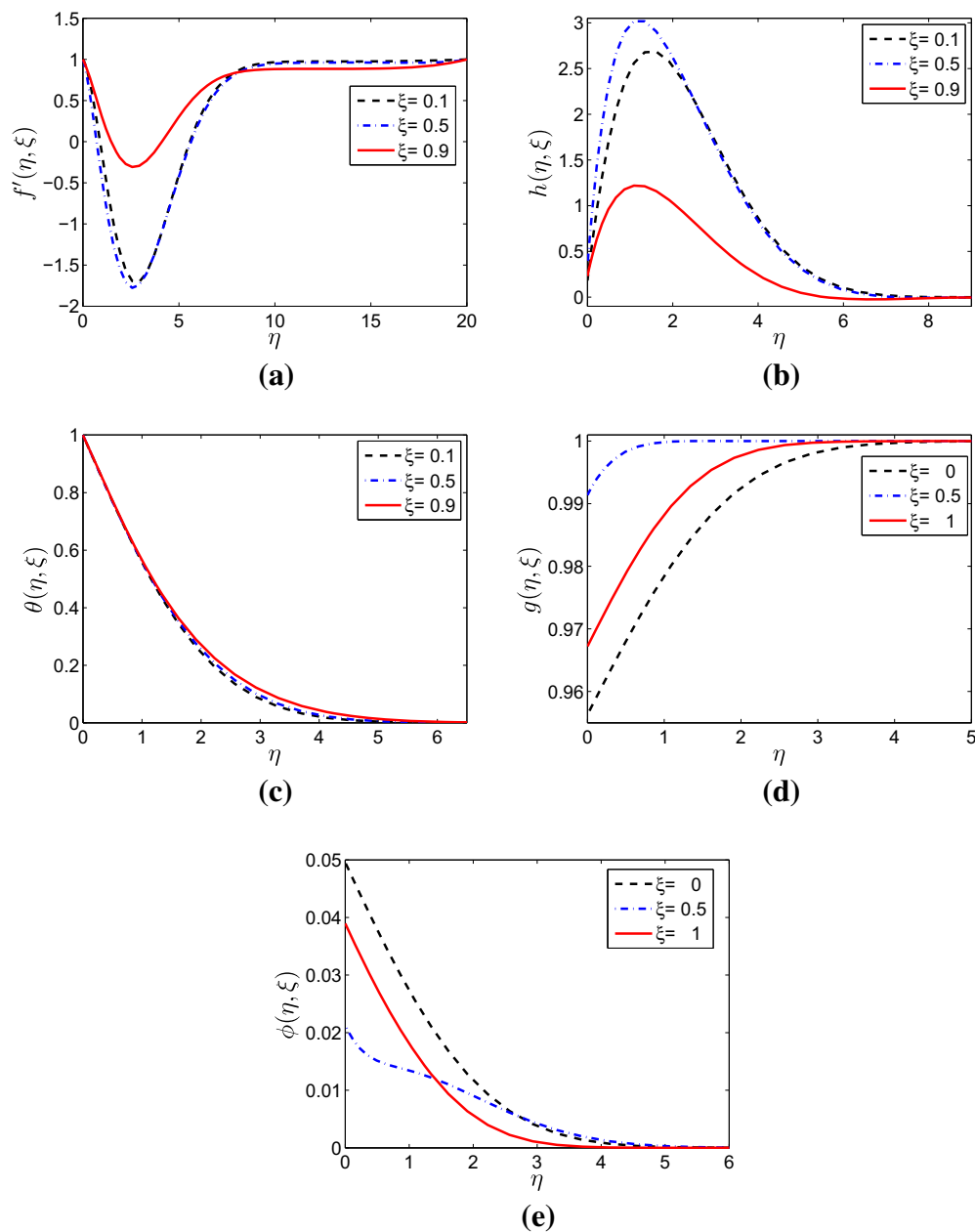
Fig. 3 Effect of varying dimensionless time ξ on **a** the velocity profile $f'(\xi, \eta)$, **b** angular momentum $h(\xi, \eta)$, **c** temperature profile $\theta(\xi, \eta)$, **d** homogeneous profile $g(\xi, \eta)$ and **e** heterogeneous profile $\phi(\xi, \eta)$

The results are consistent and less than 10^{-7} to 10^{-12} after 4 iterations. This analysis of the convergence and accuracy of the method of solution show that we can trust the numerical solutions obtained using the BSLLM.

Figure 3 illustrate the effect of increasing time ξ on the velocity profiles, angular velocity profiles, temperature profiles and homogeneous–heterogeneous profiles against the space η with $K = 1$, $Ha = 2$, $Pr = 6.8$, $N_b = 1$, $N_t = 0.05$, $S_{CA} = 0.94$, $\epsilon = 1.5$, $\delta = 0.1$, $\lambda = 0.5$, $n = 1/2$, and $K_s = 0.025$. When $\xi = 0$ and $\xi = 1$ Eqs. (11)–(15) reduces to
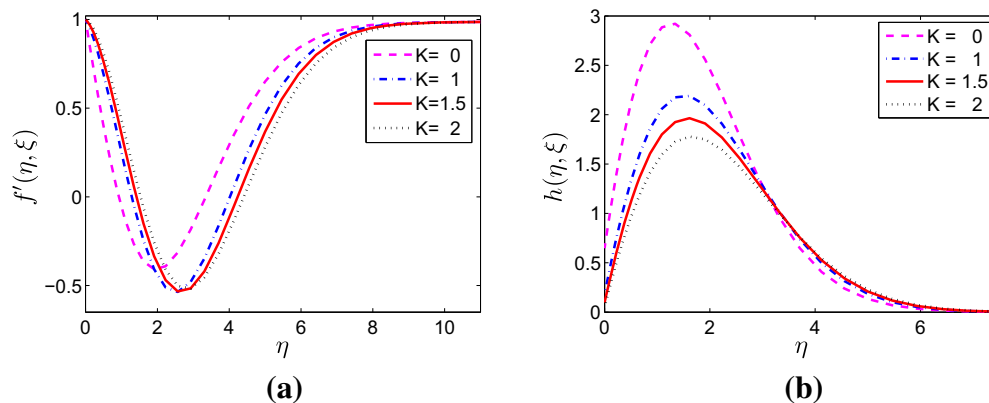
Fig. 4 Effect of varying material parameter K on **a** the velocity profiles $f'(\xi, \eta)$, **b** angular velocity $h(\xi, \eta)$
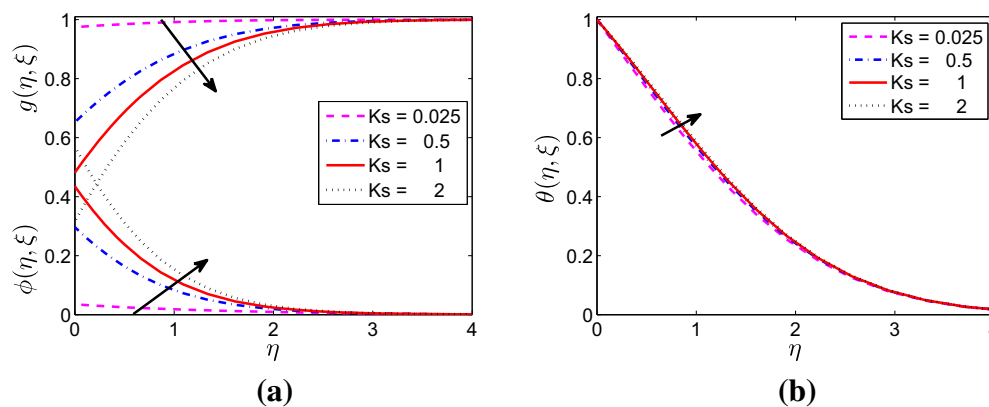
Fig. 5 Effect of the heterogeneous reaction parameter K_s on **a** the concentration profiles $g(\xi, \eta)$ and $\phi(\xi, \eta)$, **b** temperature profile $h(\xi, \eta)$

ordinary differential equations. These results show that the velocity profiles decrease when at $0 \leq \eta \leq 8$ while the opposite trend is observed for the angular velocity and temperature profiles. The reaction rate profiles increase with the time variable ξ, whereas for $n = 1/2$. It is evident from this figure that there is a smooth transition from small time solution $\xi = 0$ to large time solution $\xi = 1$.

The effect of the material parameter K on the velocity profile $f'(\xi, \eta)$ and microrotation $h(\xi, \eta)$ is plotted in Fig. 4 for $Ha = 2$, $Pr = 0.72$, $N_b = 1$, $N_t = 0.05$, $S_{CA} = 0.94$, $\epsilon = 1.5$, $\delta = 0.1$, $\lambda = 0.1$, $n = 0.5$, $K_s = 0.025$. At the place surface the velocity is initially equal to 1, and decreases to a minimum value. It then increases again away from the plate until it reaches a free stream value of unity that satisfies the boundary conditions. Increasing the material parameter K has a noticeable effect on the non-dimensional velocity as it can be seen in Fig. 4a. For $\eta < 3$, velocity increase with K while for $\eta > 3$, velocity decreases with an increases in K. In Fig. 4b the angular velocity increases with the material parameter K.

The impact of varying the strength of the heterogenous chemical reaction K_s is shown in Fig. 5a for both species A $g(\xi, \eta)$ and species B $\phi(\xi, \eta)$, $K = 3$, $Pr = 0.72$, $N_b = 1$, $N_t = 0.05$, $S_{CA} = 0.94$, $\epsilon = 1.5$, $\delta = 0.1$, $\lambda = 0.1$, $n = 0.5$ and heterogenous chemical reaction Ks increases, g decreases. As heterogenous chemical reaction K_s increases, ϕ increases. Both the decrease and the increase in the concentration profiles can be observed near the wall. At

97

Int. J. Appl. Comput. Math   (2019) 5:12   Page 13 of 14   12
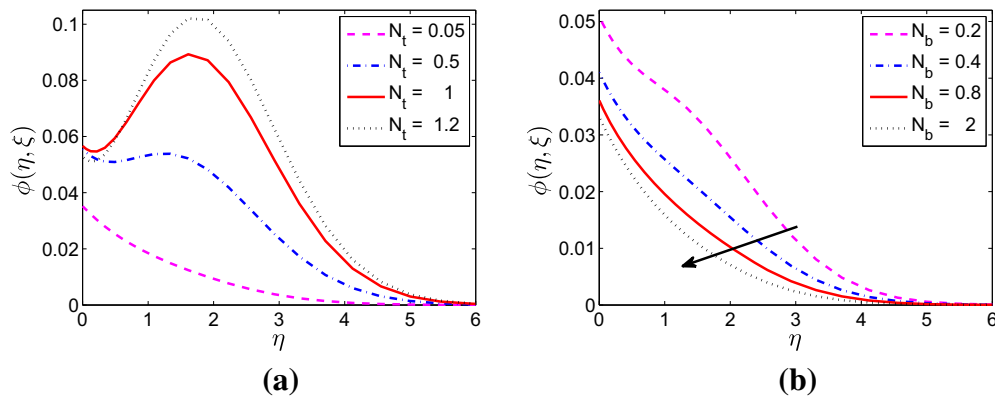
Fig. 6 Effect of the thermophoresis parameter Nt and Brownian motion parameter Nb on the concentration profiles $\phi(\xi, \eta)$

the free stream the concentration profiles asymptotically approaches 1 and 0, satisfying the boundary conditions. Figure 5b shows that increasing the heterogenous chemical reaction Ks increases the temperature.

Increasing the values of N_t increases the concentration profiles $\phi(\xi, \eta)$, see in Fig. 6a $K = 3$, $N_b = 1$, $N_t = 0.05$, $S_{CA} = 0.94$, $\epsilon = 1.5$, $\delta = 0.1$, $\lambda = 0.1$, $n = 0.5$ Increasing the Brownian motion parameter N_b reduces the concentration profiles $\phi(\xi, \eta)$, as can be observed Fig. 6b.

Conclusion

In this study we have investigated heat and mass transfer in a micropolar nanofluid flow with homogeneous–heterogeneous reactions. The conservation equations have been solved using the bivariate spectral quasiliearization method. The novelty of this article is in the study of hydromagnetic flow of micropolar nanofluid due to a stretching surface with homogeneous–heterogeneous reactions and heat generation, and the use of a novel solution method for the nonlinear conservation equations. The main observations from this study maybe listed as follows:

(i)   The fluid concentration distribution increases when particle thermophoresis increases.
(ii) The concentration profiles decreases with increasing particle Brownian motion parameter.
(iv) The material parameter enhances the linear and angular velocity profiles.

Compliance with ethical standards

Conflicts of interest The authors declare that there is no conflict of interests regarding the publication of this article.

References

1. Kumari, M., Slaouti, A., Takhar, H.S., Nakamura, S., Nath, S.: Unsteady free convection flow over a continuous moving vertical surface. Acta Mech. **116**, 75–82 (1996)
2. Pal, D., Chatterjee, S.: Heat and mass transfer in MHD non-Darcian flow of a micropolar fluid over a stretching sheet embedded in a porous media with non-uniform heat source and thermal radiation. Commun. Nonlinear Sci. Numer. Simulat. **15**, 1843–1857 (2010)
3. Sithole, H., Mondal, H., Sibanda, P.: Entropy generation in a second grade magnetohydrodynamic nanofluid flow over a convectively heated stretching sheet with nonlinear thermal radiation and viscous dissipation. Result Phys. **9**, 1077–1085 (2018)
4. Ishak, A., Nazar, R., Pop, I.: Heat transfer over a stretching surface with variable surface heat flux in micropolar fluids. Phys. Lett. A **372**, 559–561 (2008)
5. Muthuraj, R., Srinivas, S.: Fully developed MHD flow of a micropolar and viscous fluids in a vertical porous space using HAM. Int. J. Appl. Math. Mech. **6**(11), 55–78 (2010)
6. Shercliff, J.A.: A Text Book of Magnetohydrodynamics. Pergamon Press Inc., New York (1965)
7. Pal, D., Mondal, H.: Soret and Dufour effects on MHD non-Darcian mixed convection heat and mass transfer over a stretching sheet with non-uniform heat source/sink. Phys. B **407**, 642–651 (2012)
8. Sarkar, A., Kundu, P.K.: Outcomes of non-uniform heat source/sink on micropolar nanofluid flow in presence of slip boundary conditions. Int. J. Appl. Comput. Math. **3**, 801–812 (2017)
9. Kameswaran, P.K., Shaw, S., Sibanda, P., Murthy, P.V.S.N.: Homogeneous–heterogeneous reactions in a nanofluid flow due to a porous stretching sheet. Int. J. Heat Mass Transf. **57**(2), 465–472 (2013)
10. Ravikiran, G., Radhakrishnamacharya, G.: Effect of homogeneous and heterogeneous chemical reactions on peristaltic transport of a Jeffrey fluid through a porous medium with slip condition. J. Appl. Fluid Mech. **8**(3), 521–528 (2015)
11. RamReddy, C., Pradeepa, T.: Influence of convective boundary condition on nonlinear thermal convection flow of a micropolar fluid saturated porous medium with homogenous–heterogenous reactions. Front. Heat Mass Transf. **8**(6), 1–10 (2017)
12. Shaw, S., Kameswaran, P.K., Sibanda, P.: Homogeneous–heterogeneous reactions in micropolar fluid flow from a permeable stretching or shrinking sheet in a porous medium. Bound. Value Prob. **2013**, 77 (2013)
13. Magagula, V.M.: Bivariate Pseudospectral Collocation Algorithms for Nonlinear Partial Differential Equations. University of KwaZulu-Natal, Ph.D Thesis (2016)
14. Ghadikolaei, S.S., Hosseinzadeh, K., Ganji, D.D., Jafari, B.: Nonlinear thermal radiation effect on magneto Casson nanofluid flow with Joule heating effect over an inclined porous stretching sheet. Case Stud. Therm. Eng. **12**, 176–187 (2018)
15. Afridi, M.I., M, Q., Khan, I., Tlili, I.: Entropy generation in MHD mixed convection stagnation-point flow in the presence of joule and frictional heating. Case Stud. Therm. Eng. **12**, 292–300 (2018)
16. Nadeem, S., Masood, S., Mehmood, R., Sadiq, M.A.: Optimal and numerical solutions for an MHD micropolar nanofluid between rotating horizontal parallel plates. PLoS ONE. (2015). https://doi.org/10.1371/journal.pone.0124016
17. Khan, W.A., Alshomrani, A.S., Khan, M.: Assessment on characteristics of heterogeneous–homogenous processes in three-dimensional flow of Burgers fluid. Results Phys. **6**, 772–779 (2016)
18. Hayat, T., Sajjad, R., Ellahi, R., Alsaedi, A., Muhammad, T.: Homogeneous–heterogeneous reactions in MHD flow of micropolar fluid by a curved stretching surface. J. Mol. Liq. **240**, 209–220 (2017)

Chapter 7

Conclusion

In this thesis a theoretical study of heat and mass transport in non-Newtonian nanofluid models using spectral methods was performed. This was achieved by constructing, analyzing and investigating boundary layer flows in various geometrical settings and boundary conditions and subject to different source terms. The aim was to find the impact of key fluid physical parameters on the flows and on the heat and mass transfer. The non-Newtonian fluid models studied ranged from simple to complex models. These models led to highly nonlinear and coupled differential equations that required advanced numerical methods for their solution. Some recently published spectral techniques for solutions of nonlinear systems were used.

In Chapter 2, the non-Newtonian nanofluid model of interest was the upper convected Maxwell fluid model. The Maxwell nanofluid flow with magnetic field over a shrinking surface was assumed to be unsteady. Both convective and slip boundary conditions were imposed. The spectral local linearization method was used to solve the resulting system of equations. The impact and significance of Brownian motion and thermophoresis when the nanofluid particle volume fraction flux at the boundary is zero were evaluated. In terms of heat transfer coefficients, results showed that either increasing the value of particle Brownian motion or magnetic field strength reduced the heat transfer coefficient but the opposite was observed in the case of increased thermophoresis parameter. Results revealed that, with increasing values for the unsteadiness parameter, the concentration and velocity profiles both decreased whereas the temperature profile increased. Increasing particle Brownian motion leads to a reduction in the concentration profiles but concentration profiles increase with increasing thermophoresis.

In Chapter 3, the boundary layer nanofluid flow over a horizontal plate embedded in a non-Darcy porous medium was investigated, with a non-Newtonian power-law fluid being considered as the base fluid. For this model a mixed convective boundary condition was employed at the surface. The model incorporated the effects of Brownian motion and

thermophoresis. The spectral quasi- linearization method (SQLM) was used to solve the relevant equations. Both the accuracy and the convergence of the method through the evaluation of residual errors and error norms were investigated. Furthermore the impact of specific parameters on the flow behaviour and heat transfer characteristics were investigated. Results showed that the accuracy and convergence of the SQLM may depend on the choice of parameter values. For a dilatant fluid, both the heat transfer rate and the mass transfer rate increase with increasing mixed convection parameter. The Biot number enhances both the flow velocity and temperature at the surface. The heat transfer rate also increases with increasing Biot number. The mass transfer rate increases with the Biot number for smaller values of the thermophoresis parameter, but decreases for bigger values of the thermophoresis parameter.

In Chapter 4, we presented a study of heat and mass transfer for a couple stress nanofluid flow in a magneto-porous medium with thermal radiation and heat generation. The flow considered was generated by a stretching surface. The temperature and concentration distributions were studied subject to nanoparticle Brownian motion and thermophoresis effects. The resulting nonlinear model equations were solved using a spectral quasilinearization method. To determine the accuracy of the solutions and the convergence of the method, a qualitative presentation of residual errors for different parameters was given. A limited parametric study showing the influence of the flow parameters on the fluid properties was given. Results showed that the heat transfer characteristics are greatly influenced by an increase in the couple stress parameter. The boundary layer flow attains the minimum velocity for higher values of the magneto-porous parameter. The buoyancy parameter increases the velocity distribution in the momentum boundary layer. Increasing the thermal radiation leads to an increase in the temperature profiles. Increasing the Prandtl number leads to a decrease in the temperature profiles. An increase in the thermophoresis parameter leads to an increase in both the fluid temperature and concentration profiles. The Brownian motion parameter enhances the temperature in the boundary layer region. Also, increasing the Brownian motion parameter decreases concentration. The concentration profiles decrease with motion parameter decreases concentration. The concentration profiles decrease with an increase in the Lewis number. An increase in the reaction rate parameter retards the concentration distribution in the solutal boundary layer.

In Chapter 5, the second grade non-Newtonian model flow with nanofluids was considered. In this chapter the interest was on entropy generation analysis with heat and fluid flow on second grade nanofluids, in order to improve the system performance. For this reason, the entropy generation in magnetohydrodynamic flow of a second grade nanofluid over a convectively heated stretching sheet with nonlinear thermal radiation and viscous

dissipation was studied in detail. The second grade fluid was assumed to be electrically conducting. Homogeneous-heterogeneous reactions were also considered. The mathematical equations were solved using the spectral local linearization method. It was observed that enhancement occurred in the momentum and thermal boundary layer thicknesses when the second grade nanofluid parameter increased. The thermophoresis parameter acted to increase the temperature profiles. The solute concentration at the surface decreased with the strength of the homogeneous and heterogeneous reactions. Entropy generation was enhanced by the Hartmann, Reynolds and Brinkmann numbers. The entropy generation number decreased with increase of temperature difference ratio parameter.

Finally, in Chapter 6, a mathematical model of MHD micropolar nanofluid flow deformed by a stretchable surface was presented. The homogeneous–heterogeneous reactions given by isothermal cubic autocatalator kinetics and first order kinetics were considered. We assumed the existence of an induced magnetic field. The basic microrotation flow and heat mass transfer nonlinear equations in both space and time were solved using the bivariate spectral local linearization method. Analysis of the accuracy of the method was given using residual errors. The results showed that the concentration distribution was reduced by an increase in the homogenous reaction parameter. The concentration distribution was also reduced by an increase in the Schmidt number. The rate of heat transfer is enhanced by larger values of both the Prandtl number and the thermophoresis parameter. The fluid concentration distribution increased when particle thermophoresis increased. The concentration profiles decreased with increasing particle Brownian motion parameter. The material parameter enhanced the linear and angular velocity profiles.

This thesis has focused on the theoretical study of heat and mass transport in non-Newtonian nanofluid models using spectral methods. We sought to evaluate the impact of different fluid parameters on boundary layer flows for various non-Newtonian models using spectral methods. A single fluid model is inadequate to illustrate all properties of all of these fluids. We showed that one model may address only a certain number of non-Newtonian properties but fail to predict others. In this thesis, we have considered in detail five non-Newtonian models for a fluid in which nanoparticles were suspended; namely the upper convected Maxwell, power law, couple stress, second grade and micropolar fluids. Our findings showed that indeed the fluid physical parameters affect the boundary layer flow, heat and mass transfer. Our results were comparable and were in good agreement with previously published work.

The SLLM, SQLM and BSLLM methods were used to solve the equations. The methods were found to be accurate and convergent. We further discovered that some numerical

methods used may be more suitable for certain types of equations. Some numerical methods may give better accuracy for specific parameter values.

References

[1] A. Mushtaq, S. Abbasbandy, M. Mustafa, T. Hayat, and A. Alsaedi, "Numerical solution for Sakiadis flow of upper-convected Maxwell fluid using Cattaneo-Christov heat flux model," *AIP Advances*, vol. 6, no. 1, p. 015208, 2016.

[2] T. Sochi, "Flow of non-Newtonian fluids in porous media," *Journal of Polymer Science Part B: Polymer Physics*, vol. 48, no. 23, pp. 2437–2767, 2010.

[3] D. Cioranescu, V. Girault, and K. R. Rajagopal, *Mechanics and mathematics of fluids of the differential type*.

[4] R. P. Chhabra and J. F. Richardson, *Non-Newtonian flow and applied rheology: engineering applications*. Butterworth-Heinemann, 2011.

[5] S. U. S. Choi and J. A. Eastman, "Enhancing thermal conductivity of fluids with nanoparticles," *ASME-Publications-Fed*, vol. 231, pp. 99–106, 1995.

[6] S. K. Das, S. U. S. Choi, and H. E. Patel, "Heat transfer in nanofluids −a review," *Heat Transfer Engineering*, vol. 27, no. 10, pp. 3–19, 2006.

[7] B. A. Bhanvase, D. P. Barai, S. H. Sonawane, N. Kumar, and S. S. Sonawane, "Intensified heat transfer rate with the use of nanofluids," in *Handbook of Nanomaterials for Industrial Applications*, pp. 739–750, Elsevier, 2018.

[8] M. Goyal and R. Bhargava, "Boundary layer flow and heat transfer of viscoelastic nanofluids past a stretching sheet with partial slip conditions," *Applied Nanoscience*, vol. 4, no. 6, pp. 761–767, 2014.

[9] K. Sadeghy, H. Hajibeygi, and S.-M. Taghavi, "Stagnation-point flow of upper-convected Maxwell fluids," *International Journal of Non-Linear Mechanics*, vol. 41, no. 10, pp. 1242–1247, 2006.

[10] J. Choi, Z. Rusak, and J. Tichy, "Maxwell fluid suction flow in a channel," *Journal of non-Newtonian Fluid Mechanics*, vol. 85, no. 2-3, pp. 165–187, 1999.

[11] W.-T. Wu, N. Aubry, J. Antaki, and M. Massoudi, "Flow of a dense suspension modeled as a modified second grade fluid," *Fluids*, vol. 3, no. 3, p. 55, 2018.

[12] H. A. Barnes, J. F. Hutton, and K. Walters, *An introduction to rheology*. Elsevier, 1989.

[13] N. Özkaya, D. Leger, D. Goldsheyder, and M. Nordin, "Applications of statics to biomechanics," in *Fundamentals of Biomechanics*, pp. 101–139, Springer, 2017.

[14] G. Papanicolaou and S. Zaoutsos, "Viscoelastic constitutive modeling of creep and stress relaxation in polymers and polymer matrix composites," in *Creep and fatigue in polymer matrix composites*, pp. 3–59, Elsevier, 2019.

[15] L. Gargallo and D. Radic, *Physicochemical behavior and supramolecular organization of polymers*. Springer Science & Business Media, 2009.

[16] R. I. Tanner and K. Walters, *Rheology: an historical perspective*, vol. 7. Elsevier, 1998.

[17] A. Souvaliotis and A. Beris, "An extended White–Metzner viscoelastic fluid model based on an internal structural parameter," *Journal of Rheology*, vol. 36, no. 2, pp. 241–271, 1992.

[18] D. Joseph, "Hyperbolic phenomena in the flow of viscoelastic liquids," in *Trends in Applications of Pure Mathematics to Mechanics*, pp. 434–456, Springer, 1986.

[19] T. Hayat and M. Sajid, "Homotopy analysis of MHD boundary layer flow of an upper-convected Maxwell fluid," *International Journal of Engineering Science*, vol. 45, no. 2-8, pp. 393–401, 2007.

[20] D. Yang and K.-Q. Zhu, "Start-up flow of a viscoelastic fluid in a pipe with a fractional Maxwell's model," *Computers & Mathematics with Applications*, vol. 60, no. 8, pp. 2231–2238, 2010.

[21] S. Mukhopadhyay and R. S. Gorla, "Unsteady MHD boundary layer flow of an upper convected Maxwell fluid past a stretching sheet with first order constructive/destructive chemical reaction," *Journal of Naval Architecture and Marine Engineering*, vol. 9, no. 2, pp. 123–133, 2012.

[22] M. M. Rashidi, B. Rostami, N. Freidoonimehr, and S. Abbasbandy, "Free convective heat and mass transfer for MHD fluid flow over a permeable vertical stretching sheet in

the presence of the radiation and buoyancy effects," *Ain Shams Engineering Journal*, vol. 5, no. 3, pp. 901–912, 2014.

[23] S. Abbasbandy, R. Naz, T. Hayat, and A. Alsaedi, "Numerical and analytical solutions for Falkner–Skan flow of MHD Maxwell fluid," *Applied Mathematics and Computation*, vol. 242, pp. 569–575, 2014.

[24] M. Awais, T. Hayat, S. Irum, and A. Alsaedi, "Heat generation/absorption effects in a boundary layer stretched flow of Maxwell nanofluid: Analytic and numeric solutions," *PloS One*, vol. 10, no. 6, p. e0129814, 2015.

[25] M. Ramzan, M. Bilal, J. D. Chung, and U. Farooq, "Mixed convective flow of Maxwell nanofluid past a porous vertical stretched surface–An optimal solution," *Results in Physics*, vol. 6, pp. 1072–1079, 2016.

[26] M. Bilal, M. Sagheer, and S. Hussain, "Three dimensional MHD upper-convected Maxwell nanofluid flow with nonlinear radiative heat flux," *Alexandria Engineering Journal*, vol. 57, no. 3, pp. 1917–1925, 2018.

[27] T. Liu, L. Liu, and L. Zheng, "Unsteady flow and heat transfer of Maxwell nanofluid in a finite thin film with internal heat generation and thermophoresis," *Thermal Science*, vol. 22, no. 6B, pp. 2803–2813, 2018.

[28] S. K. Nandy, "Unsteady flow of Maxwell fluid in the presence of nanoparticles toward a permeable shrinking surface with Navier slip," *Journal of the Taiwan Institute of Chemical Engineers*, vol. 52, pp. 22–30, 2015.

[29] S. K. Nandy, S. Sidui, and T. R. Mahapatra, "Unsteady MHD boundary-layer flow and heat transfer of nanofluid over a permeable shrinking sheet in the presence of thermal radiation," *Alexandria Engineering Journal*, vol. 53, no. 4, pp. 929–937, 2014.

[30] R. S. Rivlin and J. L. Ericksen, "Stress-deformation relations for isotropic materials," in *Collected Papers of RS Rivlin*, pp. 911–1013, Springer, 1997.

[31] C.-S. Man and Q.-X. Sun, "On the significance of normal stress effects in the flow of glaciers," *Journal of Glaciology*, vol. 33, no. 115, pp. 268–273, 1987.

[32] M. Ramzan and M. Bilal, "Time dependent mhd nano-second grade fluid flow induced by permeable vertical sheet with mixed convection and thermal radiation," *PloS One*, vol. 10, no. 5, p. e0124929, 2015.

[33] T. Hayat, M. Qasim, S. Shehzad, and A. Alsaedi, "Unsteady stagnation point flow of second grade fluid with variable free stream," *Alexandria Engineering Journal*, vol. 53, no. 2, pp. 455–461, 2014.

[34] K. Das, R. P. Sharma, and A. Sarkar, "Heat and mass transfer of a second grade magnetohydrodynamic fluid over a convectively heated stretching sheet," *Journal of Computational Design and Engineering*, vol. 3, no. 4, pp. 330–336, 2016.

[35] M. Jamil, A. Rauf, C. Fetecau, and N. Khan, "Helical flows of second grade fluid due to constantly accelerated shear stresses," *Communications in Nonlinear Science and Numerical Simulation*, vol. 16, no. 4, pp. 1959–1969, 2011.

[36] S. Nadeem, A. Rehman, C. Lee, and J. Lee, "Boundary layer flow of second grade fluid in a cylinder with heat transfer," *Mathematical Problems in Engineering*, vol. 2012, 2012.

[37] T. E. Akinbobola and S. S. Okoya, "The flow of second grade fluid over a stretching sheet with variable thermal conductivity and viscosity in the presence of heat source/sink," *Journal of the Nigerian Mathematical Society*, vol. 34, no. 3, pp. 331–342, 2015.

[38] M. Turkyilmazoglu, "Dual and triple solutions for MHD slip flow of non-Newtonian fluid over a shrinking surface," *Computers & Fluids*, vol. 70, pp. 53–58, 2012.

[39] M. E. Erdoğan and C. E. Imrak, "Steady flow of a second-grade fluid in an annulus with porous walls," *Mathematical Problems in Engineering*, vol. 2008, 2008.

[40] T. Hayat, A. Aziz, T. Muhammad, and B. Ahmad, "On magnetohydrodynamic flow of second grade nanofluid over a nonlinear stretching sheet," *Journal of Magnetism and Magnetic Materials*, vol. 408, pp. 99–106, 2016.

[41] M. Ramzan, M. Bilal, U. Farooq, and J. D. Chung, "Mixed convective radiative flow of second grade nanofluid with convective boundary conditions: an optimal solution," *Results in physics*, vol. 6, pp. 796–804, 2016.

[42] S. Zuhra, N. S. Khan, and S. Islam, "Magnetohydrodynamic second-grade nanofluid flow containing nanoparticles and gyrotactic microorganisms," *Computational and Applied Mathematics*, vol. 37, no. 5, pp. 6332–6358, 2018.

[43] V. K. Stokes, "Couple stresses in fluids," *The physics of fluids*, vol. 9, no. 9, pp. 1709–1715, 1966.

[44] S. Islam and C. Zhou, "Exact solutions for two dimensional flows of couple stress fluids," *Zeitschrift für angewandte Mathematik und Physik*, vol. 58, no. 6, pp. 1035–1048, 2007.

[45] S. Islam, C.-y. Zhou, and X.-j. Ran, "Exact solutions for different vorticity functions of couple stress fluids," *Journal of Zhejiang University-SCIENCE A*, vol. 9, no. 5, pp. 672–680, 2008.

[46] E. Walicki and A. Walicka, "Interia effect in the squeeze film of a couple-stress fluid in biological bearings," *Applied Mechanics and Engineering*, vol. 4, no. 2, pp. 363–373, 1999.

[47] P. Hiremath and P. Patil, "Free convection effects on the oscillatory flow of a couple stress fluid through a porous medium," *Acta Mechanica*, vol. 98, no. 1-4, pp. 143–158, 1993.

[48] T. Hayat, M. Mustafa, Z. Iqbal, and A. Alsaedi, "Stagnation-point flow of couple stress fluid with melting heat transfer," *Applied Mathematics and Mechanics*, vol. 34, no. 2, pp. 167–176, 2013.

[49] H. Bakhti and L. Azrar, "Steady flow of couple-stress fluid in constricted tapered artery: Effects of transverse magnetic field, moving catheter, and slip velocity," *Journal of Applied Mathematics*, vol. 2016, 2016.

[50] H. S. Takhar, A. K. Singh, and G. Nath, "Unsteady MHD flow and heat transfer on a rotating disk in an ambient fluid," *International Journal of Thermal Sciences*, vol. 41, no. 2, pp. 147–155, 2002.

[51] N. A. Khan, S. Aziz, and N. A. Khan, "Numerical simulation for the unsteady MHD flow and heat transfer of couple stress fluid over a rotating disk," *Plos One*, vol. 9, no. 5, p. e95423, 2014.

[52] J. Umavathi, J. P. Kumar, and A. J. Chamkha, "Convective flow of two immiscible viscous and couple stress permeable fluids through a vertical channel," *Turkish Journal of Engineering and Environmental Sciences*, vol. 33, no. 4, pp. 221–244, 2010.

[53] M. S. Sarojini, M. V. Krishna, and C. U. Shankar, "MHD flow of a couple stress fluid through a porous medium in a parallel plate channel in presence of effect of inclined magnetic field," *International Journal of Physics and Mathematical Sciences*, vol. 1, pp. 9–18, 2011.

[54] F. Awad, N. Haroun, P. Sibanda, and M. Khumalo, "On couple stress effects on unsteady nanofluid flow over stretching surfaces with vanishing nanoparticle flux at the wall," *Journal of Applied Fluid Mechanics*, vol. 9, no. 4, pp. 1937–1944, 2016.

[55] R. Ellahi, A. Zeeshan, F. Hussain, and A. Asadollahi, "Peristaltic blood flow of couple stress fluid suspended with nanoparticles under the influence of chemical reaction and activation energy," *Symmetry*, vol. 11, no. 2, p. 276, 2019.

[56] A. R. Hadjesfandiari and G. F. Dargush, "Evolution of generalized couple-stress continuum theories: a critical analysis," *arXiv preprint arXiv:1501.03112*, 2014.

[57] W. Schowalter, "The application of boundary-layer theory to power-law pseudoplastic fluids: Similar solutions," *AIChE Journal*, vol. 6, no. 1, pp. 24–28, 1960.

[58] A. Acrivos, M. Shah, and E. Petersen, "Momentum and heat transfer in laminar boundary-layer flows of non-Newtonian fluids past external surfaces," *AIChE Journal*, vol. 6, no. 2, pp. 312–317, 1960.

[59] A. M. Ishak and N. Bachok, "Power-law fluid flow on a moving wall," *European Journal of Scientific Research*, vol. 34, no. 1, pp. 55–60, 2009.

[60] B. S. Reddy, N. Kishan, and M. Rajasekhar, "Mhd boundary layer flow of a non-newtonian power-law fluid on a moving flat plate," *Adv. Appl. Sci. Res*, vol. 3, pp. 1472–1481, 2012.

[61] D. O. de Almeida Cruz, J. N. N. Quaresma, C. E. Maneschy, and E. N. Macêdo, "A turbulence model for non-Newtonian power-law fluids in ducts,"

[62] P. Bose, T. Rakib, S. Das, K. M. Rabbi, and S. Mojumder, "MHD mixed convection analysis of non-Newtonian power law fluid in an open channel with round cavity," in *AIP Conference Proceedings*, vol. 1851, p. 020057, AIP Publishing, 2017.

[63] A. Sojoudi, S. C. Saha, Y. Gu, and M. Hossain, "Steady natural convection of non-Newtonian power-law fluid in a trapezoidal enclosure," *Advances in Mechanical Engineering*, vol. 5, p. 653108, 2013.

[64] S. Thohura, M. M. Molla, and M. M. A. Sarker, "Numerical simulation of non-Newtonian power-law fluid flow in a lid-driven skewed cavity," *International Journal of Applied and Computational Mathematics*, vol. 5, no. 1, p. 14, 2019.

[65] J. Bear and Y. Bachmat, *Introduction to modeling of transport phenomena in porous media*, vol. 4. Springer Science & Business Media, 2012.

[66] D. B. Ingham and I. Pop, *Transport phenomena in porous media.* Elsevier, 1998.

[67] J. H. Lehr and J. K. Lehr, *Standard handbook of environmental science, health, and technology.* McGraw Hill Professional, 2000.

[68] M. Honarpour and S. M. Mahmood, "Relative-permeability measurements: An overview," *Journal of Petroleum Technology*, vol. 40, no. 08, pp. 963–966, 1988.

[69] H. P. G. Darcy, *Les Fontaines publiques de la ville de Dijon. Exposition et application des principes à suivre et des formules à employer dans les questions de distribution d'eau, etc.* V. Dalmont, 1856.

[70] Z. Zeng and R. Grigg, "A criterion for non-Darcy flow in porous media," *Transport in Porous Media*, vol. 63.

[71] J. Prasad, Hemalatha, and Prasad, "Mixed convection flow from vertical plate embedded in non-Newtonian fluid saturated non- Darcy Porous Medium with Thermal Dispersion-Radiation and Melting Effects," *Journal of Applied Fluid Mechanics*, vol. 7, no. 385, p. 394, 2011.

[72] R. Kairi, P. Narayana, and P. Murthy, "The effect of double dispersion on natural convection heat and mass transfer in a non-Newtonian fluid saturated non-Darcy porous medium," *Transport in porous media*, vol. 68, no. 3, pp. 377–390, 2009.

[73] M. Kumari and S. Jayanthi, "Non-Darcy non-Newtonian free convection flow over a horizontal cylinder in a saturated porous medium," *International communications in heat and mass transfer*, vol. 31, no. 8, pp. 1219–1226, 2010.

[74] H. Hadim, "Non-Darcy natural convection of a non-Newtonian fluid in a porous cavity," *International communications in heat and mass transfer*, vol. 33, no. 10, pp. 1179–1189, 2006.

[75] A. Chamka, S. Abbasbandy, and A. Rashad, "Non-Darcy natural convection flow for non-Newtonian nanofluid over cone saturated in porous medium with uniform heat and volume fraction fluxes," *International Journal of Numerical Methods for Heat & Fluid Flow*, vol. 25, pp. 422–437, 2015.

[76] P. Kameswaran and P. Sibanda, "Thermal dispersion effects on convective heat and mass transfer in an Ostwald de Waele nanofluid flow in porous media," *Boundary Value Problems*, p. 243, 2013.

[77] A. C. Eringen, "Theory of micropolar fluids," *Journal of Mathematics and Mechanics*, pp. 1–18, 1966.

[78] M. S. Uddin, K. Bhattacharyya, S. Shafie, *et al.*, "Micropolar fluid flow and heat transfer over an exponentially permeable shrinking sheet," *Propulsion and Power Research*, vol. 5, no. 4, pp. 310–317, 2016.

[79] J. Peddieson and M. R, "Boundary-layer theory for a micropolar fluid recent," *Adv. Eng. Sci.*, vol. 5, pp. 405–476, 1970.

[80] A. C. Eringen, "Theory of thermomicrofluids," *Journal of Mathematical Analysis and Applications*, vol. 38, no. 2, pp. 480–496, 1972.

[81] H. Kümmerer, "Similar laminar boundary layers in incompressible micropolar fluids," *Rheologica Acta*, vol. 16, no. 3, pp. 261–265, 1977.

[82] K. K. Sankara and L. T. Watson, "Micropolar flow past a stretching sheet," *Zeitschrift für angewandte Mathematik und Physik*, vol. 36, no. 6, pp. 845–853, 1985.

[83] M. W. Heruska, L. T. Watson, and K. K. Sankara, "Micropolar flow past a porous stretching sheet," *Computers & fluids*, vol. 14, no. 2, pp. 117–129, 1986.

[84] I. Hassanien and R. Gorla, "Heat transfer to a micropolar fluid from a non-isothermal stretching sheet with suction and blowing," *Acta Mechanica*, vol. 84, no. 1-4, pp. 191–199, 1990.

[85] M. M. Rahman, A. Aziz, and M. A. Al-Lawatia, "Heat transfer in micropolar fluid along an inclined permeable plate with variable fluid properties," *International Journal of Thermal Sciences*, vol. 49, no. 6, pp. 993–1002, 2010.

[86] K. Das, "Influence of thermophoresis and chemical reaction on MHD micropolar fluid flow with variable fluid properties," *International Journal of Heat and Mass Transfer*, vol. 55, no. 23-24, pp. 7166–7174, 2012.

[87] K. Bhattacharyya, S. Mukhopadhyay, G. Layek, and I. Pop, "Effects of thermal radiation on micropolar fluid flow and heat transfer over a porous shrinking sheet," *International Journal of Heat and Mass Transfer*, vol. 55, no. 11-12, pp. 2945–2952, 2012.

[88] S. Mishra, S. Baag, and D. Mohapatra, "Chemical reaction and Soret effects on hydromagnetic micropolar fluid along a stretching sheet," *Engineering Science and Technology, an International Journal*, vol. 19, no. 4, pp. 1919–1928, 2016.

[89] S. Atif, S. Hussain, and M. Sagheer, "Numerical study of MHD micropolar carreau nanofluid in the presence of induced magnetic field," *AIP Advances*, vol. 8, no. 3, p. 035219, 2018.

[90] M. Alizadeh, A. Dogonchi, and D. Ganji, "Micropolar nanofluid flow and heat transfer between penetrable walls in the presence of thermal radiation and magnetic field," *Case studies in thermal engineering*, vol. 12, pp. 319–332, 2018.

[91] N. Abbas, S. Saleem, S. Nadeem, A. Alderremy, and A. Khan, "On stagnation point flow of a micro polar nanofluid past a circular cylinder with velocity and thermal slip," *Results in Physics*, vol. 9, pp. 1224–1232, 2018.

[92] Z. Shah, S. Islam, H. Ayaz, and S. Khan, "Radiative heat and mass transfer analysis of micropolar nanofluid flow of Casson fluid between two rotating parallel plates with effects of Hall current," *Journal of Heat Transfer*, vol. 141, no. 2, p. 022401, 2019.

[93] M. Chaudhary and J. Merkin, "A simple isothermal model for homogeneous-heterogeneous reactions in boundary-layer flow. I Equal diffusivities," *Fluid dynamics research*, vol. 16, no. 6, p. 311, 1995.

[94] M. Chaudhary and J. Merkin, "A simple isothermal model for homogeneous-heterogeneous reactions in boundary-layer flow. II Different diffusivities for reactant and autocatalyst," *Fluid dynamics research*, vol. 16, no. 6, p. 335, 1995.

[95] P. Kameswaran, S. Shaw, P. Sibanda, and P. Murthy, "Homogeneous–heterogeneous reactions in a nanofluid flow due to a porous stretching sheet," *International journal of heat and mass transfer*, vol. 57, no. 2, pp. 465–472, 2013.

[96] G. Ravikiran and G. Radhakrishnamacharya, "Effect of homogeneous and heterogeneous chemical reactions on peristaltic transport of a jeffrey fluid through a porous medium with slip condition," 2015.

[97] S. Shaw, P. K. Kameswaran, and P. Sibanda, "Homogeneous-heterogeneous reactions in micropolar fluid flow from a permeable stretching or shrinking sheet in a porous medium," *Boundary Value Problems*, vol. 2013, no. 1, p. 77, 2013.

[98] W. Yu, D. M. France, J. L. Routbort, and S. U. Choi, "Review and comparison of nanofluid thermal conductivity and heat transfer enhancements," *Heat Transfer Engineering*, vol. 29, no. 5, pp. 432–460, 2008.

[99] Y. Xuan and Q. Li, "Heat transfer enhancement of nanofluids," *International Journal of heat and fluid flow*, vol. 21, no. 1, pp. 58–64, 2000.

[100] S. P. Jang and S. U. Choi, "Cooling performance of a microchannel heat sink with nanofluids," *Applied Thermal Engineering*, vol. 26, no. 17-18, pp. 2457–2463, 2006.

[101] S.-C. Tzeng, C.-W. Lin, and K. Huang, "Heat transfer enhancement of nanofluids in rotary blade coupling of four-wheel-drive vehicles," *Acta Mechanica*, vol. 179, no. 1-2, pp. 11–23, 2005.

[102] D. P. Kulkarni, D. K. Das, and R. S. Vajjha, "Application of nanofluids in heating buildings and reducing pollution," *Applied Energy*, vol. 86, no. 12, pp. 2566–2573, 2009.

[103] T. P. Otanicar, P. E. Phelan, R. S. Prasher, G. Rosengarten, and R. A. Taylor, "Nanofluid-based direct absorption solar collector," *Journal of renewable and sustainable energy*, vol. 2, no. 3, p. 033102, 2010.

[104] N. M. Arifin, R. Nazar, and I. Pop, "Free-and mixed-convection flow past a horizontal surface in a nanofluid," *Journal of Thermophysics and Heat Transfer*, vol. 26, no. 2, pp. 375–382, 2012.

[105] A. Chamkha, S. Abbasbandy, and A. Rashad, "Non-darcy natural convection flow for non-newtonian nanofluid over cone saturated in porous medium with uniform heat and volume fraction fluxes," *International Journal of Numerical Methods for Heat & Fluid Flow*, vol. 25, no. 2, pp. 422–437, 2015.

[106] S. Mondal, S. Nandy, and P. Sibanda, "MHD Flow and Heat Transfer of Maxwell Nanofluid Over an Unsteady Permeable Shrinking Sheet with Convective Boundary Conditions," *Journal of Nanofluids*, vol. 7, no. 5, pp. 995–1003, 2018.

[107] S. Bilal, Z. Mustafa, K. U. Rehman, and M. Malik, "MHD second grade nanofluid flow induced by a rotatory cone," *Journal of Nanofluids*, vol. 8, no. 4, pp. 876–884, 2019.

[108] C. B. Sobhan and G. P. Peterson, *Microscale and nanoscale heat transfer: fundamentals and engineering applications*. CRC Press, 2008.

[109] T. L. Bergman, F. P. Incropera, D. P. DeWitt, and A. S. Lavine, *Fundamentals of heat and mass transfer*. John Wiley & Sons, Hoboken, 2011.

[110] Y. A. Cengel and A. Ghajar, *Heat and mass transfer (a practical approach, SI version)*. McGraw-Hill Education,, McGraw-Hill Education, New York, 2011.

[111] C. A. Yunus and J. G. Afshin, *Heat and mass transfer: fundamentals and applications*. Tata McGraw-Hill, New Delhi, 2011.

[112] W. M. Kays, *Convective heat and mass transfer*. Tata McGraw-Hill Education, 2012.

[113] R. Malik, M. Khan, A. Munir, and W. A. Khan, "Flow and heat transfer in sisko fluid with convective boundary condition," *Plos one*, vol. 9, no. 10, p. e107989, 2014.

[114] O. D. Makinde and A. Aziz, "Boundary layer flow of a nanofluid past a stretching sheet with a convective boundary condition," *International Journal of Thermal Sciences*, vol. 50, no. 7, pp. 1326–1332, 2011.

[115] M. J. Uddin, W. A. Khan, and A. I. Ismail, "MHD free convective boundary layer flow of a nanofluid past a flat vertical plate with Newtonian heating boundary condition," *PLoS One*, vol. 7, no. 11, p. e49499, 2012.

[116] D. Pal and H. Mondal, "The influence of thermal radiation on hydromagnetic Darcy-Forchheimer mixed convection flow past a stretching sheet embedded in a porous medium," *Meccanica*, vol. 46, no. 4, pp. 739–753, 2011.

[117] D. Pal, "Heat and mass transfer in stagnation-point flow towards a stretching surface in the presence of buoyancy force and thermal radiation," *Meccanica*, vol. 44, no. 2, pp. 145–158, 2009.

[118] S. Aïboud and S. Saouli, "Entropy analysis for viscoelastic magnetohydrodynamic flow over a stretching surface," *International Journal of Non-Linear Mechanics*, vol. 45, no. 5, pp. 482–489, 2010.

[119] A. S. Butt, S. Munawar, A. Ali, and A. Mehmood, "Entropy generation in hydrodynamic slip flow over a vertical plate with convective boundary," *Journal of mechanical science and technology*, vol. 26, no. 9, pp. 2977–2984, 2012.

[120] M. Magherbi, H. Abbassi, N. Hidouri, and A. Brahim, "Second law analysis in convective heat and mass transfer," *Entropy*, vol. 8, no. 1, pp. 1–17, 2006.

[121] N. Hidouri, M. Magherbi, H. Abbassi, and A. Ben Brahim, "Entropy generation in double diffusive convection in presence of the Soret effect," *Progress in Computational Fluid Dynamics, an International Journal*, vol. 7, no. 5, pp. 237–246, 2007.

[122] A. Lopez, G. Ibanez, J. Pantoja, J. Moreira, and O. Lastres, "Entropy generation analysis of MHD nanofluid flow in a porous vertical microchannel with nonlinear thermal radiation, slip flow and convective-radiative boundary conditions," *International Journal of Heat and Mass Transfer*, vol. 107, pp. 982–994, 2017.

[123] I. Khan, S. Ullah, M. Malik, and A. Hussain, "Numerical analysis of MHD Carreau fluid flow over a stretching cylinder with homogenous-heterogeneous reactions," *Results in Physics*, vol. 9, pp. 1141–1147, 2018.

[124] R. Sharma, R. Bhargava, and P. Bhargava, "A numerical solution of unsteady MHD convection heat and mass transfer past a semi-infinite vertical porous moving plate using element free Galerkin method," *Computational Materials Science*, vol. 48, no. 3, pp. 537–543, 2010.

[125] K.-J. Bathe and L. Zhang, "The finite element method with overlapping elements–a new paradigm for CAD driven simulations," *Computers & Structures*, vol. 182, pp. 526–539, 2017.

[126] K. Vajravelu and K. V. Prasad, *Keller-box method and its application*, vol. 8. Walter de Gruyter GmbH & Co KG, 2014.

[127] A. Asaithambi, "A second-order finite-difference method for the Falkner–Skan equation," *Applied Mathematics and Computation*, vol. 156, no. 3, pp. 779–786, 2004.

[128] B. Bin-Mohsin, "Buoyancy Effects on MHD Transport of Nanofluid Over a Stretching Surface With Variable Viscosity," *IEEE Access*, vol. 7, pp. 75398–75406, 2019.

[129] D. Anderson, J. C. Tannehill, and R. H. Pletcher, *Computational fluid mechanics and heat transfer*. CRC Press, 2016.

[130] S. S. Motsa, "A new spectral local linearization method for nonlinear boundary layer flow problems," *Journal of Applied Mathematics*, vol. 2013, Article ID 423628, 2013.

[131] M. Solecki, *Mass transfer: Advancement in process modelling*. InTech Open, 2015.

[132] S. Motsa and S. Shateyi, "Successive linearisation analysis of unsteady heat and mass transfer from a stretching surface embedded in a porous medium with suction/injection and thermal radiation effects," *The Canadian Journal of Chemical Engineering*, vol. 90, no. 5, pp. 1323–1335, 2012.

[133] R. E. Bellman and R. E. Kalaba, "Quasilinearization and nonlinear boundary-value problems," 1965.

[134] S. S. Motsa, P. G. Dlamini, and M. Khumalo, "Spectral relaxation method and spectral quasilinearization method for solving unsteady boundary layer flow problems," *Advances in Mathematical Physics*, vol. 2014, Article ID 341964, 2014.

[135] S. Shateyi and G. T. Marewo, "On a new numerical analysis of the hall effect on mhd flow and heat transfer over an unsteady stretching permeable surface in the presence of thermal radiation and heat source/sink," *Boundary Value Problems*, vol. 2014, no. 1, p. 170, 2014.

[136] S. Motsa, Z. Makukula, and S. Shateyi, "Spectral local linearisation approach for natural convection boundary layer flow," *Mathematical Problems in Engineering*, vol. 2013, 2013.

[137] S. S. Motsa, "On the practical use of the spectral homotopy analysis method and local linearisation method for unsteady boundary-layer flows caused by an impulsively stretching plate," *Numerical Algorithms*, vol. 66, no. 4, pp. 865–883, 2014.

[138] S. Motsa, "On the new bivariate local linearisation method for solving coupled partial differential equations in some applications of unsteady fluid flows with heat and mass transfer," in *Marek Solecki, Mass Transfer-Advancement in Process Modelling*, IntechOpen, 2015.